19700002308
70N11612

NASA TECHNICAL NOTE

NASA TN D-5502

NASA TN D-5502

A MINIMUM-ENERGY MISSION PLAN FOR THE MANNED EXPLORATION OF MARS

by James J. Taylor and Sam W. Wilson, Jr.

Manned Spacecraft Center
Houston, Texas

NATIONAL AERONAUTICS AND SPACE ADMINISTRATION • WASHINGTON, D. C. • NOVEMBER 1969

1. REPORT NO.	2. GOVERNMENT ACCESSION NO.	3. RECIPIENT'S CATALOG NO.
NASA TN D-5502		

4. TITLE AND SUBTITLE	5. REPORT DATE
A MINIMUM-ENERGY MISSION PLAN FOR THE MANNED EXPLORATION OF MARS	November 1969
	6. PERFORMING ORGANIZATION CODE

7. AUTHOR(S)	8. PERFORMING ORGANIZATION REPORT NO.
James J. Taylor, MSC, and Sam W. Wilson, Jr., TRW Systems Group	S-209

9. PERFORMING ORGANIZATION NAME AND ADDRESS	10. WORK UNIT NO.
Manned Spacecraft Center Houston, Texas 77058	909-40-30-00-72
	11. CONTRACT OR GRANT NO.

12. SPONSORING AGENCY NAME AND ADDRESS	13. REPORT TYPE AND PERIOD COVERED
National Aeronautics and Space Administration Washington, D.C. 20546	Technical Note
	14. SPONSORING AGENCY CODE

15. SUPPLEMENTARY NOTES

16. ABSTRACT

A minimum-energy mission profile and launch-window analysis for a manned exploration of Mars is evaluated for the period from 1977 to 1985. Four launches of an uprated Saturn V booster, each capable of placing a 400 000-pound payload into a 260-nautical-mile orbit, are used to assemble the spacecraft and the trans-Mars-injection stages. The launch window for the minimum-energy mission is relatively insensitive to delayed launches or interrupted departure sequences. From technological considerations, the minimum-energy mission is feasible and permits the accomplishment of an increased list of scientific objectives.

17. KEY WORDS (SUPPLIED BY AUTHOR)

- Mars
- Mars Orbit
- Orbital Departure
- Assembly Orbits
- Mars Mission Plan
- Mars Manned Exploration
- Launch Window
- Minimum Energy Mission

18. DISTRIBUTION STATEMENT

Unclassified - Unlimited

19. SECURITY CLASSIFICATION (THIS REPORT)	20. SECURITY CLASSIFICATION (THIS PAGE)	21. NO. OF PAGES	22. PRICE
Unclassified	Unclassified	81	* $3.00

* For sale by the Clearinghouse for Federal Scientific and Technical Information
Springfield, Virginia 22151

CONTENTS

TABLES

FIGURES

A MINIMUM-ENERGY MISSION PLAN FOR THE MANNED EXPLORATION OF MARS

By James J. Taylor and Sam W. Wilson, Jr.*
Manned Spacecraft Center

SUMMARY

A minimum-energy mission profile for a manned conjunction-class Mars mission is described. The mission is designed to minimize propulsion requirements without compromising mission objectives. The heliocentric phases consist of two near-Hohmann transfers separated by a Mars-orbital stay of approximately 1 year (about one-third the total trip time of approximately 3 years). Trans-Mars injection is accomplished with a series of near-perigee burns to minimize gravity losses. The elliptical Mars parking orbit benefits from Mars oblateness perturbations which reduce the Mars-orbital-insertion and trans-Earth-injection propulsion requirements.

Mission opportunities are evaluated for the period from 1977 to 1985. The 1983 mission opportunity requires the most propulsion, and the 1977 opportunity requires the least propulsion. A non-mission-dependent velocity budget is developed which requires the addition of 600 fps to the impulsive trans-Mars-injection maneuver and 1650 fps to the spacecraft impulsive propulsion requirements. The maximum Earth-entry velocity does not exceed 40 000 fps, which is within current Apollo technology.

Four launches of an uprated Saturn V booster, each capable of placing a 400 000-pound payload into a 260-nautical-mile circular assembly orbit, are used to assemble the spacecraft and the trans-Mars-injection stages. The first launch places the manned spacecraft (without the Mars lander module) into the assembly orbit. The second launch places the first orbital-launch vehicle (liquid oxygen and hydrogen fueled) and the Mars lander module into the assembly orbit. The third and fourth launches place two additional orbital-launch vehicles (also liquid oxygen and hydrogen fueled) into the assembly orbit. The total vehicle weight, assembled in orbit and prepared for trans-Mars injection, is 1 461 600 pounds. The spacecraft, which includes a 90 000-pound manned Mars lander module, 9000 pounds of scientific equipment, 20 000 pounds of jettisonable probes, and a two-stage propulsion system, is assumed to weigh 450 000 pounds.

An analysis of the Earth-departure launch window is presented. The multiple-impulse technique provides trans-Mars-injection launch windows of 28 to 33 days for

---

*TRW Systems Group, Houston, Texas.

an optimally oriented rendezvous-compatible assembly orbit. Exemplary launch schedules, based on assumed launch-facility limitations, are presented. Interrupted departure sequences are investigated, and orbital departure is found to be still possible after several days of coast in an intermediate elliptical orbit. Extensions to the orbital-launch window are possible by deliberate insertion into a holding orbit.

INTRODUCTION

The feasibility of manned interplanetary missions for the exploration of Mars has been documented in numerous reports (e.g., refs. 1 to 8). The mission plans that demonstrate this feasibility are varied and show considerable ingenuity. Multiple-planet flybys, aerodynamic capture, "perihelion kick," and many other techniques have been used to reduce the performance requirements for short-duration missions of less than 700 days. However, the minimum-energy mission, which requires longer trip times, has received much less attention, and the actual penalties of the shorter trip times cannot be determined unless they are compared with parameters of the minimum-energy mission without regard to trip time. Mission energy is defined as the summation of the required velocity increments, including atmospheric and propulsive maneuvers, for all phases of the mission except during the Mars-orbital phase.

The primary objective of this report is to present the minimum-energy mission plan in sufficient detail to provide a comparative basis for determining the effectiveness of other mission plans. The measure of this effectiveness is a combination of such factors as cost, scientific return, program schedule, and so forth. The determination of the comparative effectiveness of the mission profiles presented in the literature is beyond the scope of this report. The basic mission profile for the minimum-energy mission (which is a conjunction-class mission) is presented in the section of this report entitled "Nominal Mission Profile."

Although the major penalty of conjunction-class missions is extended trip time, many advantages are realized in comparison to the higher energy mission profiles. The total mission energy requirements, including Earth-entry velocity, are significantly reduced in conjunction-class missions. The reduced energy requirements, for a given mass in Earth orbit, permit an increased functional payload. The conjunction-class mission profile is bounded by the orbits of Earth and Mars; therefore, close approach to the Sun and passage through the asteroid belt beyond Mars are avoided. The conjunction-class mission also provides for a greatly increased Mars-orbital stay time for extended scientific observation. The increased functional payload can be used to offset penalties associated with the extended trip time.

After mission opportunities and energy requirements are determined, spacecraft system performance is discussed. Although many assumptions concerning spacecraft performance are possible, a particular set of assumptions is necessary to conduct a realistic launch-window analysis. The techniques developed in this section are valid, regardless of the assumptions; but the quantitative results are dependent on the assumptions. A portion of the launch-window data presented has been published previously (ref. 9).

SYMBOLS

h_A assembly-orbit apogee altitude

h_P assembly-orbit perigee altitude

i assembly-orbit inclination relative to the equator

M number of orbital revolutions between the direct-rendezvous opportunity in the northeast quadrant and the succeeding opportunity in the southeast quadrant

N number of orbital revolutions between each direct-rendezvous opportunity in a given launch-azimuth quadrant

N_D approximate number of anomalistic launch windows in nodal launch window

N_M number of in-plane launch opportunities in main-spacecraft ascent window

N_S number of in-plane launch opportunities in orbital-launch-vehicle ascent window

R radius from center of planet, n. mi.

t time, sec

t_0 epoch, departure date for minimum $\vec{V}_\infty$, days after Julian date 2 440 000

$t_{D,1}$ date orbital-departure window opens

$t_{D,2}$ date orbital-departure window closes

$t_{M,1}$ date main-spacecraft ascent window opens

$t_{M,2}$ time main-spacecraft ascent window closes

$t_{S,1}$ date orbital-launch-vehicle-stage ascent window opens, $\approx$5.5 days before $t_{D,1}$

$t_{S,2}$ date orbital-launch-vehicle-stage ascent window closes, $\approx$4.0 days before $t_{D,2}$

u_0 argument of position measured in the plane of the orbit from the right ascending node, at epoch t_0

$\vec{V}_{AZ}$ horizontal component of velocity vector (fig. 18)

$\vec{V}_0$ matched-conic velocity vector at the sphere of influence, fps

$\vec{V}_\infty$ hyperbolic-excess-velocity vector

W plane-change wedge angle (fig. 18)

α_0 right ascension of the Earth-departure asymptote at t_0

Δt launch interval between launches on a given azimuth, hr

Δt_D width of nodal launch window, days

Δt_M width of main-spacecraft ascent window, days

Δt_p time available for pad turnaround, days

Δt_S width of orbital-launch-vehicle ascent window, days

ΔV impulsive-velocity increment, fps

ΔV_1 impulsive velocity to transfer from assembly orbit to first intermediate orbit, fps

ΔV_2 impulsive velocity to transfer from first intermediate orbit to second intermediate orbit, fps

ΔV_3 impulsive velocity to transfer from second to third intermediate orbit, fps

ΔV_4 plane-change maneuver, if required

ΔV_5 impulsive velocity to transfer from final ellipse to departure hyperbola

$\Delta\Omega_0$ change in right ascension of assembly-orbit ascending node at t_0, deg

$\Delta\omega_0$ change in assembly-orbit argument of perigee at epoch t_0, deg

δ_0 declination of the Earth-departure asymptote at t_0

δt launch interval between the northeast and southeast launch azimuths, hr

Ω right ascension of the departure asymptote

Ω_0 right ascension of assembly-orbit ascending node at t_0, deg

ω_0 assembly-orbit argument of perigee at epoch t_0, deg

NOMINAL MISSION PROFILE

The mission objectives assumed for the analysis are as follows:

1. To photograph the Mars surface during season changes
2. To map the Mars surface features
3. To research the Mars atmosphere
4. To research the Mars surface with unmanned soft landers
5. To explore the Mars surface with a manned lander
6. To investigate one or both of the Martian moons with a manned excursion vehicle

Heliocentric Phase

The heliocentric phase of the nominal minimum-energy mission profile is illustrated in figure 1. The conjunction-class mission profile uses near-Hohmann (near-180°) transfers between the two orbits of the planets. A limited analysis of two- and three-impulse trajectories (refs. 10 and 11) indicates that the minimum-energy transfer to Mars is a two-impulse trajectory and that a large launch window is available before three-impulse trajectories can appreciably reduce the velocity requirements. Two impulses are used for each leg of the trajectory, one at Earth (or Mars) departure and one at planet arrival. The aerodynamic entry into the Earth atmosphere replaces the second impulse for the return leg of the trajectory. The other impulses are propulsive and consist of multiple thrusting maneuvers. However, from a heliocentric point of view, these multiple thrusts are equivalent to single impulses.

The velocity and trip-time requirements vary continuously with a given class of mission. The conjunction-class Mars missions have total trip times of 950 to 1000 days. However, when the energy requirements are allowed to increase by 50 percent or more, the total trip time can be reduced to 450 days. A continuous velocity and total-trip-time trade-off from conjunction- to opposition-class missions is possible, but a local maximum occurs in the energy requirements at the 600- to 700-day total trip time. This local maximum is approximately 80 percent greater than the minimum energy requirements and may require additional heliocentric impulses.

There are other classes of missions, such as single- and dual-planet flyby missions, which have total trip times in the 600- to 700-day range, but the velocity requirements are still approximately 30 percent higher than the minimum. There is also a multiple-heliocentric-orbit class of missions which has minimum-energy velocity requirements but longer trip times (approximately 1300 days). This class of mission involves Hohmann transfers with an additional full orbit coast. The minimum energy is not reduced, and the missions are effective only for phasing as in an abort.

The minimum-energy, 1000-day mission profile has several desirable features, as viewed in the heliocentric phase (fig. 1). The trajectories are contained between the Earth and Mars orbits. Thus, both close approach to the Sun, as in the Venus-flyby and opposition-class missions, and traverse of the asteroid belt beyond Mars are avoided. The spacecraft design problems associated with solar-radiation protection, temperature control, meteoroid protection, and solar-electric panels (if used as the power source) should therefore be simplified.

The Mars-orbital stay time, indicated by the dashed curve in figure 1, is approximately one-third of the total trip time. Since the exploration of Mars is the primary purpose of the mission, it is desirable that the stay time be as long as practical. A longer orbital stay time permits observation of Mars during seasonal changes, more time for detailed surface exploration, and visits to one or both of the Mars moons. The transfer times out and return are approximately the same, as required for the shorter duration missions. Shorter total times are obtained by reducing the available exploration time at the planet to approximately one-tenth of the total trip time.

Trans-Mars Injection

The Earth-to-Mars heliocentric phase of the mission defines the target conditions for trans-Mars injection (TMI) in terms of the asymptotic direction and required energy of the departure hyperbola (i.e., the $\vec{V}_\infty$ direction and magnitude). To achieve these conditions, the spacecraft and orbital-launch vehicles are assembled in a low, rendezvous-compatible Earth orbit (either elliptical or circular) and then injected into the departure hyperbola with a series of thrusting maneuvers, as illustrated in figure 2. Each thrusting period occurs near periapsis and is followed by a coast in an intermediate elliptical orbit. The actual size and number of the intermediate orbits control the magnitude of each velocity maneuver and the associated gravity losses. The use of this technique is documented in reference 12, in which the use of nuclear orbital-launch vehicles is assumed. A set of guidance equations which achieve near-optimal steering for the thrusting maneuvers has been developed (ref. 13). The guidance equations were designed to maintain periapsis altitude, and an engine "switching" logic was developed to minimize the gravity loss for each burn. The simulation of the gravity losses approaches the minimum as the number of intermediate orbits approaches infinity. The minimum gravity loss is zero for parabolic injection and increases as the $\vec{V}_\infty$ magnitude increases, the thrust-to-weight ratio decreases, or both. However, the time available for injection and assembly is finite, and the gravity losses will never actually be minimum.

Spacecraft assembly may be delayed because of unexpected launch delays, problems with spacecraft and orbital-launch-vehicle (OLV) rendezvous, systems checkout difficulties, and many other potential problems. The TMI sequence may be interrupted for similar operational reasons. Therefore, a launch and injection window is required for a reasonable probability of achieving the desired heliocentric trajectory. Since the detailed analysis of the launch and injection window depends largely upon spacecraft performance, OLV performance, operational constraints, and mission-energy requirements, the analysis is presented after discussion of these items.

Mars-Orbit Design

The parking orbit about Mars (fig. 3) is elliptical with a periapsis altitude of 200 nautical miles and an apoapsis altitude of approximately 10 000 nautical miles. The orbit is designed so that the perturbations of the oblate gravitational potential field assist in reducing the velocity required for Mars-orbital insertion (MOI) and trans-Earth injection (TEI). The use of planetary oblateness for parking-orbit alinement is discussed in references 14 and 15. The procedure used is to establish the periapsis altitude as low as possible, but well above Mars atmospheric perturbations (chosen at 200 nautical miles for this analysis). The apoapsis altitude and orbital inclination are then chosen so that the resulting nodal and apsidal motions will shift the original orbit into proper alinement for TEI.

Many combinations of apoapsis altitude and orbital inclinations result in proper parking-orbit alinement. However, the mission objectives provide constraints that narrow the choice. Because of the preliminary nature of the analysis, the following constraints are not all-inclusive, but do establish the major design goals.

The manned-landing maneuvers require posigrade orbital inclination. Since the rotational period of Mars approximates that of Earth (although the Mars diameter is much less than the Earth diameter), a large landing velocity penalty occurs as the orbital inclination is increased from 0° (posigrade equatorial) to 180° (retrograde equatorial). The Mars moons are in a near-equatorial posigrade orbit; therefore, the velocity requirements for rendezvous with the Mars moons are also adversely affected by high orbit inclinations.

To reduce the MOI and TEI velocity requirements, the apoapsis altitude should be high. A high apoapsis reduces velocity requirements for a Mars moon rendezvous, but increases the landing velocity requirements. The periapsis position should remain in sunlight both prior to landing (for site selection) and after landing (for mapping of the surface, observation of seasonal changes, and so forth). Limited control of the initial periapsis latitude is available by variation of the inclination of the approach hyperbola and by acceptance of the penalty resulting from an increased plane change at MOI.

The inclination to the Mars equator of the nominal Mars parking orbit is between 0° and 30°. The periapsis altitude is 200 nautical miles, and the apoapsis altitude varies between 9000 and 10 000 nautical miles, depending on the selected inclination, the declination of periapsis, and the orbital stay time.

A manned Mars landing is accomplished after sufficient landing-site data are obtained from orbit. The Mars lander is manned and checked out by the crew, separates from the main spacecraft, and descends to the surface with a retrograde propulsion maneuver. A near-Hohmann descent is used, with the landing site located near the periapsis position of the main spacecraft to reduce the lander propulsion requirements. The surface stay time of approximately 30 days permits scientific exploration of the accessible regions. Following surface exploration, the crew returns to the main spacecraft in the ascent stage of the lander.

A rendezvous with Deimos, the outer moon, and the return to the main spacecraft can be accomplished with a 6000-fps velocity change, including 200 fps for midcourse corrections and final breaking. Exploration of Phobos, the inner moon, requires a 6500-fps velocity change. These numbers are based on a 200- by 10 000-nautical-mile parking orbit, with the rendezvous maneuvers timed to coincide with the passage of the parking-orbit line of apsides through the plane of the moon orbit. The final maneuver in a Mars moon rendezvous is more accurately described as docking rather than landing because of the low masses of both bodies. The gravitational acceleration at the surface of Phobos is expected to be 0.037 fps/sec, based on Phobos having a density similar to the density of Earth. Deimos, which is a smaller moon than Phobos, has only a 0.025-fps/sec gravitational acceleration. The round-trip moon rendezvous requires approximately 2 days for Phobos and 5 days for Deimos.

Because of the large size of the Mars-orbital spacecraft, Mars moon rendezvous is assumed to be accomplished with a small module staged from the main spacecraft. This module would be similar to the Apollo lunar-module ascent stage. A module of this size can carry two men on a round trip to one of the moons or on a round trip to each moon if a refueling capability exists.

Mars-Orbital Insertion

The manned Mars lander module is to have atmospheric-entry capability and a landing propulsion system. It might therefore be feasible to stage the lander module prior to MOI for aerodynamic capture and then rendezvous with the lander module after the spacecraft has completed MOI. A flight plan (fig. 4) has been developed to study this technique and determine its relative advantages.

Aerodynamic probes are released from the spacecraft shortly after entering the Mars sphere of influence. The probes are targeted to enter the atmosphere and transmit density-profile data back to the spacecraft prior to the lander module entering the Mars atmosphere.

The lander module is staged (unmanned) from the main spacecraft and targeted for entry to occur immediately prior to MOI. The probe data are analyzed on board the spacecraft, and guidance corrections are sent to the lander module for flight-path-angle changes. The lander-module aerobraking phase is guided to result in an apoapsis altitude of approximately 10 000 nautical miles, coplanar with the spacecraft orbit. A velocity impulse at apoapsis is required in order to raise the periapsis out of the Mars atmosphere.

The main spacecraft achieves Mars orbit with a burn near the periapsis of the desired orbit and begins tracking the lander module. The spacecraft issues guidance commands to the lander module and effects rendezvous. The rendezvous propulsion is provided by the lander module, since it is much lighter than the spacecraft and is thus more efficient in applying velocity changes.

Trans-Earth Injection

The TEI maneuver uses a multiple-impulse technique, although the spacecraft is already in an elliptical orbit with the periapsis position almost alined for a single-impulse burn. Performance trade-offs between MOI, TEI, and parking-orbit elements do not always yield an orbit which is perfectly alined at the time of TEI; therefore, the multiple-impulse technique provides a launch window of more practical size.

The TEI maneuver is initiated with a burn near apoapsis to adjust the orbital geometry in two respects. The orbital plane is changed to include the desired departure asymptote, and the periapsis altitude is raised to reduce flight-path-angle penalties during the final departure maneuvers. The spacecraft then coasts to a position near periapsis, where the final injection burn is made. By using this technique, a 30- to 50-day launch window can be achieved with only a small penalty. A similar launch window occurs immediately following MOI. However, because of the Earth-Mars geometry at the time of MOI, multiple heliocentric circuits are required for Earth intercept, and the total trip time is not appreciably changed.

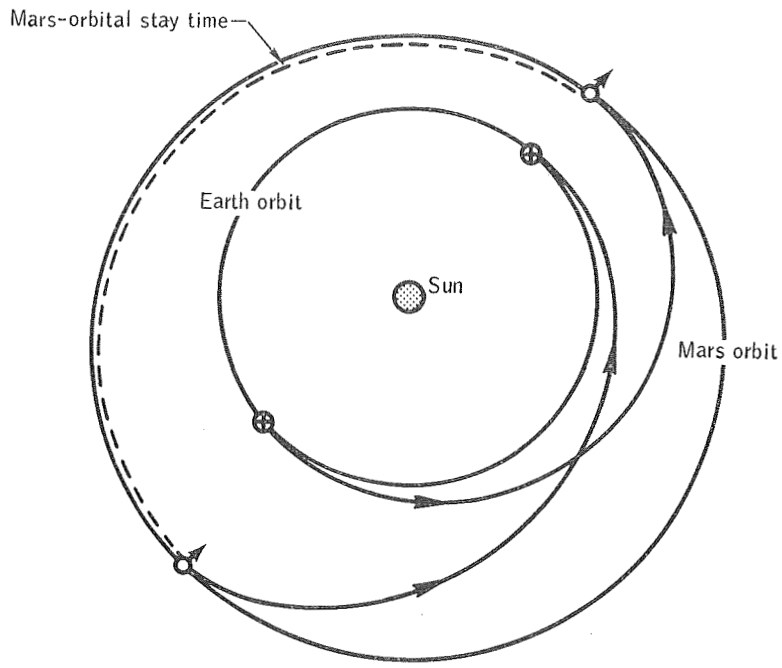

Figure 1. - Heliocentric phase of the nominal minimum-energy, Mars-landing mission profile.

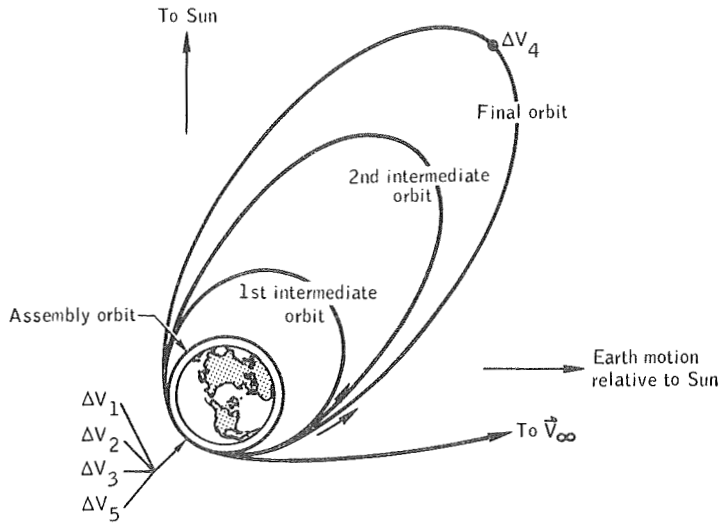

ΔV_1 Transfer from assembly orbit to 1st intermediate orbit

ΔV_2 Transfer from 1st intermediate orbit to 2nd intermediate orbit

ΔV_3 Transfer from 2nd intermediate orbit to final orbit

ΔV_4 Plane-change maneuver if required

ΔV_5 Transfer from final orbit to $\vec{V}_\infty$

Figure 2. - Earth-orbital operations for TMI.

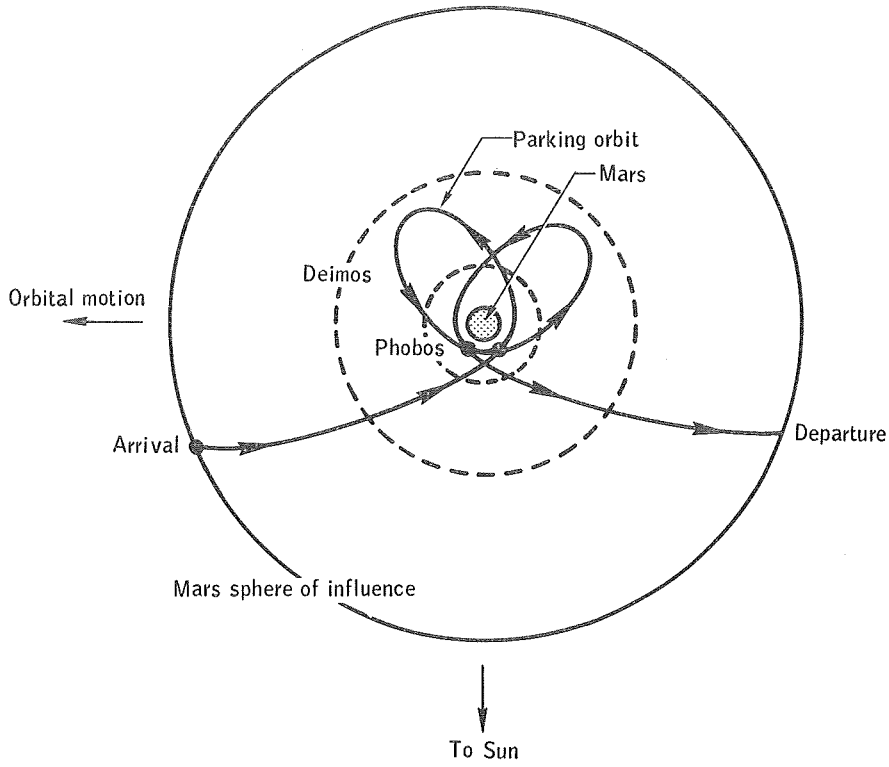

Figure 3. - Nominal mission profile for Mars-orbital operations.

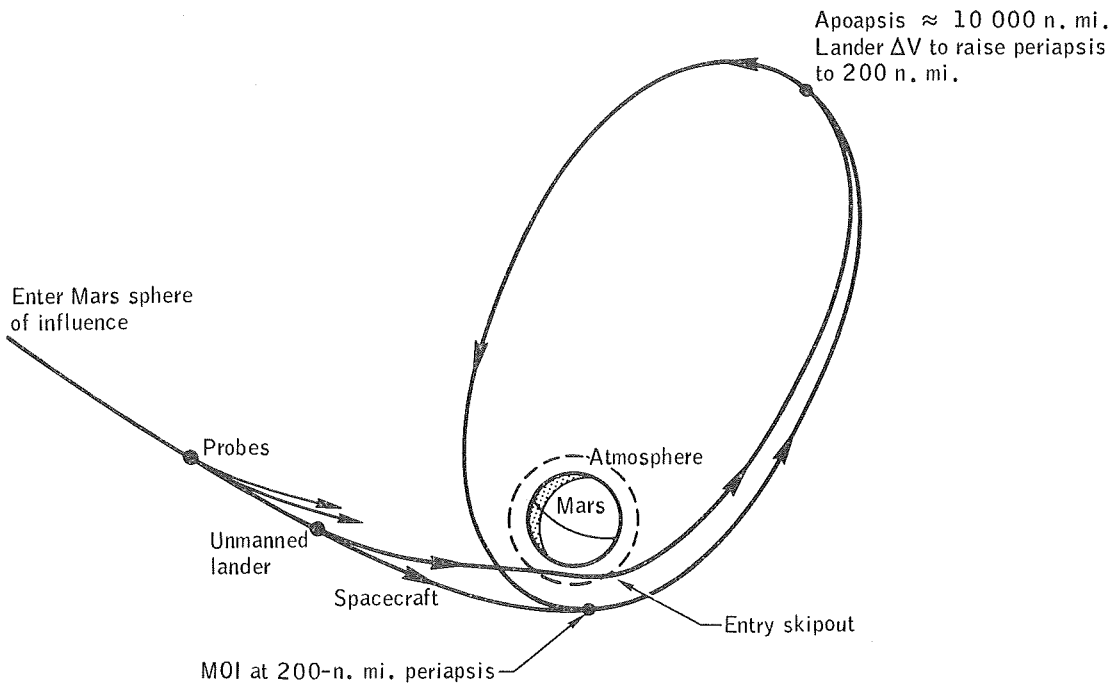

Figure 4. - Schematic of MOI.

FLIGHT-PLAN EVALUATION

Mission Opportunities

An analysis was made of the characteristics of conjunction-class missions by using data similar to the two-body approximations presented in reference 16, but with results tailored to the current analysis. This analysis includes all conjunction-class opportunities from 1977 to 1985 and the maximum-energy conjunction-class mission occurring in 1983.

A typical plot of velocity requirements for departure from Earth and arrival at Mars during the 1983 launch window is shown in figure 5. Plots were made of the velocity requirements for trip times of 160 to 400 days from which the mission trajectories were selected. The velocity data shown in figure 5 are for transfers from a 262-nautical-mile circular Earth orbit to a 200-nautical-mile circular Mars orbit. The velocity increments for other parking orbits are obtained by adding or subtracting a constant increment from the data. In figure 6, the velocity requirements for Mars departure and Earth arrival are shown for the 1983 mission, with a typical trip time of 300 days.

Minimum velocities for the Earth-to-Mars trajectories were observed on October 8, 1977; October 29, 1979; November 16, 1981; and December 21, 1983, for the departure leg at trip times of 340, 320, 300, and 280 days, respectively. Minimum velocities for return from Mars orbit were observed on July 5, 1979; July 14, 1981; August 3, 1983; and December 15, 1985. Thus, a typical minimum-energy mission leaves Earth orbit on October 8, 1977, with an outbound trip time of 340 days and arrives in Mars orbit on September 7, 1978. The next minimum-energy return after arrival is on July 5, 1979. Therefore, the Mars-orbital stay time is 295 days if the velocity increments for the mission are to be minimized.

In addition to the incremental velocity requirements of the transfer trajectories, a non-mission-dependent velocity budget (table I) was added to account for gravity losses, midcourse-correction requirements, and spacecraft attitude control. A total of 1650 fps is added to the spacecraft propulsion requirements, and 600 fps is added to the Earth-departure propulsion requirements, as determined by impulsive-velocity calculations. The TMI gravity and steering losses are low because multiple-revolution injection procedures are used. The gravity and steering losses for MOI and TEI are low for two reasons: (1) the Mars parking orbit is elliptical, which reduces the magnitude of the required velocity change (to which the gravity loss is related), and (2) the Mars parking orbit is oriented to take advantage of the oblateness of Mars so that the nominal burns occur near periapsis where the loss is usually a minimum.

The guidance velocity requirements and delivery accuracies for the various phases of the mission are discussed in detail in references 17 to 19. The midcourse-correction requirements shown in table I include an allowance for spinning the spacecraft to provide artificial gravity. This allowance is 250 fps for each heliocentric phase. If the artificial gravity is found to be unnecessary for missions of 1- to 3-year durations, then the non-mission-dependent velocity budget could be reduced by approximately 500 fps.

The nominal TMI launch windows from 1977 to 1985 are shown in figure 7. Although the velocity requirements are plotted as a function of Earth-departure date, the launch windows are actually discrete events occurring at approximately 2-year intervals — the dashed lines are drawn to show trends. The mission opportunities are indicated by the vertical bars and the year of Earth departure (e.g., 1977, 1979, etc.). In figure 7, the minimum-energy requirements are indicated by the bottom of the bar, and the requirements for a 50-day Earth-departure window are shown at the top of the bar. All velocities include the non-mission-dependent velocity budget. The MOI and TEI velocity requirements are shown as a total which represents the velocity capability required of the spacecraft. The maximum velocity requirement of 11 000 fps occurs in the 1983 TMI launch window. However, the increase in spacecraft velocity requirements for a 50-day launch window is almost constant at 300 fps. The TMI requirements are more sensitive to departure time. The 50-day TMI launch window requires from 600 to 1100 fps, depending on the TMI launch window. The maximum TMI requirements occur in the 1983 mission launch window.

The Earth-entry velocity is indicated by a point rather than by a vertical bar in figure 7 because the Mars-orbital stay time is adjusted to minimize the ΔV required for TEI, and the trans-Earth departure and arrival dates are then fixed for the entire TMI launch window. Thus, the Earth-entry velocity is constant for a given launch window, and the orbital stay time is variable. The Earth-entry velocity does not exceed 40 000 fps, and its maximum occurs in the 1983 TMI launch window. Entry is assumed to occur at an altitude of 400 000 feet.

The total trip time varies approximately 50 days for a 50-day launch window. The maximum trip time (1028 days) occurs in the 1981 mission opportunity. The 1977, 1979, 1981, and 1983 mission parameters are presented in table II for the beginning, middle, and end of the 50-day TMI launch window. The Earth-departure $\vec{V}_\infty$ vectors for the four opportunities are tabulated in the appendix. A 5-day reduction in the 1983 TMI launch window reduces the injection velocity requirements from 14 350 to 13 420 fps. Therefore, a small reduction in the 1983 TMI launch window seems advisable.

The 1983 mission opportunity apparently establishes the maximum propulsion requirements, as determined by numerical comparisons. However, geometric reasoning to support this conclusion is also possible, as illustrated in figure 8. Figure 8 is a plot of the Earth-Mars phase angle, the Mars ecliptic latitude, and the Mars-Sun heliocentric distance. The Earth-Mars phase angle is the heliocentric angle between Earth and Mars, plotted as a function of time. The Mars ecliptic latitude and the Mars-Sun distances are sinusoidal and almost in phase. Thus, the maximum and minimum Mars-Sun distances correspond to maximum and minimum latitudes. The date of TMI is indicated by a solid dot near the time scale, and Mars arrival is shown by an asterisk on each parameter curve. Trans-Earth injection occurs approximately 1 year after Mars arrival.

The 1983 mission opportunity, the maximum-energy conjunction-class mission, results in Mars arrival with Mars near perihelion at a maximum southerly latitude with respect to the ecliptic plane. Mars departure a year later occurs when Mars is

near aphelion and maximum northerly latitude. The 1977 minimum-energy conjunction-class mission results in Mars arrival and departure latitudes near zero and in a Mars-Sun distance of approximately the mean value. The cyclic nature of these ephemeris conditions at arrival and departure is apparent in figure 8.

The following are the minimum-energy Mars-landing mission requirements, assuming a 50-day orbital-departure window, for the 1977 to 1985 time period.

TMI, fps	13 600
MOI, fps	6 500
TEI, fps	4 500
Maximum Earth-entry velocity, fps	40 000
Total trip time, days	1 028

The minimum-energy mission profile has several desirable characteristics, in addition to the low spacecraft ΔV requirements. The Earth-entry velocity is always less than 40 000 fps, and entry can therefore be accomplished within current Apollo technology. The maximum spacecraft distance from the Sun is 1.7 AU when Mars is at aphelion; this distance avoids traverse of the asteroid belt and minimizes the size of solar panels, if used. Spacecraft thermal-design requirements are less constraining because the spacecraft does not approach the Sun closer than 1.0 AU.

Spacecraft Performance Requirements

The determination of the spacecraft performance requirements depends on the selected "mode," which defines the technique of accomplishing a given mission within the prescribed energy requirements. The analysis which led to the selection of the mode described in this report is given in reference 4. Other mode studies of the opposition- and conjunction-class missions (e.g., refs. 5 to 8) have been conducted and different conclusions have been reached. The differences are directly related to the assumed spacecraft module weights, with propulsion-system performance and mission-energy requirements differing only slightly.

The spacecraft module weights assumed for this study (table III) have been derived through in-house NASA studies and through contractor studies such as references 2 and 3. Uncertainty exists concerning the actual module weights because of the preliminary nature of existing design studies, and the uncertainty is indicated here by listing optimistic and pessimistic values, as well as the expected value. Spacecraft weights are based on a four-man crew, with the lander and the Mars-moon-rendezvous vehicle using two of the four crewmen.

The expected weight of the mission module (50 000 pounds) includes 6000 pounds for meteoroid protection and 9000 pounds for onboard experimental equipment. The experimental equipment is assumed to remain on board the spacecraft throughout the mission and could consist of a biological laboratory and various remote sensors, including a large astronomical telescope.

The amount of expendables (food, oxygen, water, etc.) is based on a four-man crew and expulsion at the rate of 9000 lb/yr. The expendables will probably be stored in the mission module, and the initial mission-module weight (i.e., at TMI) for a 3-year mission is expected to be 77 000 pounds. The optimistic and pessimistic values of mission-module weight, including expendables, are thus 67 000 and 87 000 pounds, respectively.

The Earth-entry module is an Apollo-type command module modified for a four-man crew and for the slightly increased entry velocity. The operational lifetime of the entry module need not exceed approximately 2 days, since the module will not be manned until shortly before entry.

The 20 000 pounds of scientific probes are assumed expended in Mars orbit prior to TEI. Atmospheric probes will actually be operated prior to MOI if the lander module is inserted into orbit by aerobraking. The assumption of carrying the scientific probes through the MOI maneuver and expending them in Mars orbit is therefore conservative. The following is a breakdown of jettisonable scientific weight: seven Mars atmospheric probes at 400 pounds each, three soft-lander modules at 2400 pounds each, a 10 000-pound Mars-moon-rendezvous vehicle, and 2500 pounds for expendable mapping and survey equipment. The spacecraft weight at TMI, excluding the MOI and TEI propulsion modules, has an expected value of 202 000 pounds with optimistic and pessimistic values of 174 500 and 229 500 pounds, respectively.

The assumed characteristics of the propulsion systems considered in this analysis are listed in table IV. The MOI module is cryogenic, with an expected specific impulse of 445 seconds. The TEI module has a required lifetime of 3 years, assuming that the module is used for midcourse corrections on the return trip, and the specific impulse of 400 seconds is based on space-storable propellant. Optimistic, expected, and pessimistic values are assigned to the propulsion-system performance parameters because of the uncertainty of preliminary design data.

The total spacecraft weight required immediately after TMI is shown in tables V and VI, in which the velocity budgeted for the MOI module is 6500 fps and the TEI module is designed for the mission requirement of 4500 fps.

The advantage of aerobraking the lander module to Mars orbit (discussed in ref. 4) is indicated by the difference in total spacecraft weight shown in tables V and VI. The advantage (i.e., reduced spacecraft weight) increases as the spacecraft module weight and propulsion-system performance tend toward pessimistic values. The current uncertainties of the Mars atmosphere require that atmospheric probes be launched from the main spacecraft to arrive prior to the lander module and to provide guidance information for targeting of the entry flight-path angle. The entry-corridor problem is complicated by the sensitivity associated with entry at near-parabolic speed and with targeting for a highly elliptical orbit. Therefore, the option to carry the lander module into Mars orbit as an integral part of the spacecraft should be retained until more lander-module design is accomplished. This option is retained by assuming sufficient performance in the MOI stage to retrofire the heavier spacecraft to Mars orbit and by providing additional payload capability from Earth orbit.

Orbital-Launch Vehicle

The Earth launch vehicle is assumed capable of placing 400 000 pounds of payload into a 260-nautical-mile circular orbit. This amounts to approximately 35 percent uprating of the Saturn V, but no attempt is made in this report to determine actual Saturn V uprating potential (ref. 8). The 400 000-pound payload capability was chosen to show that this payload is sufficient for accomplishing the Mars mission with four launches if a liquid-oxygen- and hydrogen-fuel OLV is used.

A schematic of the four launch configurations is shown in figure 9. The first launch configuration places the spacecraft, without the Mars lander module, into the assembly orbit with the crew in an Apollo command module (modified to carry the fourth crewman). This command module is used only to provide launch-abort capability and is not to be injected to Mars. The total payload available for the spacecraft is 360 000 pounds, which is determined by subtracting, from the launch-vehicle payload, 20 000 pounds for command-module crew transport, 20 000 pounds for interstages, attitude-control fuel used during Earth orbit, and so forth. The second launch configuration places the first OLV into the assembly orbit with the Mars lander module stacked on top. The first OLV propellant tanks are off-loaded to compensate for the weight of the Mars lander module. The third and fourth launch configurations place the fully tanked orbital launch vehicles into the assembly orbit.

A weight summary of the assumed OLV is presented in table VII. The propellant, which is liquid oxygen and hydrogen, has a specific impulse of 433 seconds. Each OLV stage delivers a thrust of 200 000 pounds and has an inert mass of 44 500 pounds, which consists of the dry-stage mass, the residuals, the instrumentation unit, and the forward attitude propulsion systems. The OLV-stage mass will be lower at the time of orbital departure than at the time of orbital insertion because of propellant venting (assuming 30-day maximum storage in orbit), interstage and nose-fairing jettison, and attitude-propulsion-system jettison. Thus, at the time of orbital departure, the total OLV weight is 367 200 pounds, assuming a full propellant load of 322 700 pounds.

The assembled spacecraft (including the Mars lander module) and the orbital launch vehicles have a required ideal velocity capability of 13 600 fps. The ideal velocity capability of this assembled configuration is shown in figure 10 as a function of the Mars lander-module weight. The 13 600-fps ideal velocity requirement can be met with a Mars lander module weighing 90 000 pounds (with an actual capability of 13 721 fps); thus, the total spacecraft weight injected toward Mars is 450 000 pounds. The distribution of ΔV among the OLV stages is shown in table VIII. This is a sufficient capability for all cases considered in the previous section if the lander module is placed in Mars orbit by aerobraking (table V). If the lander module is taken into Mars orbit as an integral part of the spacecraft (table VI), the 450 000-pound capability is sufficient for all (except the most pessimistic) combinations of spacecraft module weight and spacecraft propulsion-system performance.

The launch sequence indicated in this report places the Mars lander module behind the MOI module, and it is assumed that the lander module will be staged prior to MOI for aerobraking. If this sequence is not used, the lander module must be docked onto the forward end of the spacecraft some time prior to MOI.

TABLE I. - NON-MISSION-DEPENDENT VELOCITY BUDGET

Maneuver	Velocity, fps
TMI gravity and steering losses	600
Trans-Mars midcourse corrections and artificial gravity	500
MOI gravity and steering losses	100
Mars-orbital maneuvers and artificial gravity	500
TEI gravity and steering losses	50
Trans-Earth midcourse corrections and artificial gravity	500

TABLE II. - OPPORTUNITIES FOR A MINIMUM-ENERGY MARS-LANDING MISSION[a]

Calendar date, center of launch window	Date of TMI, days after Julian date 2 440 000	Trans-Mars trip time, days	Mars-orbital stay time, days	Trans-Earth trip time, days	Total trip time, days	TMI ΔV, fps	MOI ΔV, fps, (b)	TEI ΔV, fps	MOI ΔV + TEI ΔV, fps	Total ΔV, fps	Entry velocity, fps
October 8, 1977	3400	360	300	338	998	13 243	4459	4364	8 823	21 791	37 637
	3425	340	295	338	973	12 434	4295	4364	8 659	20 818	37 637
	3450	320	290	338	948	13 226	4535	4364	8 899	21 850	37 637
October 29, 1979	4150	340	310	365	1015	13 244	4738	4239	8 977	21 946	38 000
	4175	320	305	365	990	12 236	4503	4239	8 742	20 703	38 000
	4200	300	300	365	965	12 839	4669	4239	8 908	21 472	38 000
November 16, 1981	4900	320	330	378	1028	13 592	5346	4454	9 800	23 117	38 550
	4925	300	325	378	1003	12 400	5204	4454	9 658	21 783	38 550
	4950	280	320	378	978	12 685	5599	4454	10 053	22 463	38 550
December 21, 1983	5665	280	469	251	1000	14 350	6599	4376	10 975	25 050	39 760
	5670	280	465	251	996	13 420	6324	4376	10 700	23 845	39 760
	5690	280	445	251	976	12 715	6067	4376	10 443	22 838	39 760
	5710	280	425	251	956	12 395	6392	4376	10 768	22 888	39 760
	5715	280	419	251	950	12 375	6599	4376	10 975	23 075	39 760

[a]All ΔV include the non-mission-dependent velocity given in table I; a 262-n. mi. circular Earth-departure orbit is assumed.

[b]A 200- by 10 000-n. mi. Mars parking orbit is assumed.

TABLE III. - SPACECRAFT WEIGHT ASSUMPTIONS

Mission module, lb	50 000 ± 10 000
Entry module, lb	15 000 ± 2500
Mars lander, lb	90 000 ± 15 000
Expendables, lb/yr	9000
Scientific probes, lb	20 000

TABLE IV.- PROPULSION-SYSTEM PERFORMANCE ASSUMPTIONS

Space-storable systems:	
Specific impulse, sec	400 ± 15
Stage mass fraction	0.20 ± 0.05
Cryogenic systems:	
Specific impulse, sec	445 ± 15
Stage mass fraction	0.20 ± 0.05

TABLE V. - VARIATION IN TOTAL SPACECRAFT WEIGHT FOR AEROBRAKED LANDER

Propulsion-system performance	Spacecraft module weight, lb		
	Optimistic	Expected	Pessimistic
Optimistic	272 931	319 416	365 901
Expected	289 808	339 207	388 605
Pessimistic	310 262	363 213	416 164

TABLE VI. - VARIATION IN TOTAL SPACECRAFT WEIGHT FOR NON-AEROBRAKED LANDER

Propulsion-system performance	Spacecraft module weight, lb		
	Optimistic	Expected	Pessimistic
Optimistic	314 368	371 211	428 055
Expected	336 496	397 567	458 638
Pessimistic	363 112	429 275	495 438

TABLE VII. - ORBITAL-LAUNCH-VEHICLE WEIGHT SUMMARY

	Weight, lb
Dry stage	33 000
Instrumentation unit	6 000
Forward attitude propulsion system	3 000
Fuel residuals	2 500
Nose fairing[a]	2 600
Aft interstage[a]	6 300
Aft attitude propulsion system[a]	7 900
Propellant vented[a]	16 000
Usable propellant	322 700
Total launch weight	400 000

[a]This weight lost in Earth orbit prior to TMI.

TABLE VIII. - ORBITAL-LAUNCH-VEHICLE PERFORMANCE CAPABILITY

Stage	Useful propellant, lb	Burn time,	Initial thrust-to-weight ratio	Maximum ΔV, fps (a)
1	232 700	504	0.2750	5 372
2	322 700	699	.1827	4 871
3	322 700	699	.1368	3 478
Total	878 100	--	--	13 721

[a]A total spacecraft weight of 450 000 pounds and the orbital-launch-vehicle weights of table VII are assumed.

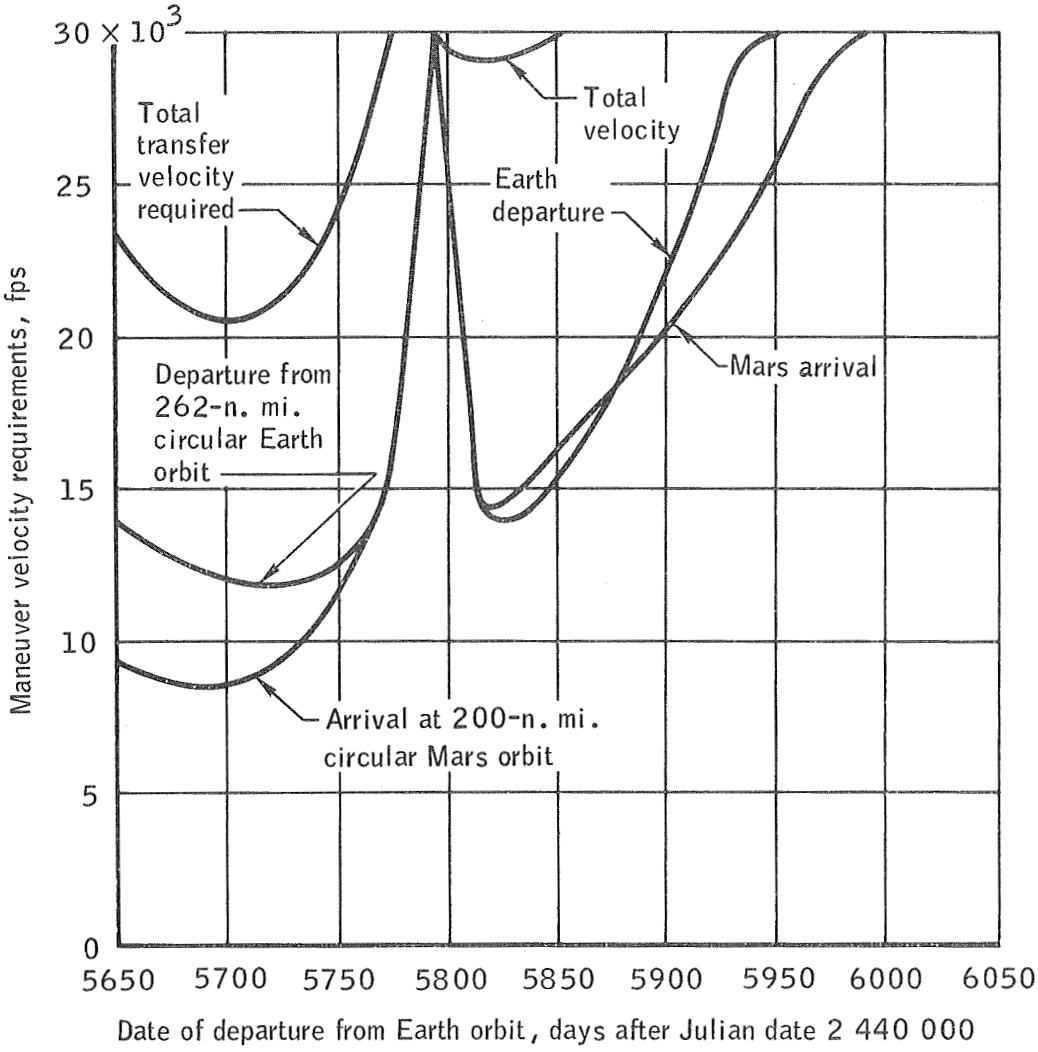

Figure 5. - Velocity requirements for transfer from Earth to Mars in 1983 with a total trip time of 280 days.

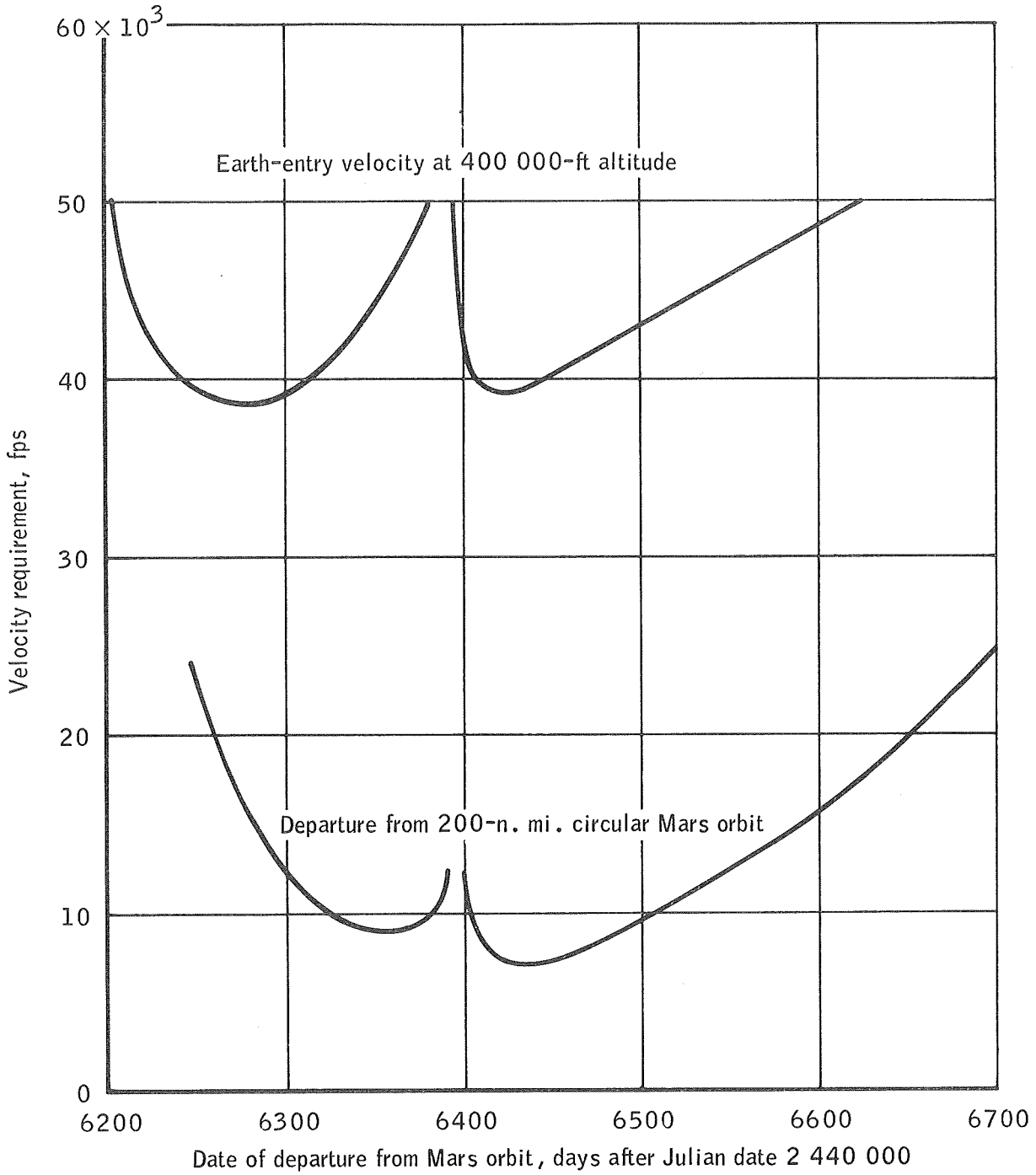

Figure 6. - Velocity requirements for transfer from Mars to Earth in 1983 with a total trip time of 300 days.

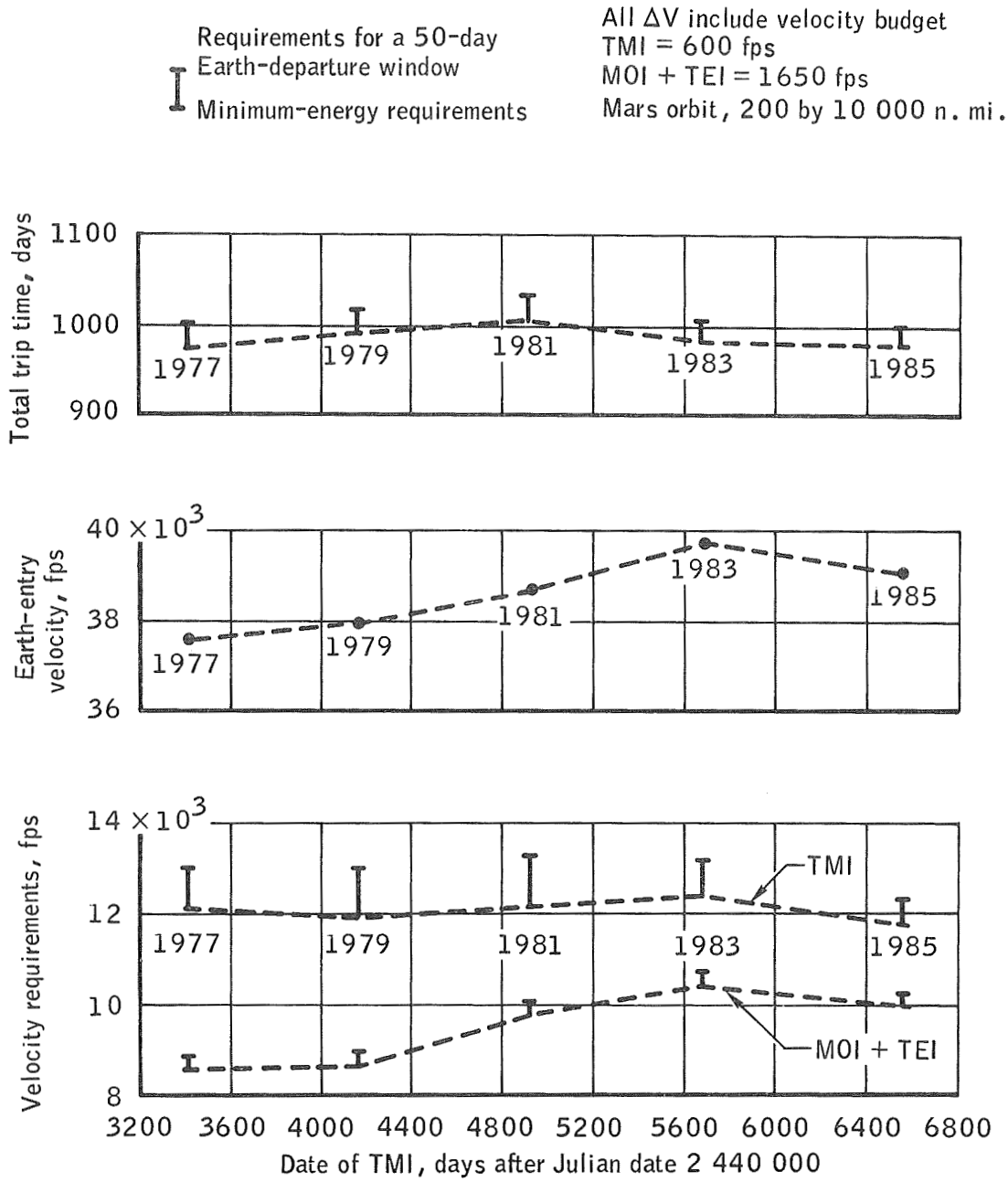

Figure 7. - Conjunction-class Mars-landing mission opportunities.

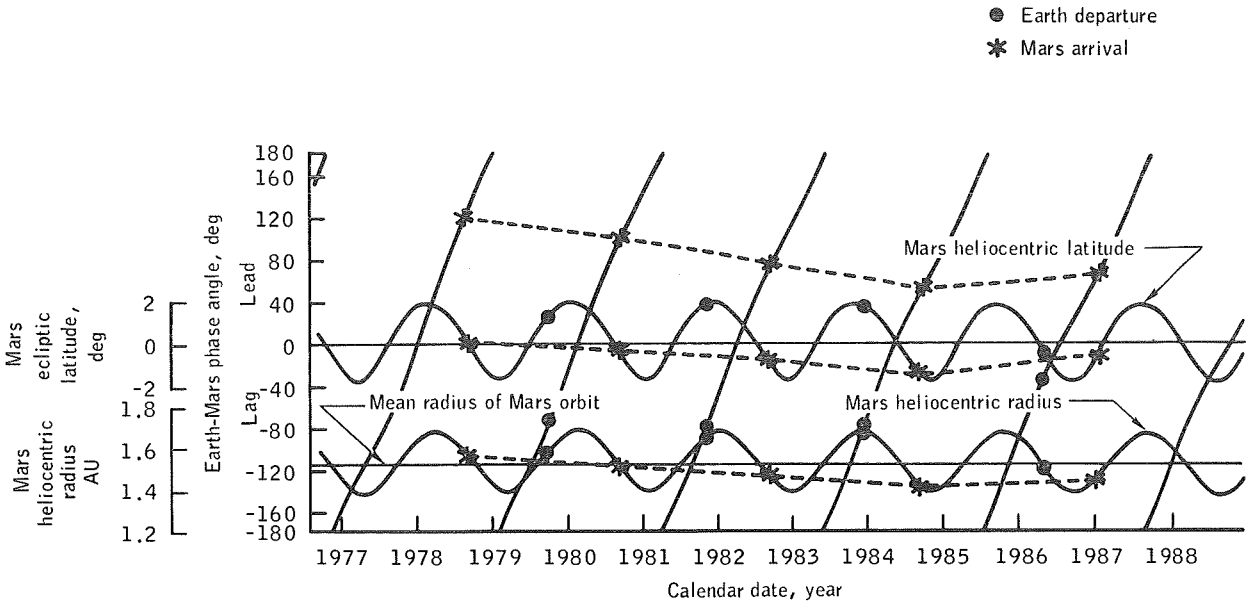

Figure 8. - Mars ephemeris parameters.

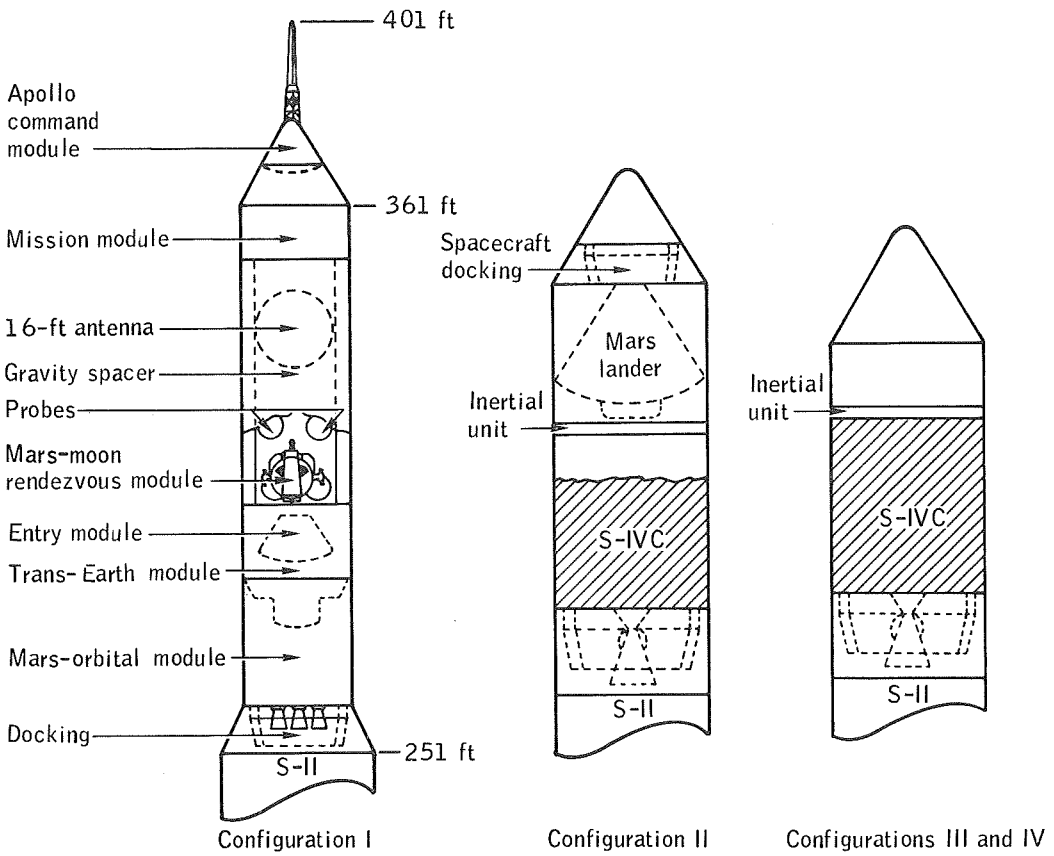

Figure 9. - Orbit-assembly launch configurations.

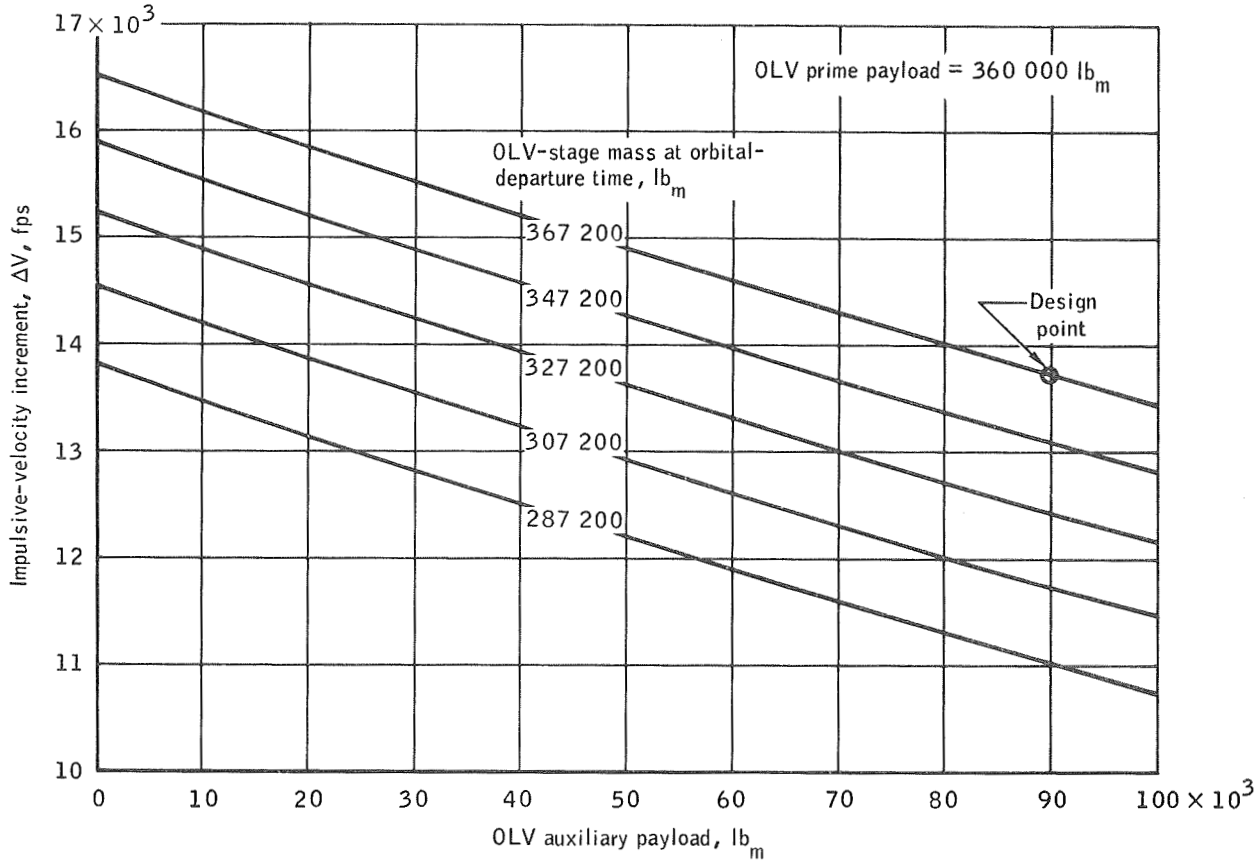

Figure 10. - Ideal ΔV as a function of OLV stage mass and auxiliary payload.

LAUNCH-WINDOW ANALYSIS

The major interactions and constraints affecting the schedule of events during the Earth-departure phase of the minimum-energy mission are illustrated schematically in figure 11. The minimum and maximum values specified in the figure are not necessarily firm requirements, but they were treated as such in this report to obtain specific numerical results.

To maintain a reasonable probability of mission success, the launch schedule should be as flexible as possible (i. e., the launch windows shown in fig. 11 should be as wide as possible) so that unpredicted operational delays can be accommodated. The orbital-departure window determines the phasing of the entire launch schedule. For this reason, and because it is rigidly constrained by astrodynamic considerations, the orbital-departure window is the most critical element in the launch schedule and is the logical starting point for analysis.

Orbital-Departure Window Definitions

The variation of the ΔV required for interplanetary departure from a circular assembly orbit is illustrated in figure 12. The lowermost curve represents the basic (or zero plane change) requirement, which reflects the variation in the magnitude of the required $\vec{V}_\infty$. Generally, $\vec{V}_\infty$ is a function of two variables, the Earth-departure date and the target-planet arrival date. In this report, it is assumed that, for a given departure date, only one arrival date will satisfy overall mission requirements and constraints. This assumption effectively frees the orbital-departure analysis from the heliocentric-mission-profile analysis. If this were not true, the basic energy curve would be replaced by a surface. It would then be possible to trade off energy and plane-change penalties by varying the arrival date to reduce the orbital-departure ΔV requirement (ref. 20). Any ΔV reductions realized from such a trade-off would be at least partially offset by payload penalties accruing from greater variability in the overall mission profile (ref. 21).

The upper dashed curve in figure 12 defines the nodal window, and the shape of the curve depends on the elements of the assembly orbit and on the orbital-departure technique. The nodal window curve is actually the envelope of minimums on a cyclic curve of ΔV requirements, of which only the lower portions of three cycles are shown. These requirements oscillate with a period approximately equal to the period of the assembly orbit. The anomalistic variations depend primarily on the angular location in the assembly orbit at which the departure maneuver is initiated. For this analysis, it is both valid and convenient to ignore the anomalistic variations and to consider the nodal window to be a continuous function. In this approach, it is assumed that departure will be initiated precisely at the correct time within a given orbital revolution. This approach is justified by the fact that the interval between anomalistic windows is small compared to the width of the nodal window that is of primary concern in this report.

The nodal window is mostly influenced by plane-change requirements that arise from nodal regression of the assembly orbit. Secondary contributions to the shape of the envelope of anomalistic minimums include variations of the hyperbolic asymptote direction and apsidal rotation in the case of elliptical assembly orbits.

The motions of the departure asymptote and an arbitrary assembly orbit relative to an inertial coordinate system are illustrated in figure 13 for a typical mission opportunity. Time is measured in days from the date of minimum V_∞ in the synodic window. The assembly orbit is oriented to contain the departure asymptote 12 days before the minimum-energy date. The assembly-orbit node rotates much more rapidly in inertial space than the departure asymptote, as usually occurs for most interplanetary mission opportunities.

Assembly-orbit and departure-asymptote coordinates are referenced to a rotating coordinate system defined by the equator and the ascending node of the assembly orbit (fig. 14). In this reference frame, the assembly orbit is stationary, and the departure asymptote appears to move quite rapidly, intersecting the assembly-orbit plane at $t = -12$ days and approximately 16 days later at $t = +4$ days. Plots in this coordinate system are helpful for evaluating the relationship of assembly-orbit inclination and asymptote declination. The orbit inclination must be equal to or greater than the absolute value of the asymptote declination if coplanar departure is to be possible.

The implication in figure 14 regarding optimal orientation of the assembly-orbit ascending node is of particular importance. To achieve maximum width of the nodal window, the ascending node should be oriented so that, on the date of minimum V_∞, this node will be approximately 90° from the right ascension of the departure asymptote. Such an orientation will allow a favorable trade-off between the ΔV contributions arising from plane-change requirements and the basic energy requirements. A rapid variation of asymptote declination or a highly nonsymmetric basic energy window implies a bias of the nodal orientation.

Multiple-Impulse Orbital-Departure Technique

To reduce the ΔV penalties arising from plane-change requirements and gravity losses, a multiple-impulse orbital-departure technique was chosen for analysis. The geometric aspects of the departure sequence are shown in figure 15. Although five impulses are used, the departure sequence is equivalent (in terms of impulsive ΔV) to a three-impulse maneuver. The technique was to optimize the sequence as if it were a three-impulse maneuver and then divide the first impulse into three colinear subimpulses to accommodate the ΔV capabilities of the individual OLV stages.

The advantage of the three-impulse maneuver over one-impulse and two-impulse maneuvers is illustrated in figure 16. A simplified computation technique which yielded only quasi-optimum results was used to reduce computation time. In the quasi-optimum three-impulse technique, the first and third impulses change only the instantaneous velocity magnitude (leaving azimuth and flight-path angle unchanged), and the second

impulse changes only the instantaneous azimuth (leaving velocity magnitude and flight-path angle unchanged). The third impulse is constrained to lie at the perigee of the final ellipse. The location (in the intermediate ellipse) of the second impulse is optimized to yield the minimum plane-change ΔV for a given relative declination and magnitude of $\vec{V}_\infty$. The location (in the assembly orbit) of the first impulse is adjusted by iteration to yield the required relative longitude of $\vec{V}_\infty$. Given the location of the first impulse, the magnitudes of the first and third impulses are determined, respectively, by the specified period of the intermediate ellipse and the magnitude of $\vec{V}_\infty$.

The accuracy of the quasi-optimum technique is discussed in reference 9, in which the technique is compared with a rigorous three-impulse optimization (ref. 22) and with one- and two-impulse optimizations (ref. 23). The total ΔV resulting from the three-impulse quasi-optimization is essentially equal to the true minimum ΔV for $\vec{V}_\infty$ magnitudes and relative declinations (measured from the assembly-orbit plane) of the order encountered in Mars conjunction-class missions.

The ΔV requirement for plane change depends on the size of the final ellipse in the departure sequence, and the ΔV decreases as the ellipse gets larger (fig. 17). A final orbital period of 48 hours was chosen for the purposes of this analysis. The plane-change ΔV requirements were computed with the assumption that the instantaneous perigee altitude would be held constant throughout the actual finite-thrust plane-change maneuver to avoid atmospheric entry in the event of a premature engine shutdown. The impulsive approximation of the characteristic velocity increment required for such a maneuver is the arc-type ΔV shown in figure 18.

Gravity Losses

In addition to reducing the impulsive ΔV requirements for out-of-plane departures, the multiple-impulse technique also reduces the gravity losses that result when the finite thrust level of the OLV is considered. The magnitude of the gravity-loss reduction depends on the performance characteristics of the OLV propulsion system and can be very significant. In this analysis, approximate gravity losses were computed and added to the impulsive ΔV for each burn in the departure sequence. For this purpose, equation (25) of reference 24 was used by multiplying with a calibration factor obtained from numerically integrating finite-burn simulations.

Assembly-Orbit Parameters

Several sets of parameters can be chosen to describe the assembly orbit. The parameters chosen for this analysis were h_P, h_A, i, Ω_0, ω_0, and u_0. The right ascension of the ascending node and the argument of perigee must be treated as functions of time in the orbital-departure-window analysis because of the significant perturbing effects of Earth oblateness. The secular effects, as defined by the equations in reference 25, of the second and fourth gravitational harmonics are included in the orbital simulations. However, the long- and short-period oblateness perturbations are ignored, as are atmospheric, lunar, and solar effects.

Since the period of any reasonable assembly orbit is short, compared to the desired width of the nodal window, the specific value given u_0 is relatively unimportant. However, to permit assembly of the spacecraft, it is necessary that all the separately launched modules eventually be injected into a common orbit in which u_0, as well as the other orbital parameters, has a specific and precise value. The rendezvous operations are simplified if the assembly-orbit parameters h_P, h_A, and i are chosen so that the values of the remaining parameters (Ω_0, ω_0, and u_0), which result from nominal insertion at the end of a standard ascent trajectory, simultaneously recur at regular launch intervals. For elliptical assembly orbits, the intervals between simultaneous recurrences are so long that they are of no practical significance. However, if a circular assembly orbit is used, ω_0 becomes meaningless, and it is necessary only that Ω_0 and u_0 recur simultaneously. Since the elliptical assembly orbit could provide significant performance gains, both types of assembly orbits are considered in the analysis.

Circular Assembly Orbits

Many circular assembly-orbit families exhibit the desired recurrence characteristic previously described. Three of these families are illustrated in figure 19. Each family is characterized by a unique integer N that corresponds to the number of orbital revolutions between each direct-rendezvous opportunity in a given launch-azimuth quadrant. Within each of these families, there are several discrete orbits for which two direct-rendezvous opportunities, one in the northeast quadrant and one in the southeast quadrant, occur during a primary recurrence interval of N orbital periods. Each discrete rendezvous-compatible orbit is characterized by a second integer M that corresponds to the number of orbital revolutions between the direct-rendezvous opportunity in the northeast quadrant and the succeeding direct-rendezvous opportunity in the southeast quadrant. Within each N-family, the index M begins at one for an inclination slightly greater than the latitude of the launch site and increases with higher inclinations.

Three rendezvous-compatible circular assembly orbits with indices of $N = 15$ and $M = 1$, $M = 2$, and $M = 3$ were chosen for this analysis. These orbits are designated in figure 19 by circles. Pertinent characteristics of these orbits are shown in table IX. The launch azimuths shown are measured in a rotating Earth reference frame and are based on analytical approximations to account for the effect of Earth rotation.

To achieve maximum flexibility in the overall launch schedule, the orbital parameter Ω_0 must be optimized to attain the maximum possible width of the nodal window. If the epoch t_0 for a given synodic period is chosen to be the date on which the required V_∞ is at a minimum, then the optimum value of Ω_0 is approximated by

$$\Omega_0 = \alpha_0 - \frac{\sin \delta_0}{|\sin \delta_0|} 90^\circ \tag{1}$$

where α_0 and δ_0 are the right ascension and declination, respectively, of the Earth-departure asymptote at t_0. This value can be used as a starting point for a more accurate numerical optimization, which is usually necessary because of variations in the asymptote direction and because of asymmetry in the curve of V_∞ versus time.

The optimization was accomplished by scanning Ω_0 at discrete intervals in the neighborhood of the value given by equation (1). Direct control of Ω_0 was exercised by fixing the lift-off time and the launch azimuth for the initial launch (i.e., the main spacecraft) to the assembly orbit and then varying the launch date. The results of a typical Ω_0 scan are shown in figure 20.

The width of the orbital-departure window is only moderately sensitive to Ω_0 in the region of the optimum value, as indicated in figure 20. Any appreciable reduction in the ΔV capability of the OLV causes a loss of several days near the center of the orbital-departure window unless Ω_0 is reselected to reduce the height of the reflected vertex of the ΔV requirement curve.

The optimization was performed within the total orbital-departure ΔV of 13 860 fps, including gravity losses, to provide a maximum width of the nodal window. This ΔV is 139 fps higher than the capability shown in table VIII for the OLV. The 1-percent discrepancy results from an upward revision of the estimate of required payload after most of the calculations had been performed and has the effect of reducing the orbital-departure window by 1 or 2 days. In view of the preliminary nature of payload information, it was not considered useful to recompute the orbital-departure-window parameters for the revised payload estimates.

The effect of assembly-orbit inclination on a typical mission opportunity is shown in figure 21. For all the mission opportunities investigated, the lower assembly-orbit inclinations consistently yielded narrower orbital-departure windows, but required less ΔV in the center of the orbital-departure window. The lowest inclination (29.16°) was selected for further analysis because the lower ΔV requirement allows a greater margin to compensate for uncertainties in the OLV performance capability. Lower inclinations generally provide for a greater payload capability into orbital and orbital-rendezvous operations.

Elliptical Assembly Orbits

Although an elliptical assembly orbit cannot provide rendezvous compatibility of the type previously described for circular assembly orbits, it does have advantages with respect to the conversion of propulsive energy to orbital energy during the Earth-departure maneuver. The basic phenomenon is illustrated in figure 22, which shows, for a representative V_∞, orbital-departure ΔV requirements as functions of the relative declination and the relative longitude of the departure asymptote. The relative longitude in this instance is measured from the perigee of the elliptical assembly

orbit. The semimajor axes of the circular and elliptical assembly orbits chosen are equal; hence, the initial orbital energies are equal. As relative longitude varies, the elliptical ΔV describes a sine curve with a mean value approximately equal to the circular ΔV requirement.

Because the line of apsides of the elliptical parking orbit rotates rapidly under the influence of Earth-oblateness effects, the optimum relative longitude occurs only briefly within an orbital-departure window. However, as indicated in figure 23, the orbital parameter ω_0 can be chosen to deepen the nodal window or to widen it at a given ΔV.

A comparison of nodal windows for circular and elliptical assembly orbits in a typical synodic period is given in figure 24. The values of ω_0 and Ω_0 are optimized to yield maximum nodal window width at a ΔV of 13 860 fps. The perigee altitude of the elliptical assembly orbit is arbitrarily set at 100 nautical miles, and the apogee altitude is adjusted to equate the inserted payload capability to the payload capability of the corresponding circular assembly orbit. In the four mission opportunities studied, the elliptical assembly orbits yielded deeper nodal windows and greater orbital-departure-window widths than the circular assembly orbits for the ΔV chosen.

The use of an elliptical assembly orbit provides efficient payload flexibility by raising or lowering the apogee altitude. However, in a comparison of the nodal windows, it should be emphasized that atmospheric perturbations were not included in the mathematical simulations. The circular-assembly-orbit altitude (260.33 n. mi.) is high enough that atmospheric decay should be negligible over the period of interest. Although it is not expected to be sufficient to alter any conclusions regarding orbital-departure feasibility, atmospheric drag at the 100-nautical-mile perigee altitude of the elliptical assembly orbit is expected to have a perceptible effect on the nodal window.

TABLE IX. - CIRCULAR ASSEMBLY-ORBIT PARAMETERS[a]

Inclination, deg	Altitude, n. mi.	Launch azimuth, deg		Launch interval, hr	
		Northeast	Southeast	δt (b)	Δt (c)
29.16	260.33	83.12	97.51	1.66	23.49
31.08	260.83	75.36	105.28	3.33	23.50
34.70	261.87	66.33	114.30	4.99	23.52

[a]Phased for twice-a-day standard rendezvous.

[b]Between the northeast and southeast launch azimuths.

[c]Between launches on a given azimuth.

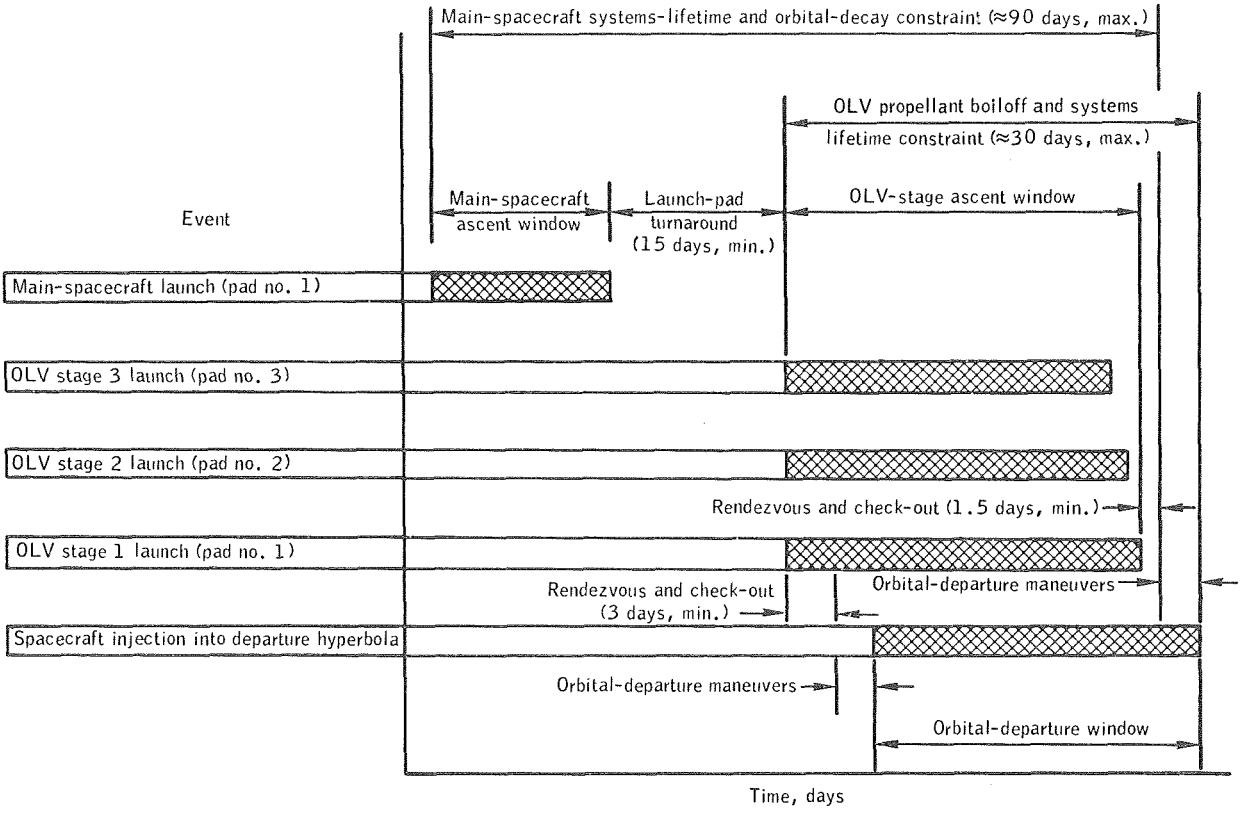

Figure 11. - Launch schedule constraints and interactions.

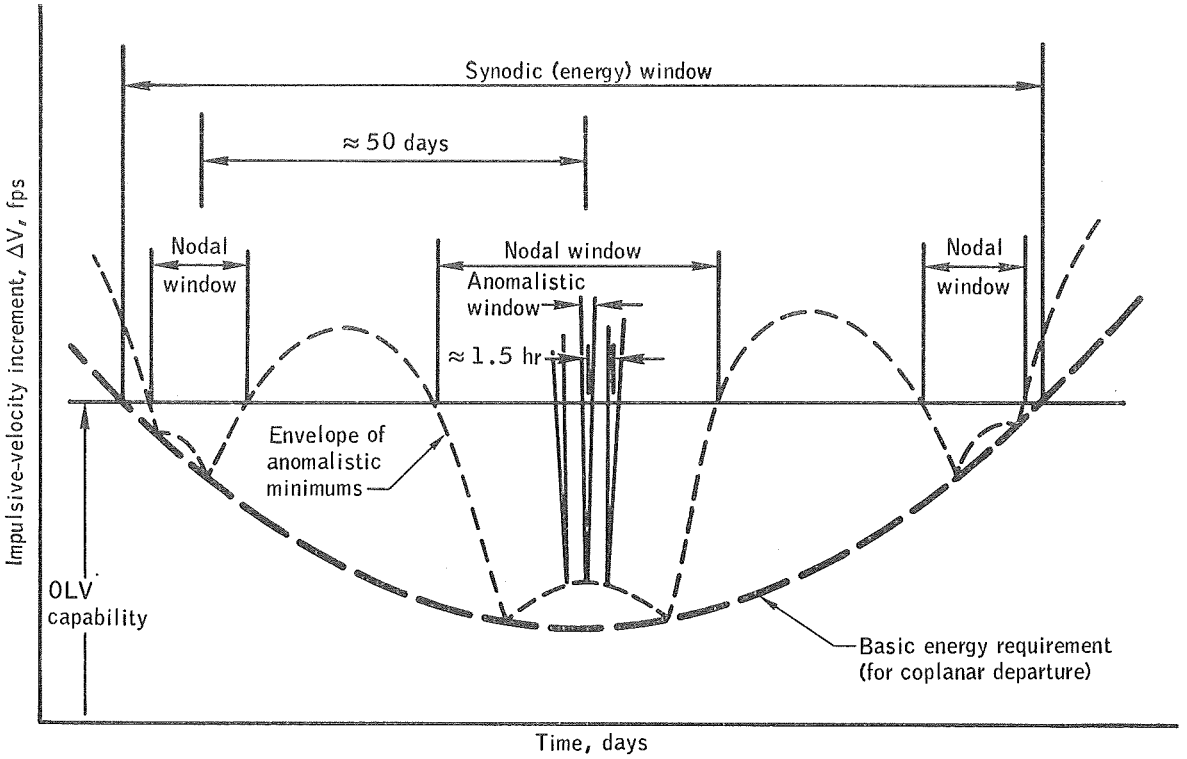

Figure 12. - Definition of orbital-departure windows.

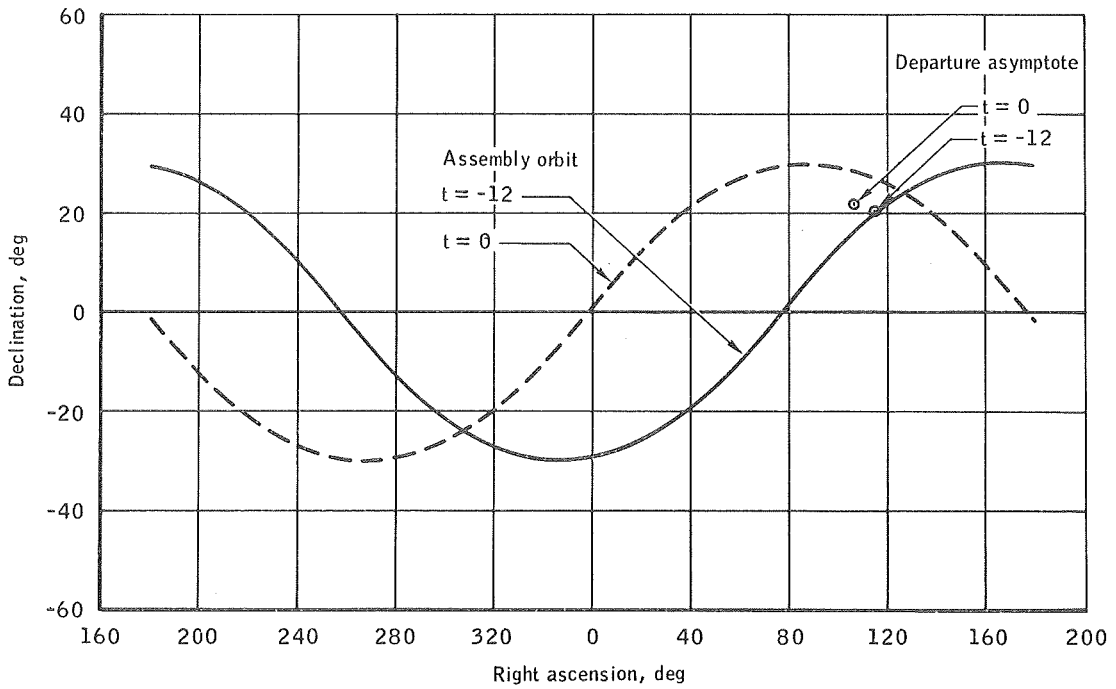

Figure 13. - Assembly-orbit and departure-asymptote coordinates relative to equinox and equator.

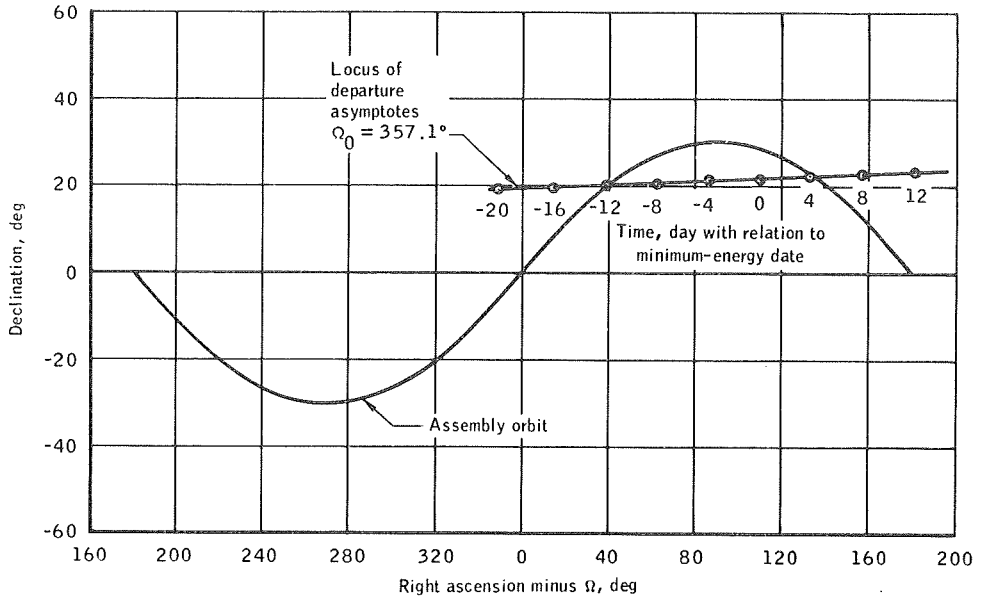

Figure 14. - Assembly-orbit and departure-asymptote coordinates relative to assembly-orbit node and equator.

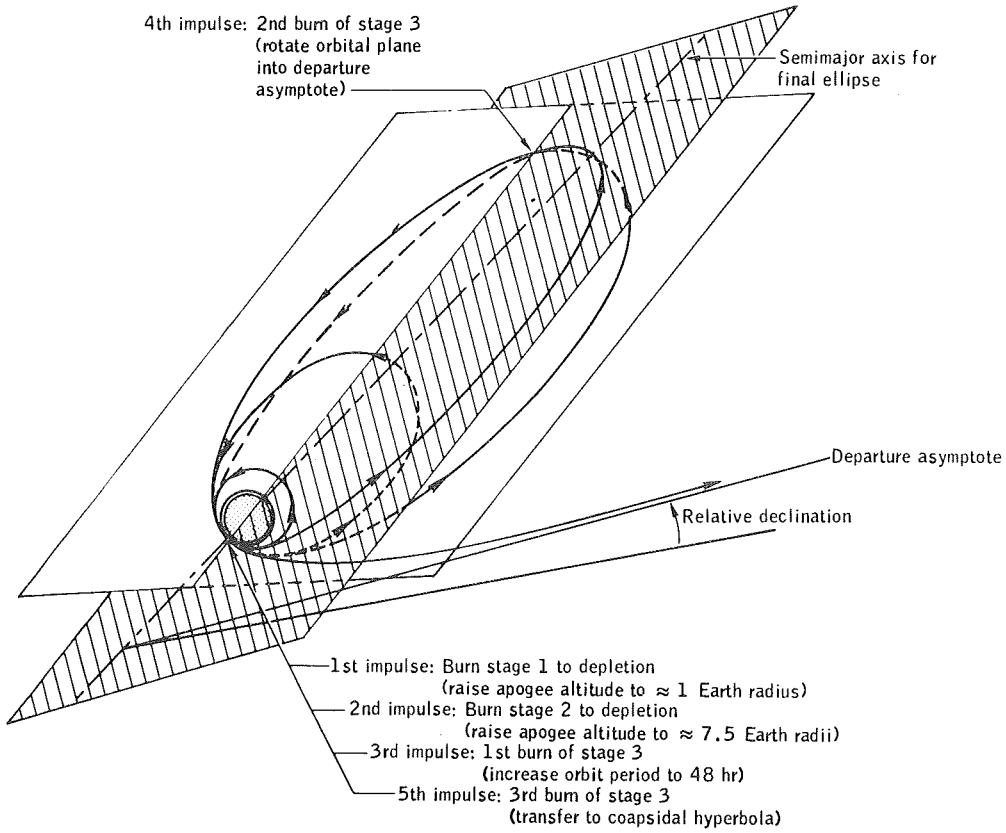

Figure 15. - Geometry of the five-impulse departure technique.

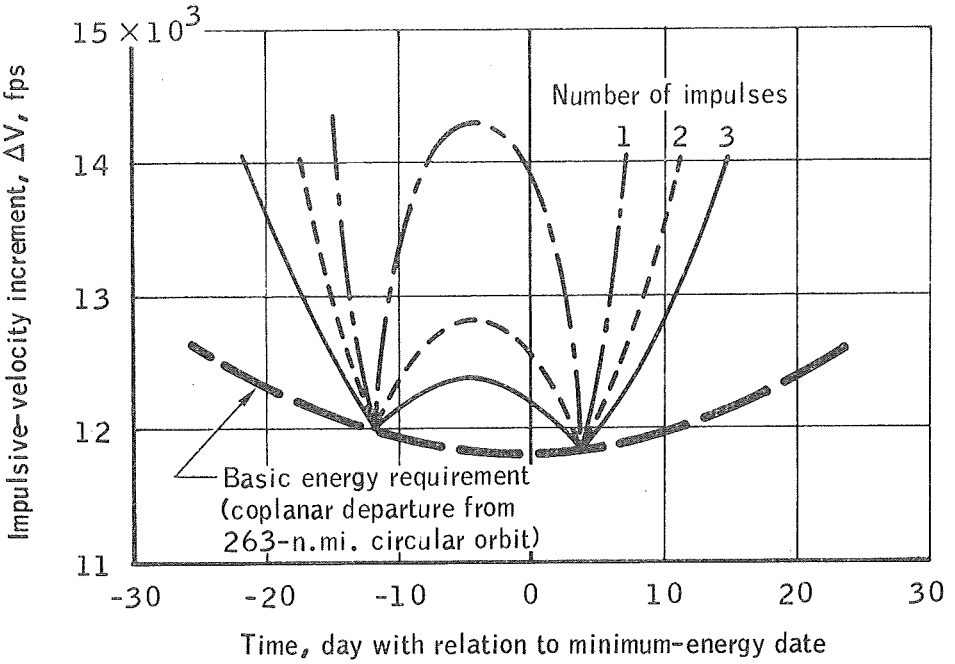

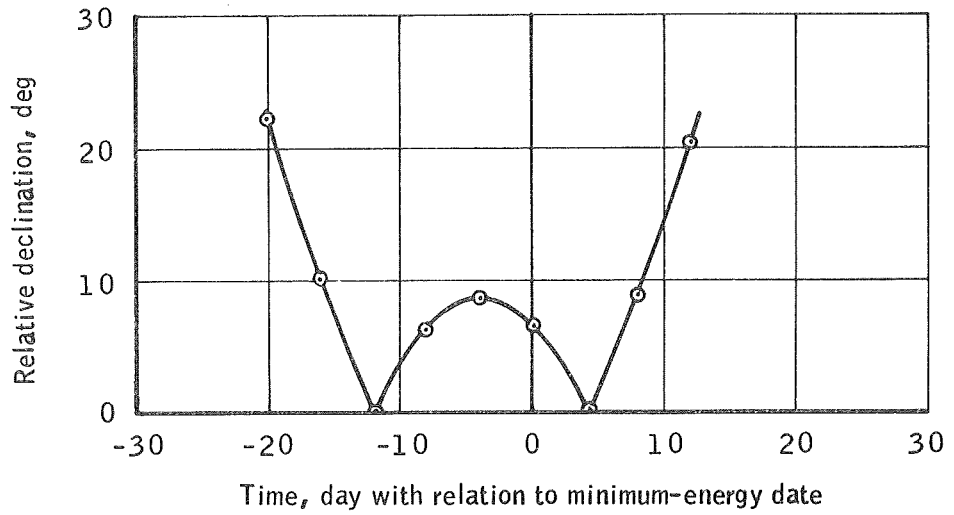

Figure 16. - Comparison of nodal windows for one-impulse, two-impulse, and three-impulse departures.

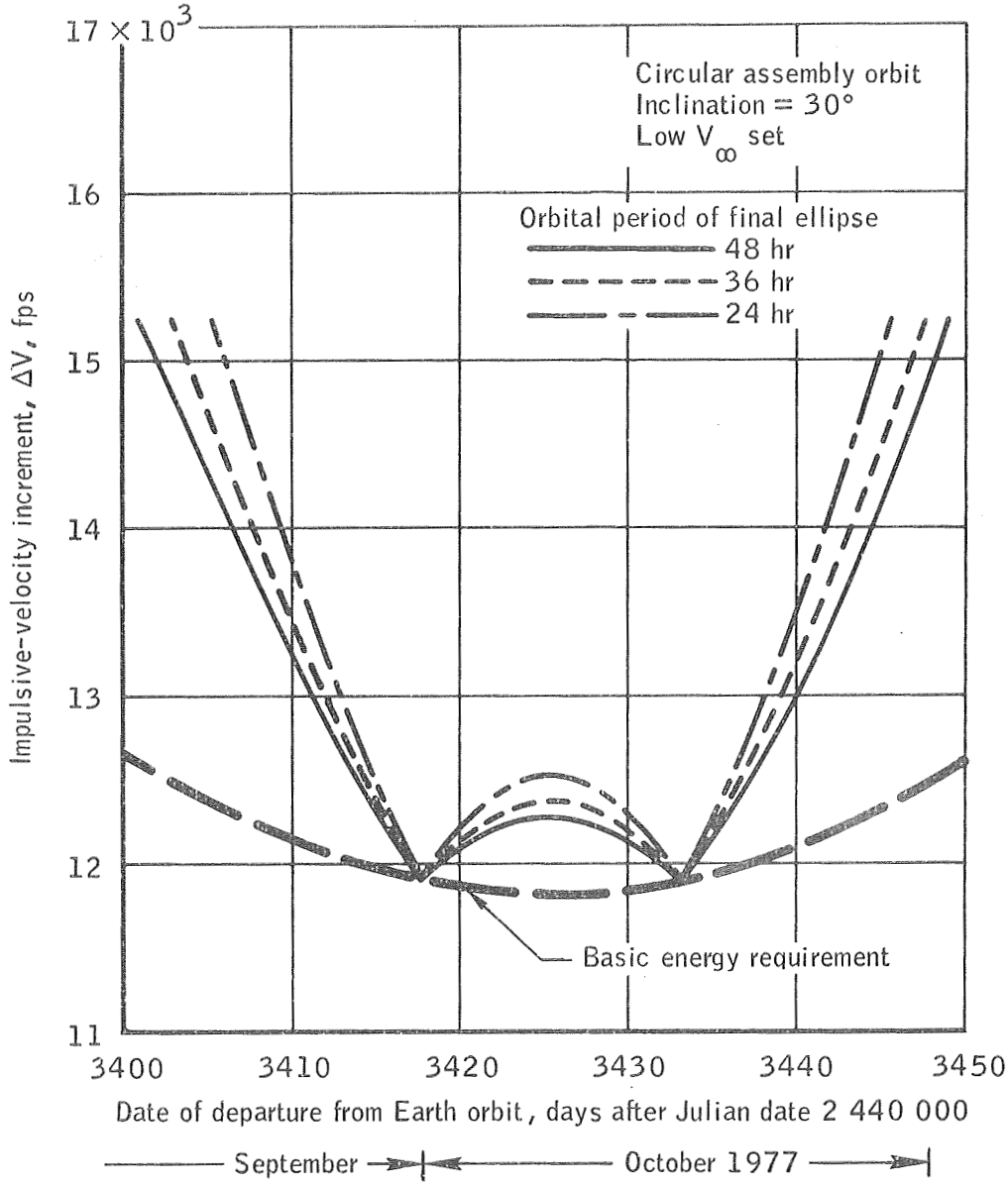

Figure 17. - Effect of final ellipse size on nodal window (nominal orbit orientation), 1977 mission opportunity.

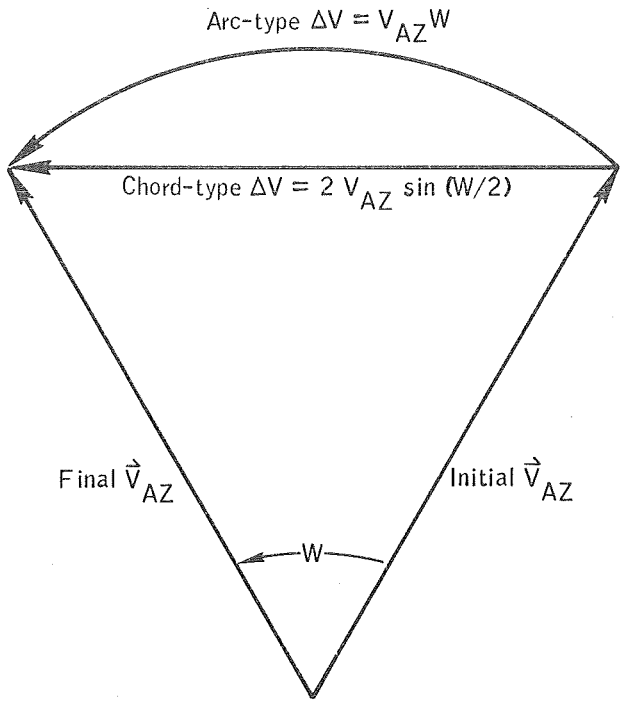

Figure 18. - Comparison of chord-type and arc-type plane-change velocity increments.

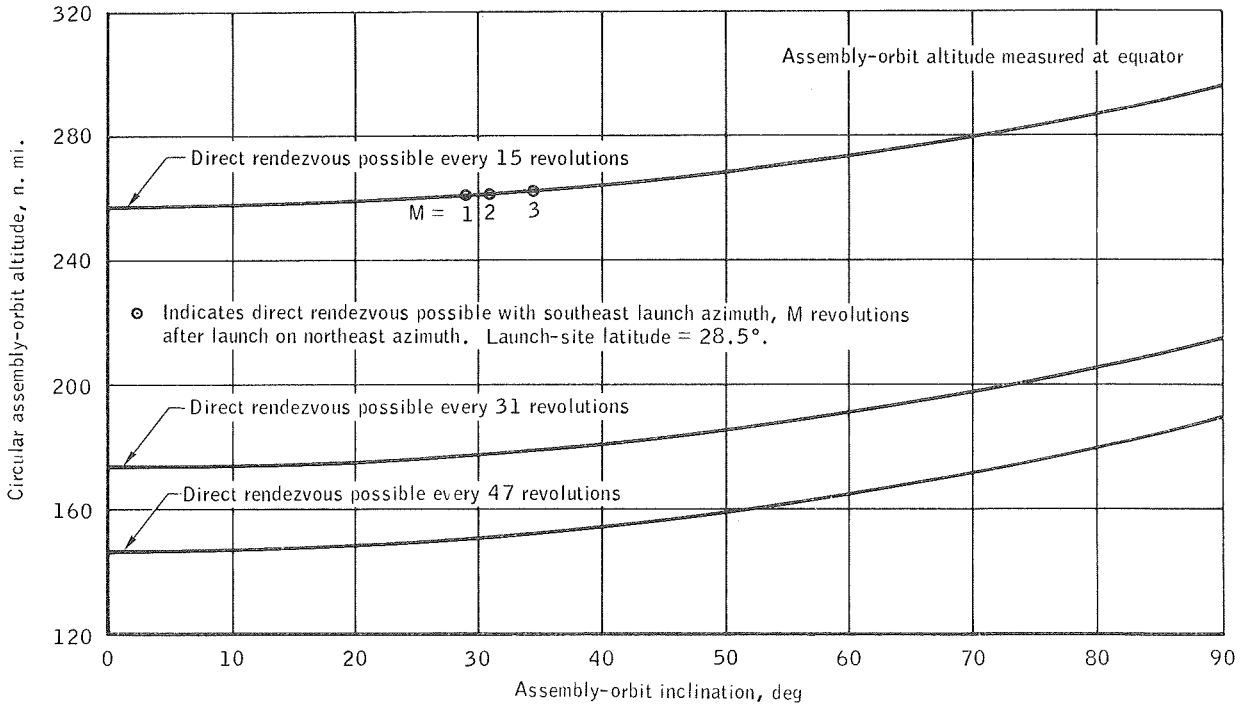

Figure 19. - Circular assembly-orbit altitudes to provide direct-rendezvous capability.

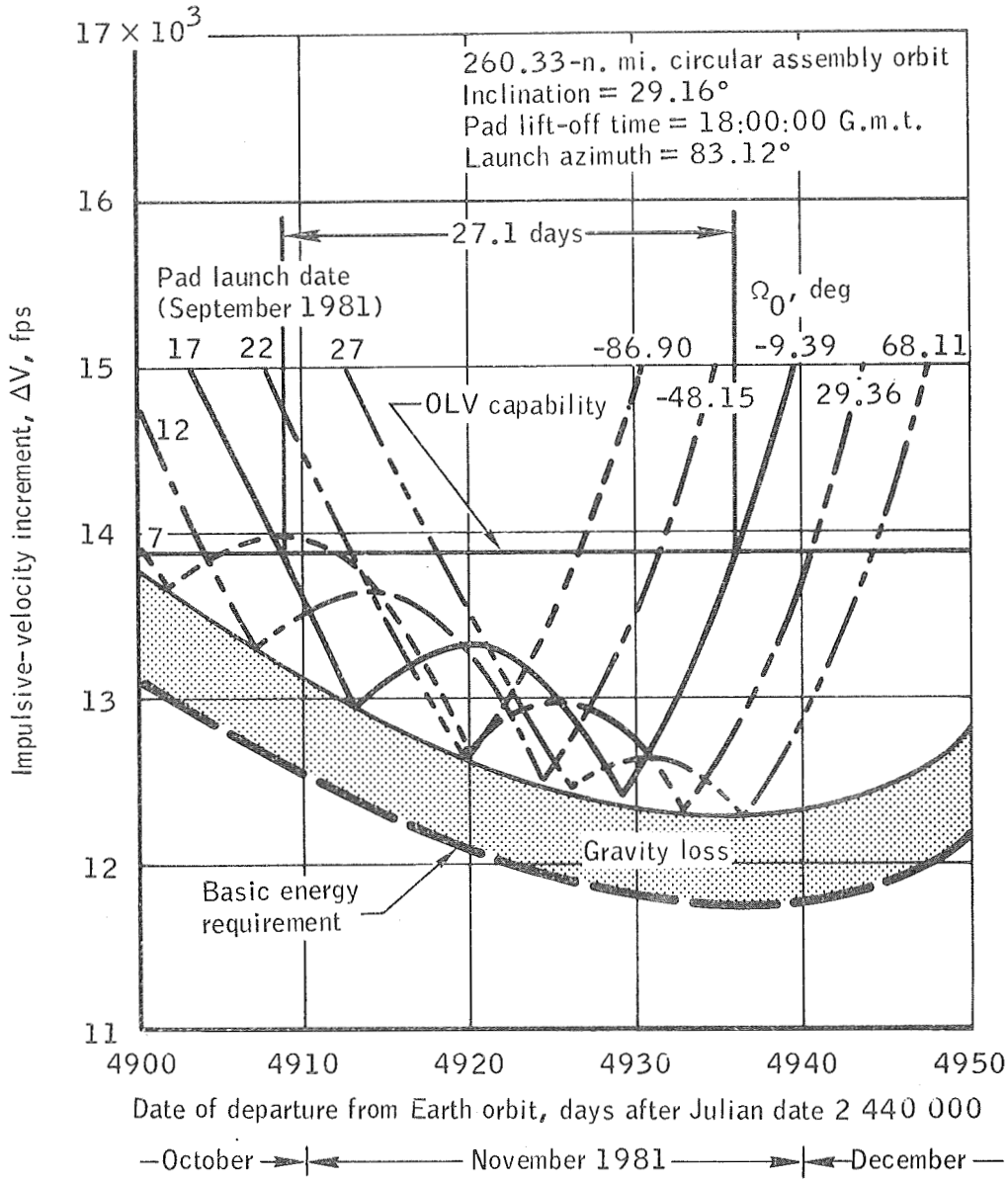

Figure 20. - Effect of Ω_0 on nodal window for circular assembly orbit (gravity losses included), 1981 mission opportunity.

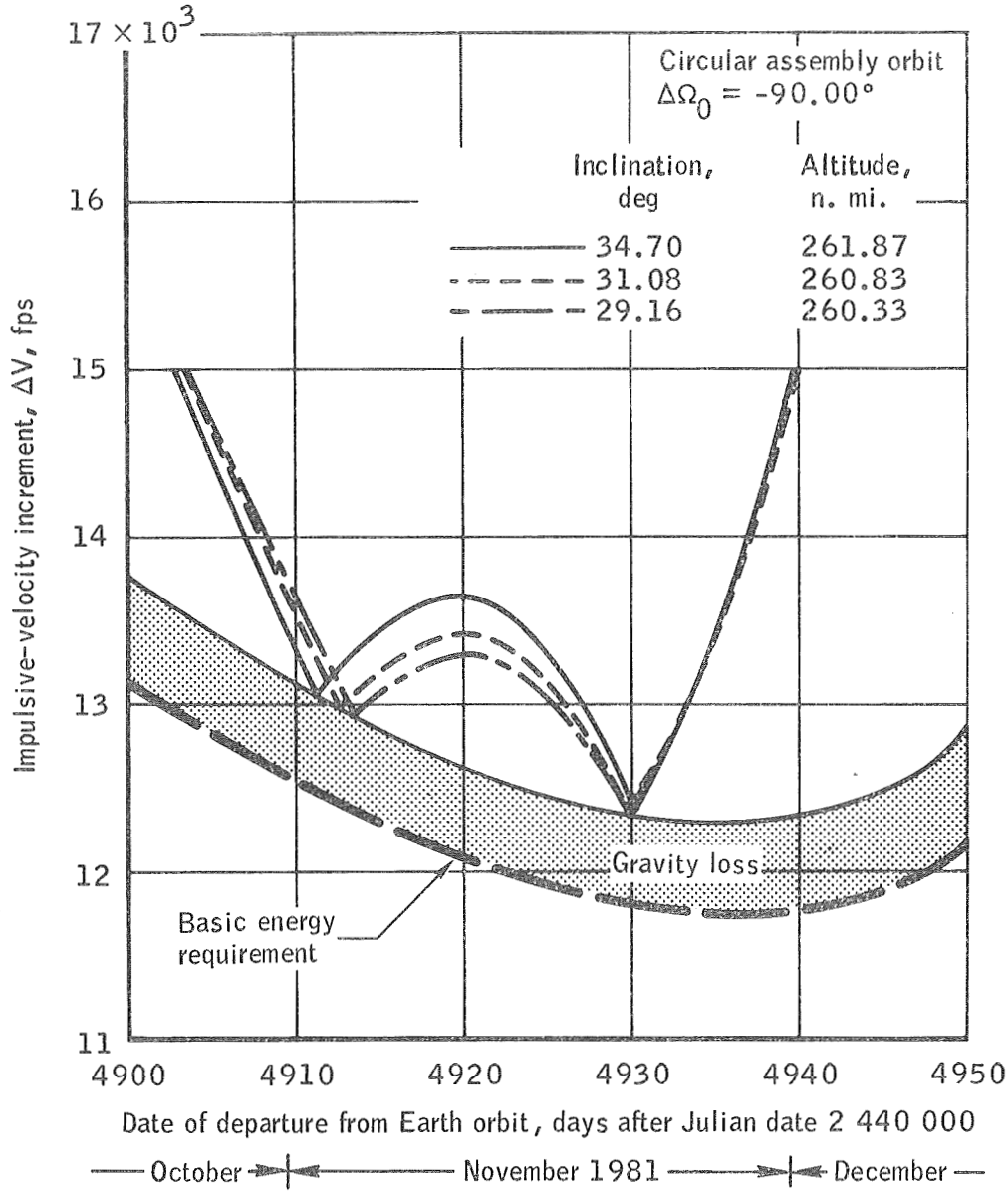

Figure 21. - Effect of inclination on nodal window for circular assembly orbit (gravity losses included), 1981 mission opportunity.

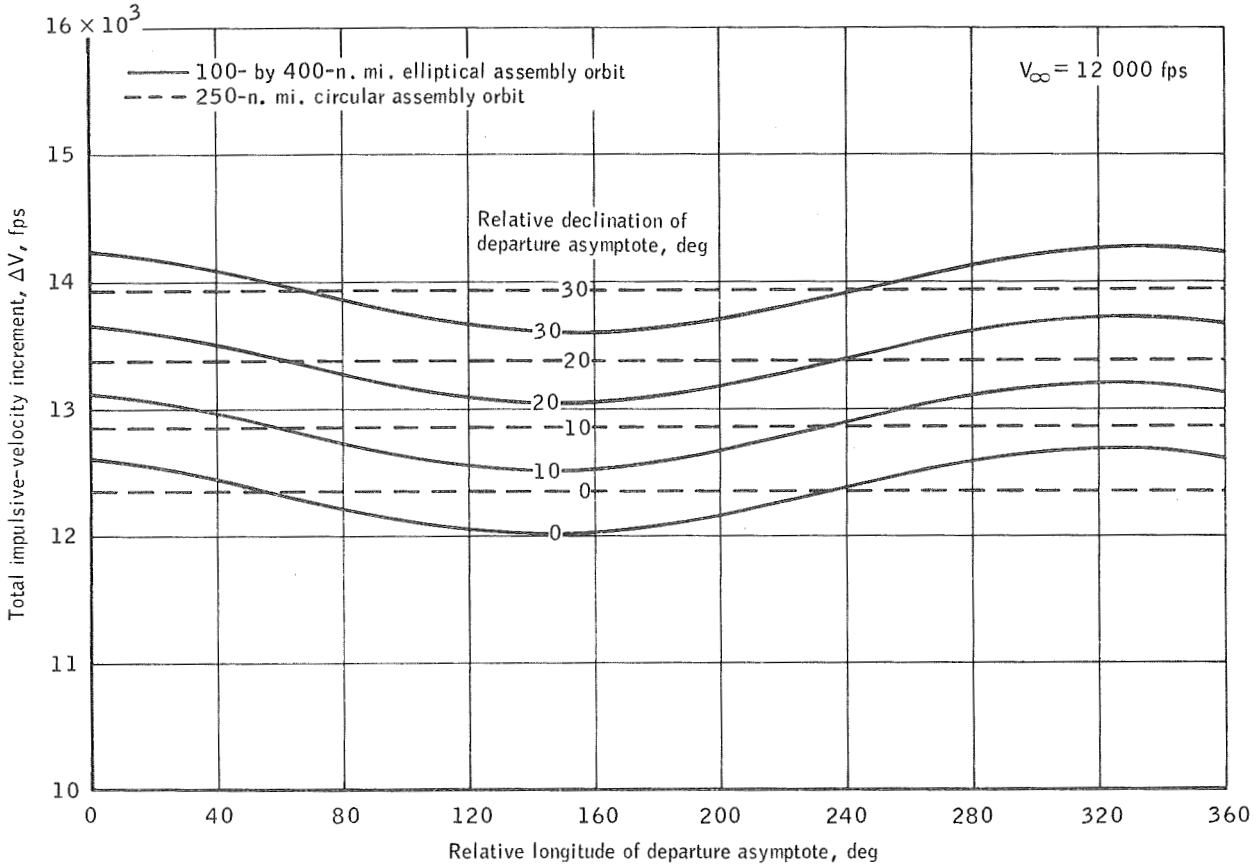

Figure 22. - Three-impulse total ΔV as a function of relative longitude and relative declination of departure asymptote.

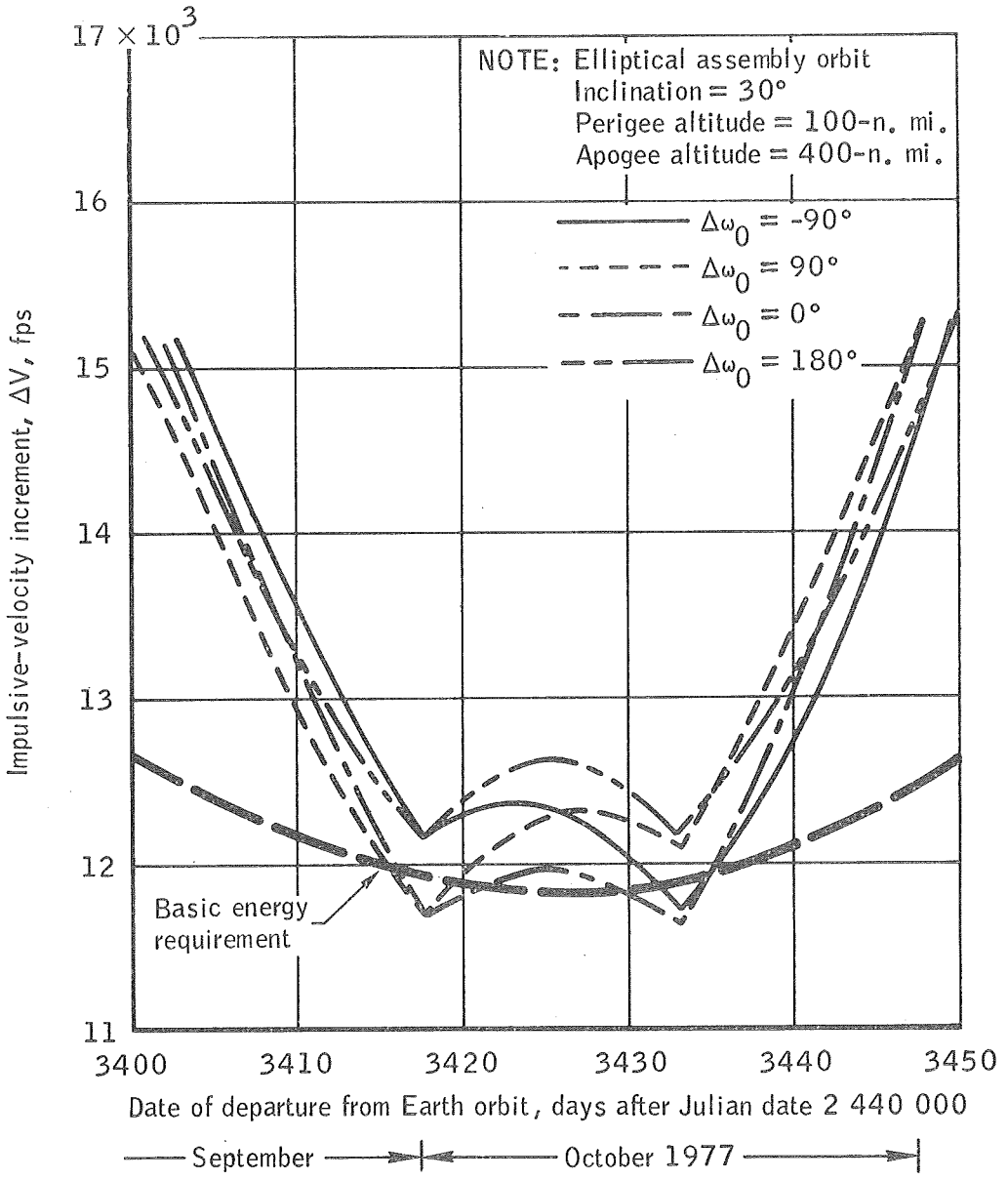

Figure 23. - Effect of apsidal orientation on nodal window (nominal nodal orientation), 1977 mission opportunity.

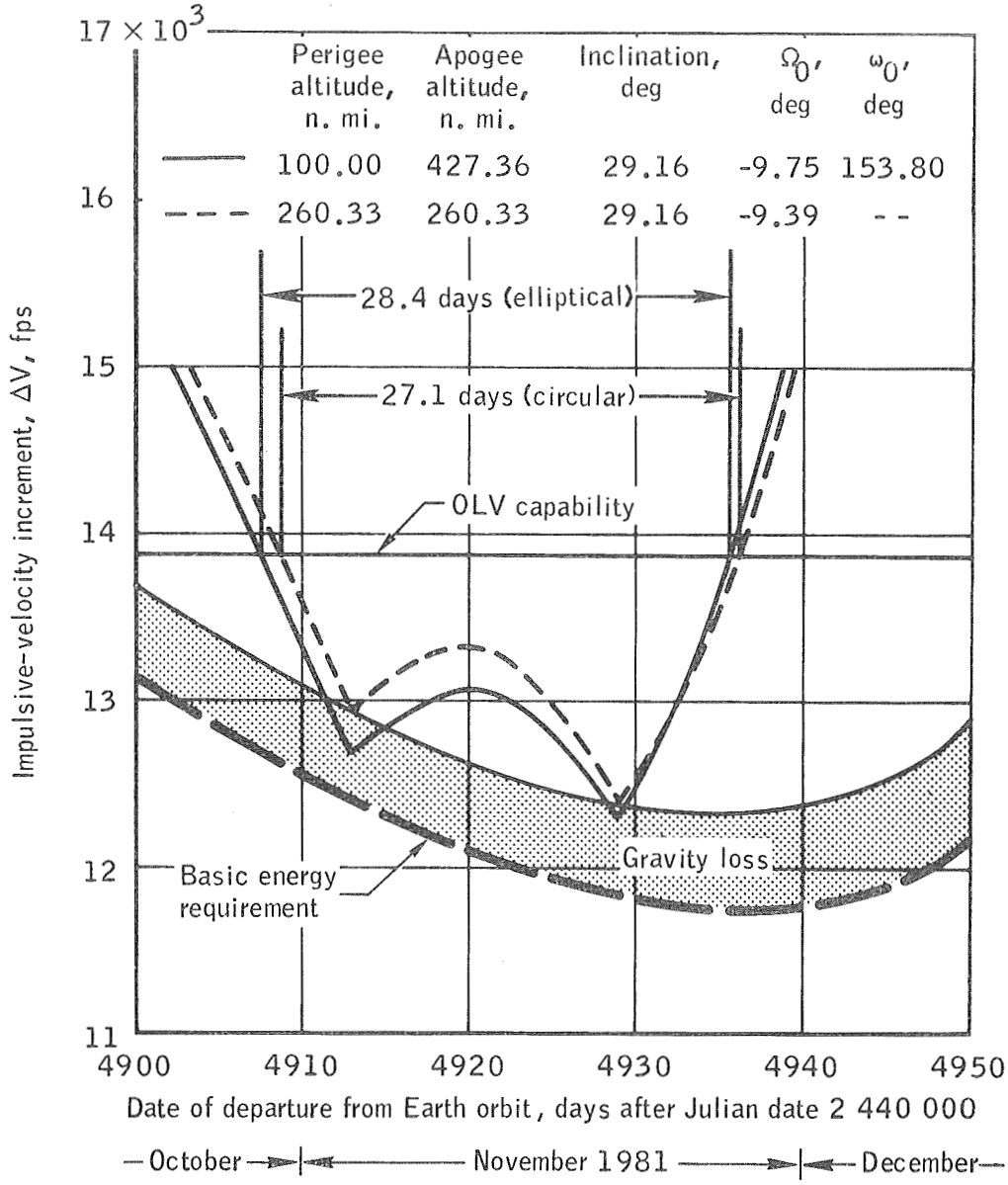

Figure 24. - Comparison of orbital-departure windows for elliptical and circular assembly orbits, 1981 mission opportunity.

LAUNCH SCHEDULES

Table X is a summary of the launch schedules for each of the four mission opportunities investigated. These schedules are based on the use of optimally oriented circular and elliptical assembly orbits with inclinations of 29.16°.

The overall circular assembly-orbit launch schedule for each of the four mission opportunities is illustrated in figures 25 to 28. Figures 29 to 32 illustrate the launch schedules for elliptical assembly orbits. The circular and triangular symbols shown in figures 25 to 32 indicate the lift-off time for each in-plane launch opportunity within the appropriate ascent window.

The lift-off times for the first launch were constrained to lie between 13:00 and 18:00 hours G.m.t. This constraint was necessary to ensure favorable lighting conditions in the suborbital abort recovery area and was based on the assumption that the main spacecraft would be manned during the ascent to the assembly orbit. The limits are probably more restrictive than would be necessary.

The main-spacecraft ascent window can be widened by relaxing the lift-off time constraint (as indicated by the dashed lines in figs. 25 to 32). Alternatively, if the launch of the main spacecraft slips beyond the closing date of the nominal ascent window, the lift-off time can be held at the constraining value, which allows $\dot{\Omega}_0$ to vary from its optimum value. This procedure causes the orbital-departure window (hence, the OLV ascent window) to shift toward the right and to become progressively smaller (fig. 33). However, a delay of several days can be accommodated without a serious degradation of the orbital-departure window. The indication in figure 33, that the opening date of the orbital-departure window advances at almost exactly the same rate as the date of lift-off, is important. Therefore, the time interval available for pad refurbishment remains almost constant, although the main-spacecraft launch may be delayed several days beyond the nominal closing date. Table XI summarizes the effects of main-spacecraft launch delays in all four mission opportunities, assuming the lift-off time constraint is maintained.

In figures 34 to 41, ΔV requirements are shown for interrupted orbital-departure sequences. At selected points within the optimum circular-orbit departure window for each of the four mission opportunities, delays are assumed to occur after the first burn (figs. 34 to 37) and after the second burn (figs. 38 to 41) in the normal departure sequence. Such delays may be either inadvertent as a result of resolvable system malfunctions or deliberate. For example, if a malfunction is detected in an upper OLV stage or in the main spacecraft near the end of the nodal window, it may be possible to save the mission by burning one or both of the lower OLV stages to achieve a holding orbit which has a lower nodal regression rate and thus to extend the orbital-departure window.

With regard to propulsion requirements, orbital departure is usually still possible after a delay of several days in an intermediate ellipse, and impressive extensions of the orbital-departure window are possible by deliberately firing into a holding orbit (figs. 34 to 41). However, holding in a high ellipse for an extended time requires repeated passes through the Van Allen radiation belts. An evaluation of the inherent radiation hazards must be made before the holding maneuver can be considered practical as a contingency measure.

TABLE X. - LAUNCH-SCHEDULE SUMMARY FOR MARS CONJUNCTION-CLASS MISSIONS[a]

Event or mission parameter		Mission opportunity			
Symbol	Description	1977	1979	1981	1983
t_0	Epoch; departure date for minimum V_∞, days after Julian date 2 440 000	3426.0 (3426.0)	4182.0 (4182.0)	4936.0 (4936.0)	5715.0 (5716.0)
Ω_0	Right ascension of assembly-orbit ascending node at t_0, deg	-18.97 (-19.30)	-40.32 (-25.17)	-9.39 (-9.75)	0.66 (23.54)
ω_0	Assembly-orbit argument of perigee at t_0, deg	-- (18.77)	-- (102.30)	-- (153.80)	-- (175.60)
$t_{M,\,1}$	Date main spacecraft ascent window opens (lift-off time for northeast launch, 18:00 G.m.t.)	Aug. 4 (Aug. 4)	Aug. 24 (Aug. 26)	Sept. 17 (Sept. 17)	Nov. 1 (Nov. 4)
Δt_M	Width of main spacecraft ascent window; (constant Ω_0 and ω_0), days	12.8 (12.8)	12.8 (12.8)	12.8 (12.8)	12.8 (12.8)
N_M	Number of in-plane launch opportunities in main spacecraft ascent window	22 (22)	22 (22)	22 (22)	22 (22)
$t_{M,\,2}$	Date main spacecraft ascent window closes (lift-off time for southeast launch, 13:00 G.m.t.)	Aug. 17 (Aug. 17)	Sept. 6 (Sept. 8)	Sept. 30 (Sept. 30)	Nov. 14 (Nov. 17)
Δt_p	Time available for pad turnaround, days	>29 (>29)	>27 (>26)	>25 (>24)	>22 (>21)
$t_{S,\,1}$	Date OLV-stage ascent window opens, $\approx$ 5.5 days before $t_{D,\,1}$	Sept. 15 (Sept. 15)	Oct. 3 (Oct. 4)	Oct. 25 (Oct. 23)	Dec. 6 (Dec. 8)
Δt_S	Width of OLV ascent window, days	31.4 (31.4)	29.4 (29.4)	28.5 (28.4)	32.4 (33.3)
N_S	Number of in-plane launch opportunities in OLV ascent window	66 (66)	62 (62)	60 (60)	68 (70)
$t_{S,\,2}$	Date OLV-stage ascent window closes, $\approx$ 4.0 days before $t_{D,\,2}$	Oct. 17 (Oct. 17)	Nov. 2 (Nov. 3)	Nov. 23 (Nov. 22)	Jan. 8, 1984 (Jan. 11, 1984)
$t_{D,\,1}$ (b)	Date orbital-departure window opens (ΔV = 13 860 fps)	Sept. 21 (Sept. 20)	Oct. 9 (Oct. 10)	Oct. 31 (Oct. 30)	Dec. 12 (Dec. 14)
Δt_D	Width of nodal orbital-departure window, days	30.5 (30.5)	27.9 (28.3)	27.1 (28.4)	31.2 (32.0)
N_D	Approximate number of anomalistic orbital-departure windows in nodal orbital-departure window	466 (465)	426 (432)	414 (433)	477 (488)
$t_{D,\,2}$ (b)	Date orbital-departure window closes (ΔV = 13 860 fps)	Oct. 21 (Oct. 21)	Nov. 6 (Nov. 7)	Nov. 27 (Nov. 27)	Jan. 12, 1984 (Jan. 15, 1984)

[a]The values shown are for a 260.33-n. mi. circular assembly orbit, and the data enclosed in parentheses apply to a 100- by 427.36-n. mi. elliptical assembly orbit. The orbital inclination in both cases is 29.16°.

[b]Time of final transplanetary-injection burn — first burn in orbital-departure sequence occurs 2.5 days earlier.

TABLE XI. - ORBITAL-DEPARTURE WINDOWS FOR DELAYED SPACECRAFT LAUNCHES[a]

Mission opportunity	Width of nodal window for main-spacecraft launch delay of — (b)			
	0 to 13 days (c)	20 days	25 days	30 days
1977	30.5	30.0	28.0	[d]22.0
1979	27.9	27.6	26.0	22.5
1981	27.1	26.9	25.3	22.5
1983	31.2	[d]28.0	[d]22.8	[d]17.0

[a]260.33-n. mi. circular assembly orbit with an inclination of 29.16°.

[b]Width of nodal window in days, assuming OLV capability = 13 860 fps.

[c]Nominal main-spacecraft ascent window (constant Ω_0).

[d]Launch window limited by mission constraint on orbital-departure date rather than by excessive ΔV requirement.

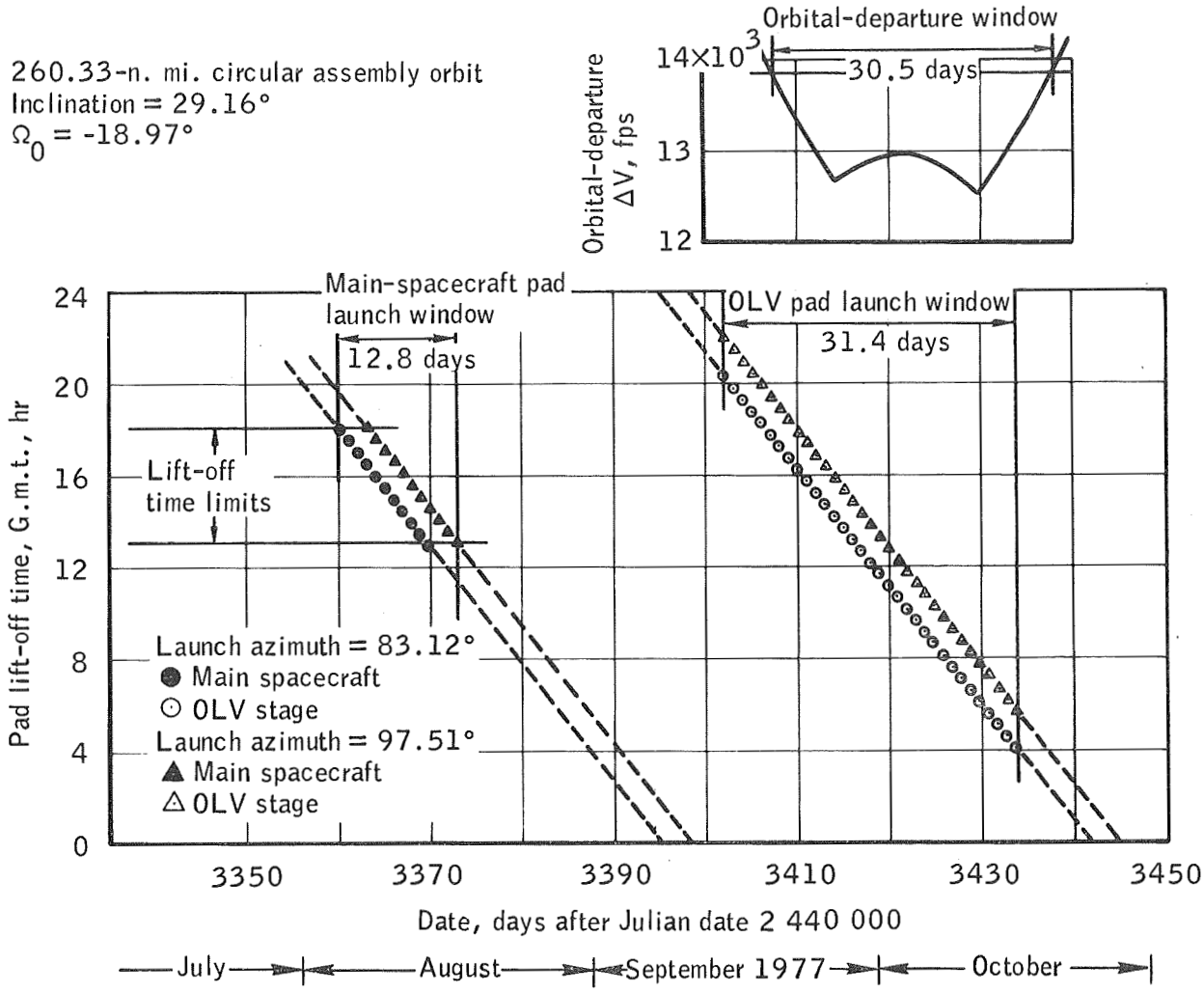

Figure 25. - Launch schedule for the 1977 mission opportunity using circular assembly orbits.

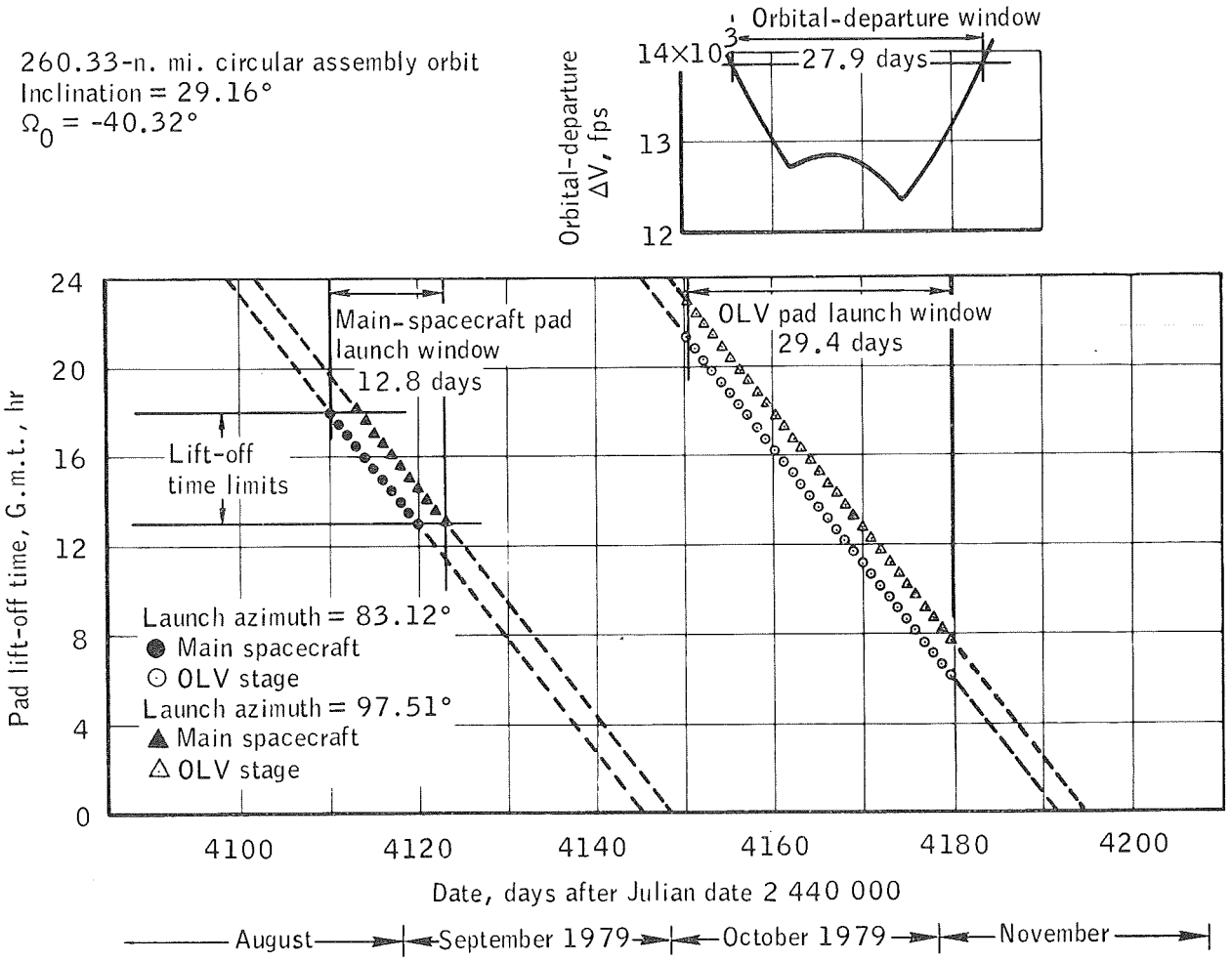

Figure 26. - Launch schedule for the 1979 mission opportunity using circular assembly orbits.

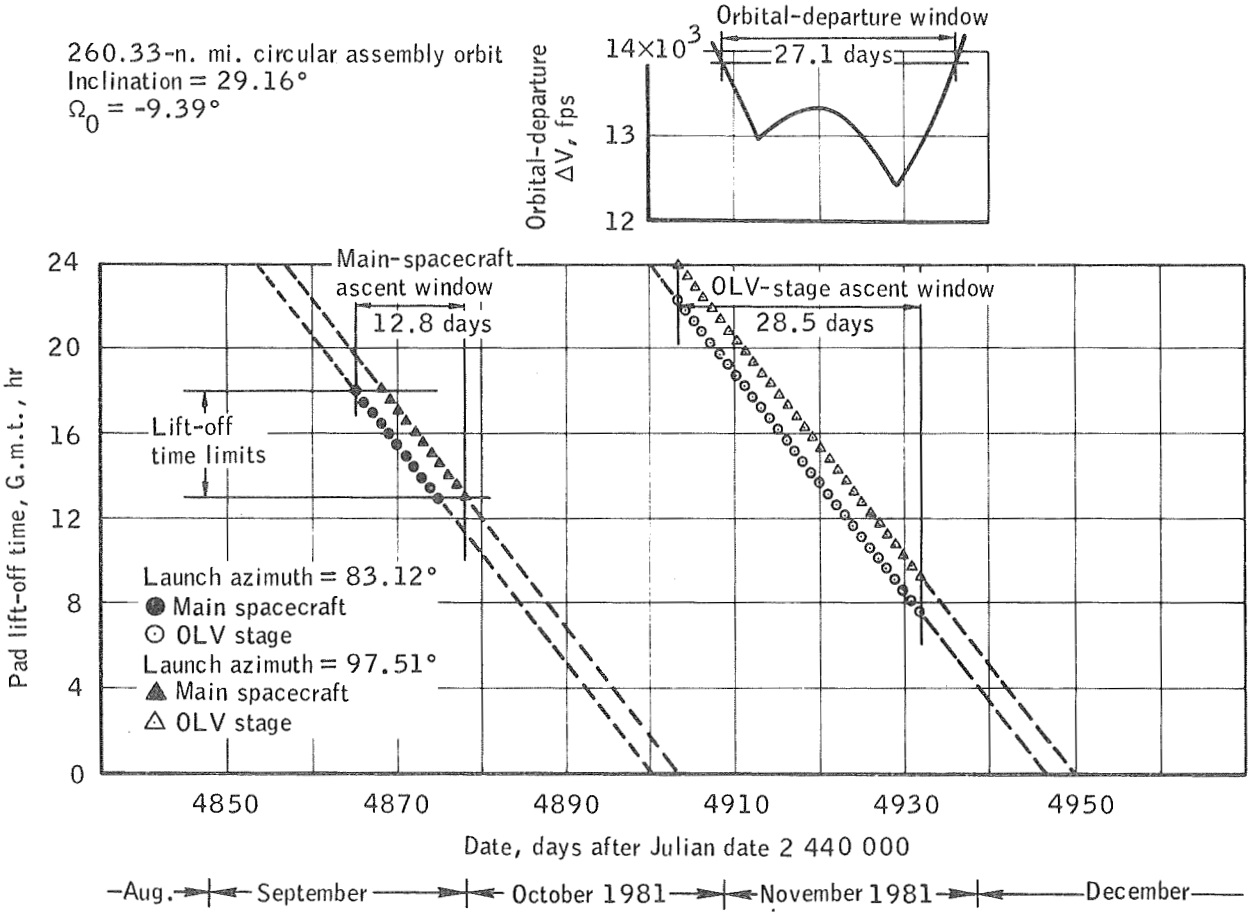

Figure 27. - Launch schedule for the 1981 mission opportunity using circular assembly orbits.

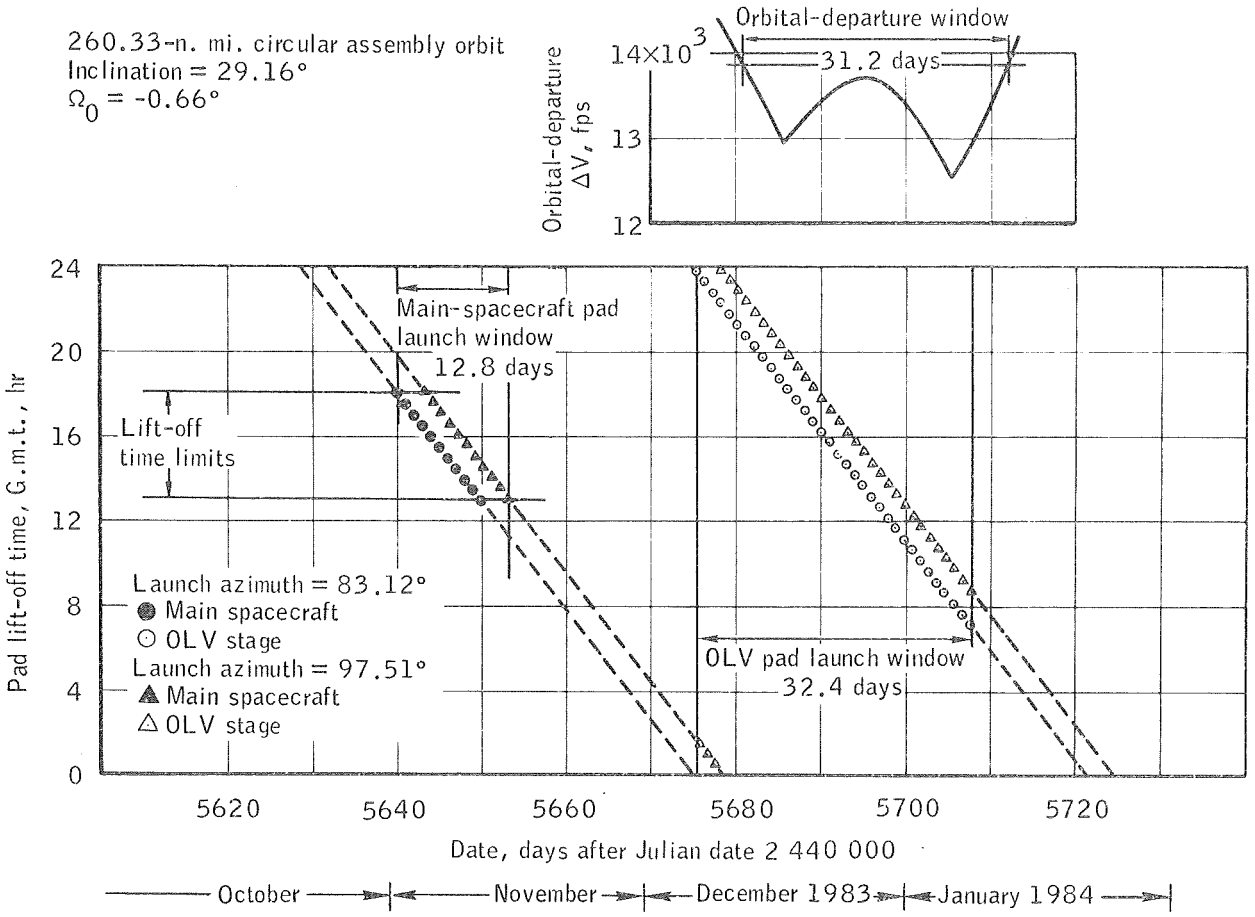

Figure 28. - Launch schedule for the 1983 mission opportunity using circular assembly orbits.

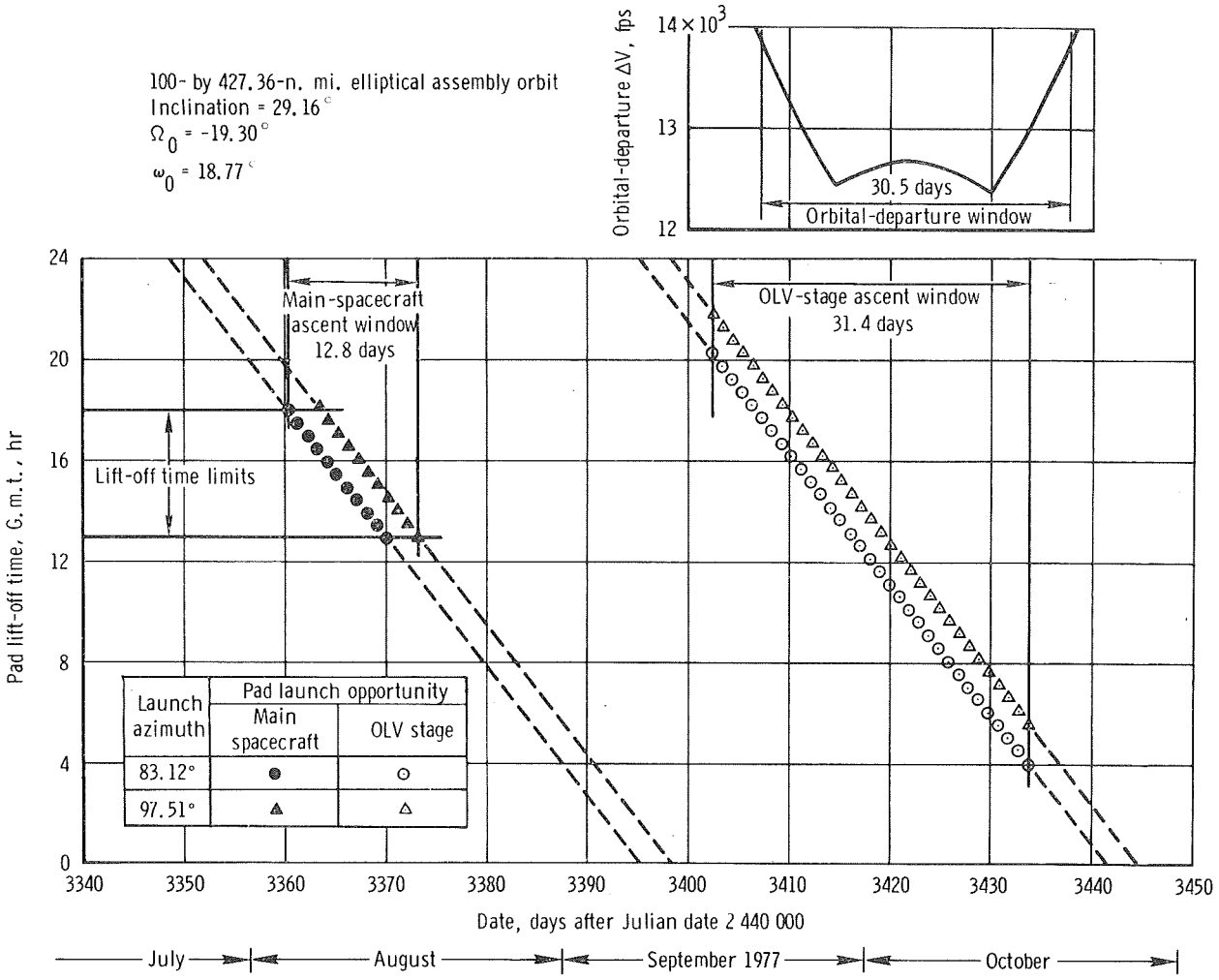

Figure 29. - Launch schedule for the 1977 mission opportunity using elliptical assembly orbits.

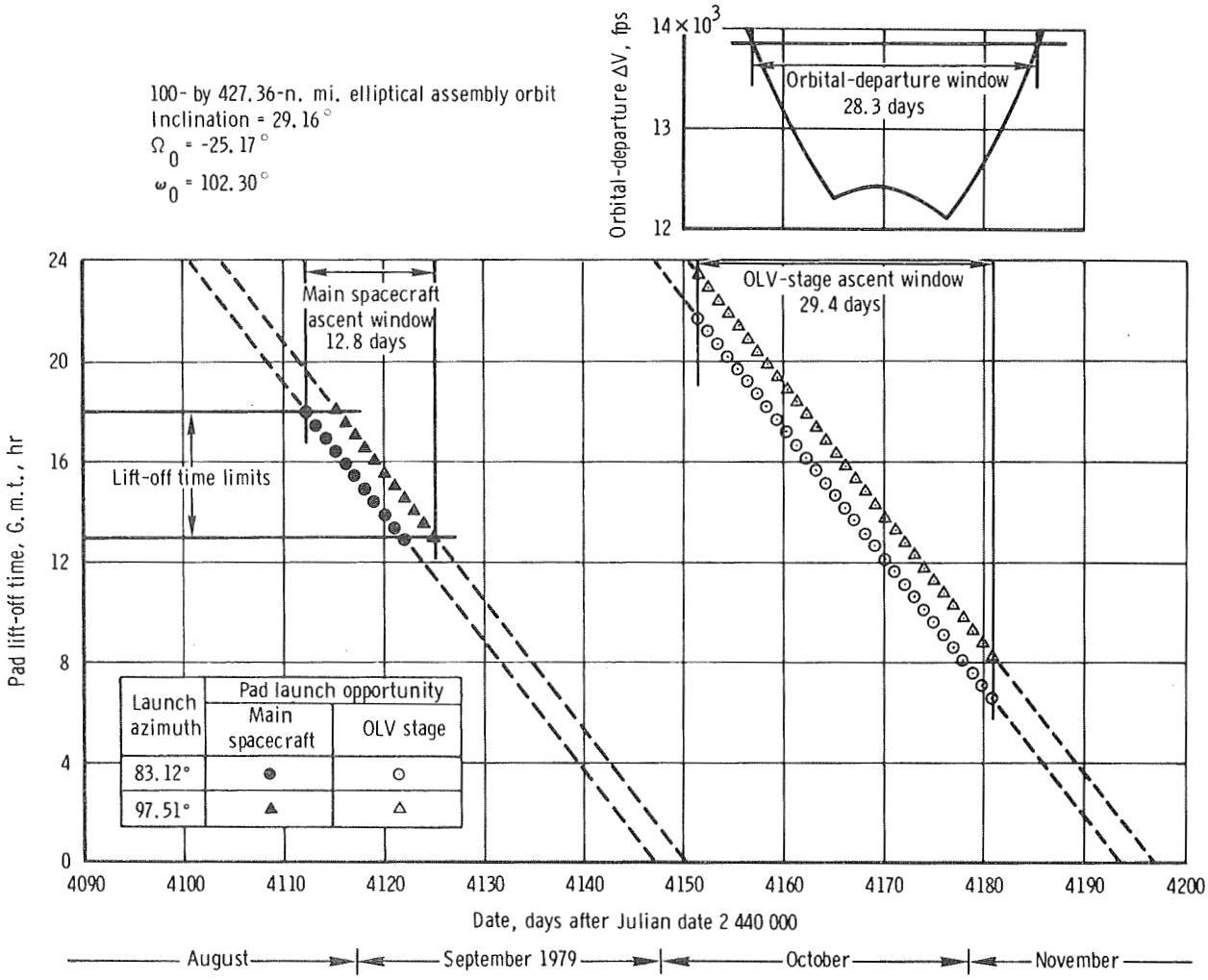

Figure 30. - Launch schedule for the 1979 mission opportunity using elliptical assembly orbits.

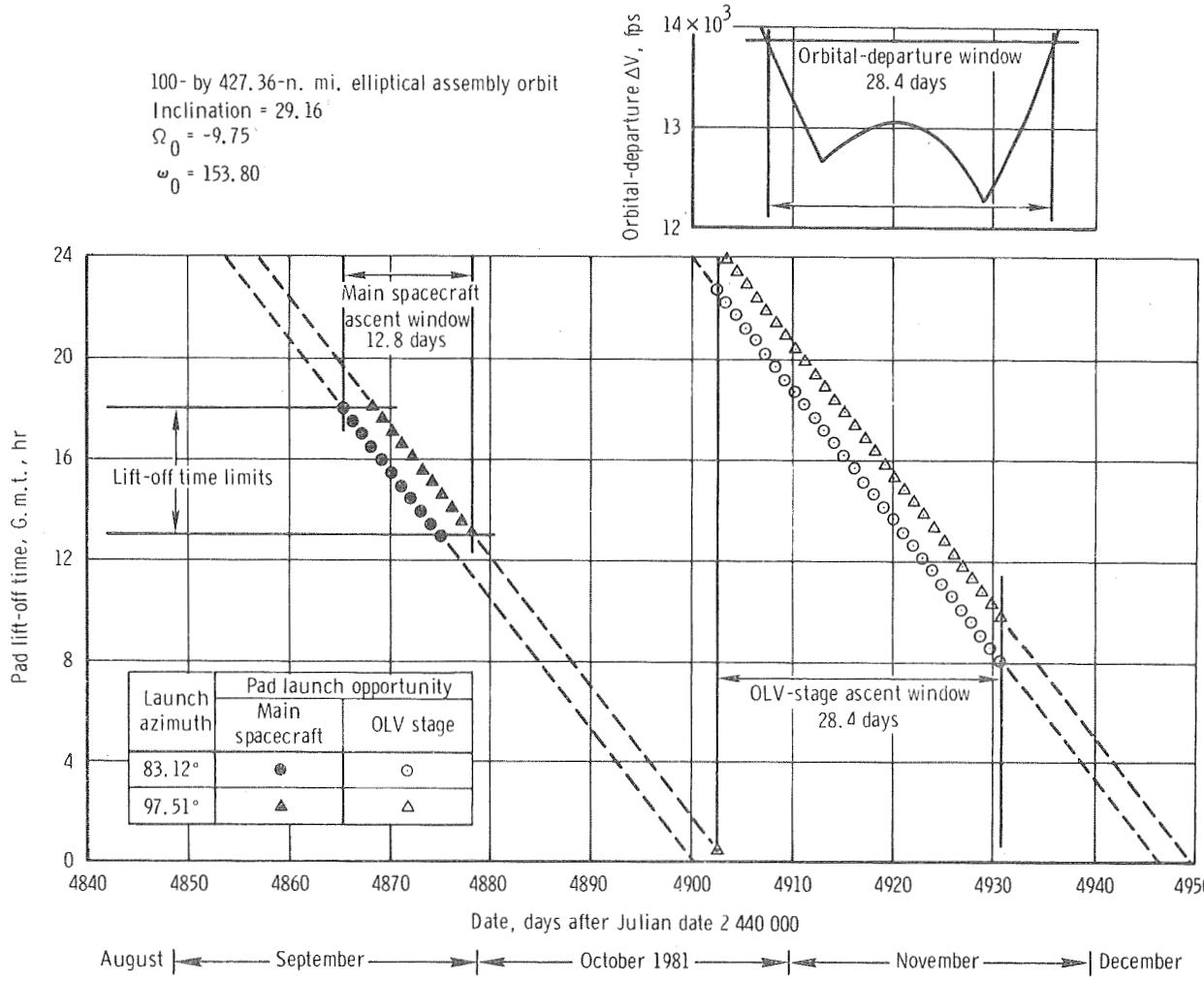

Figure 31. - Launch schedule for the 1981 mission opportunity using elliptical assembly orbits.

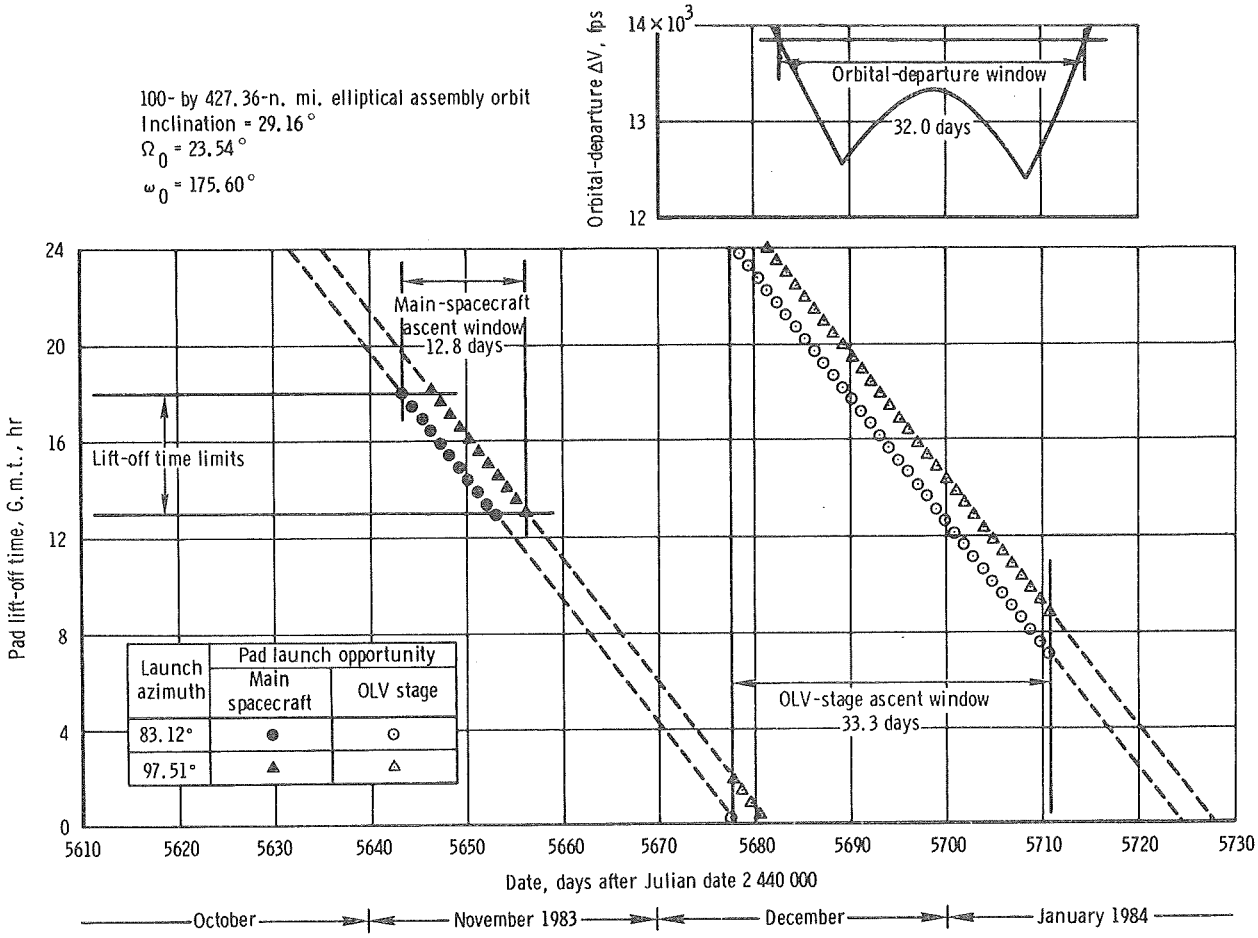

Figure 32. - Launch schedule for the 1983 mission opportunity using elliptical assembly orbits.

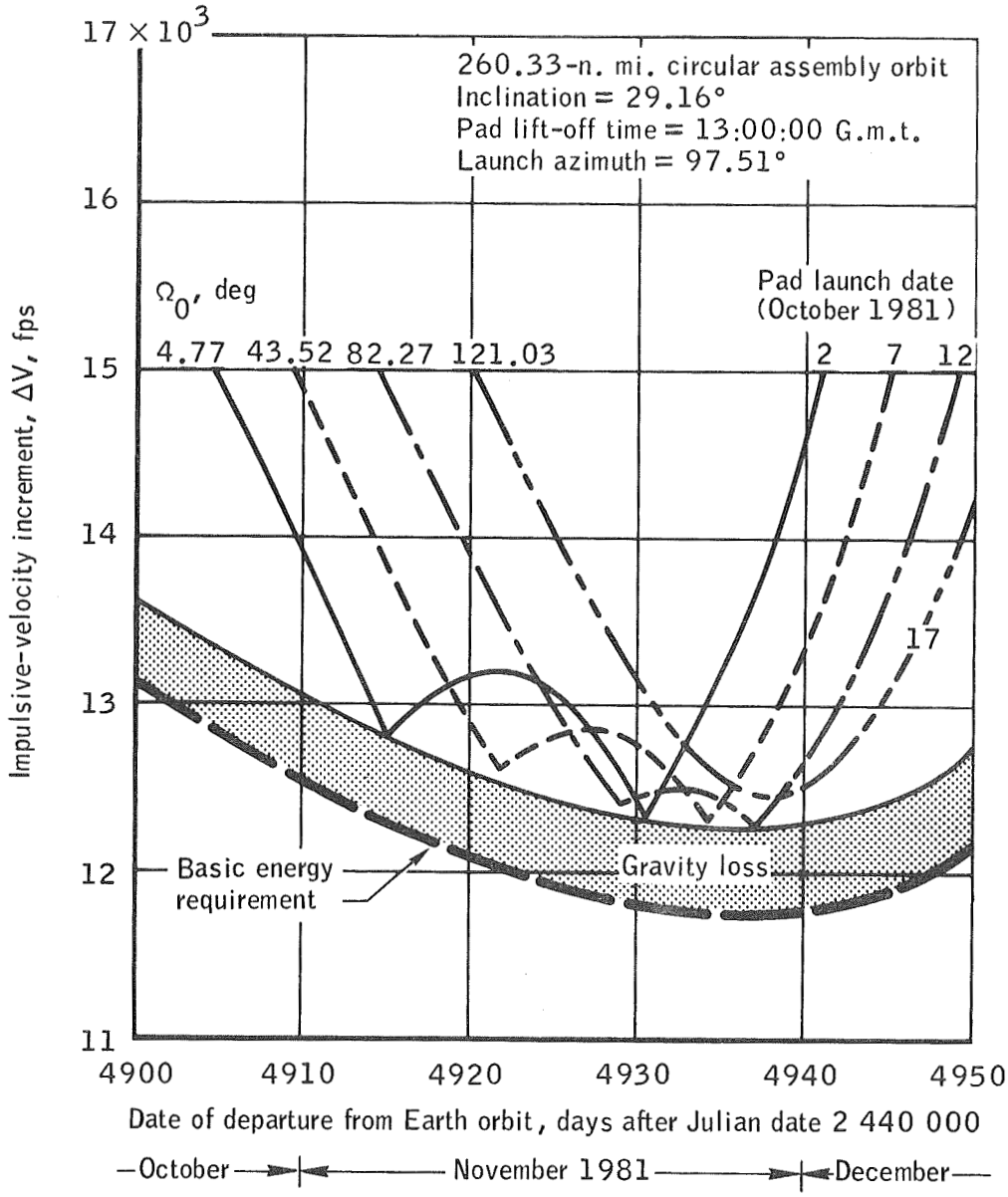

Figure 33. - Effect of pad launch date on nodal window for a circular assembly orbit during the 1981 mission opportunity.

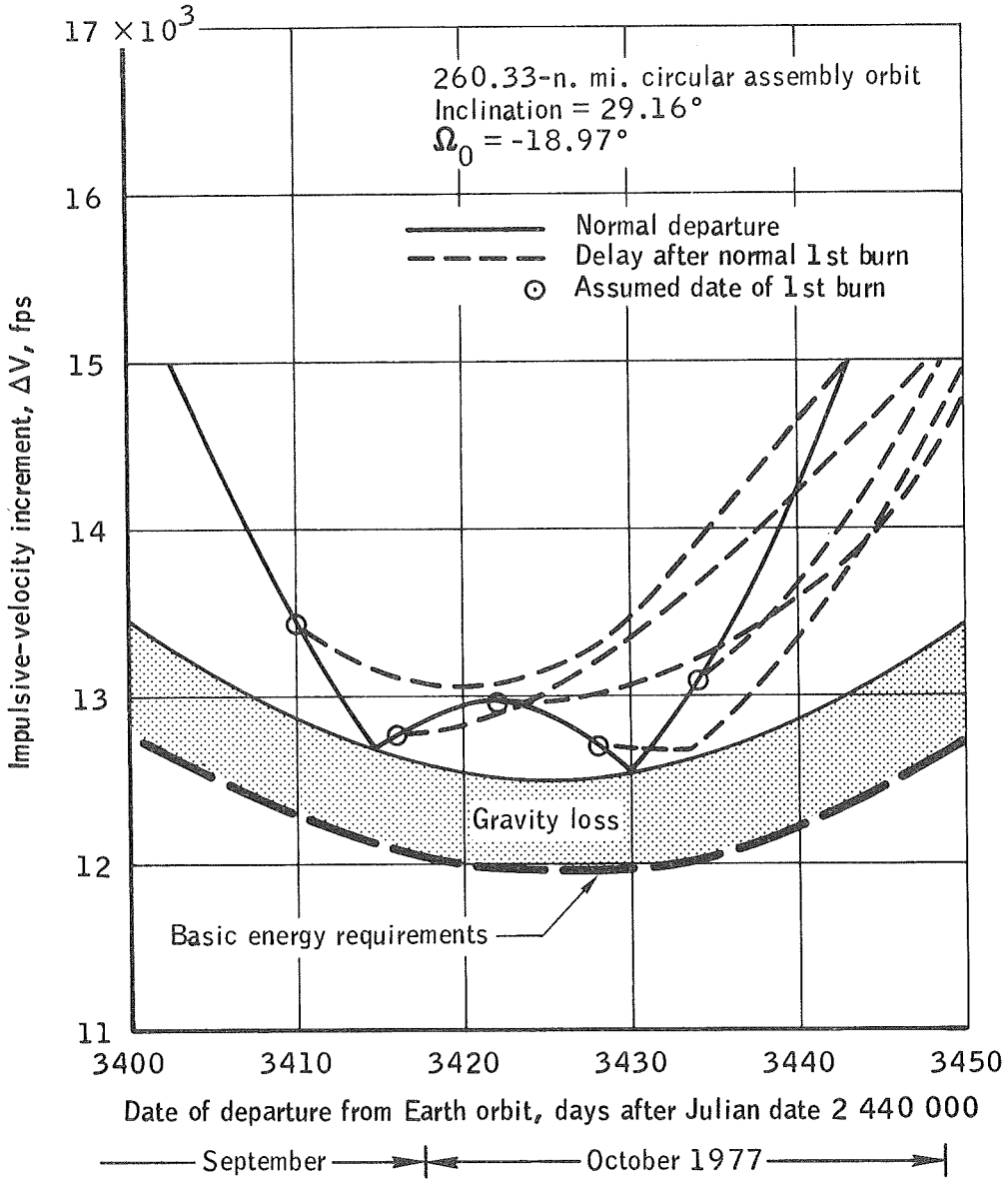

Figure 34. - Interrupted departure sequence for the 1977 mission opportunity (delay following first burn).

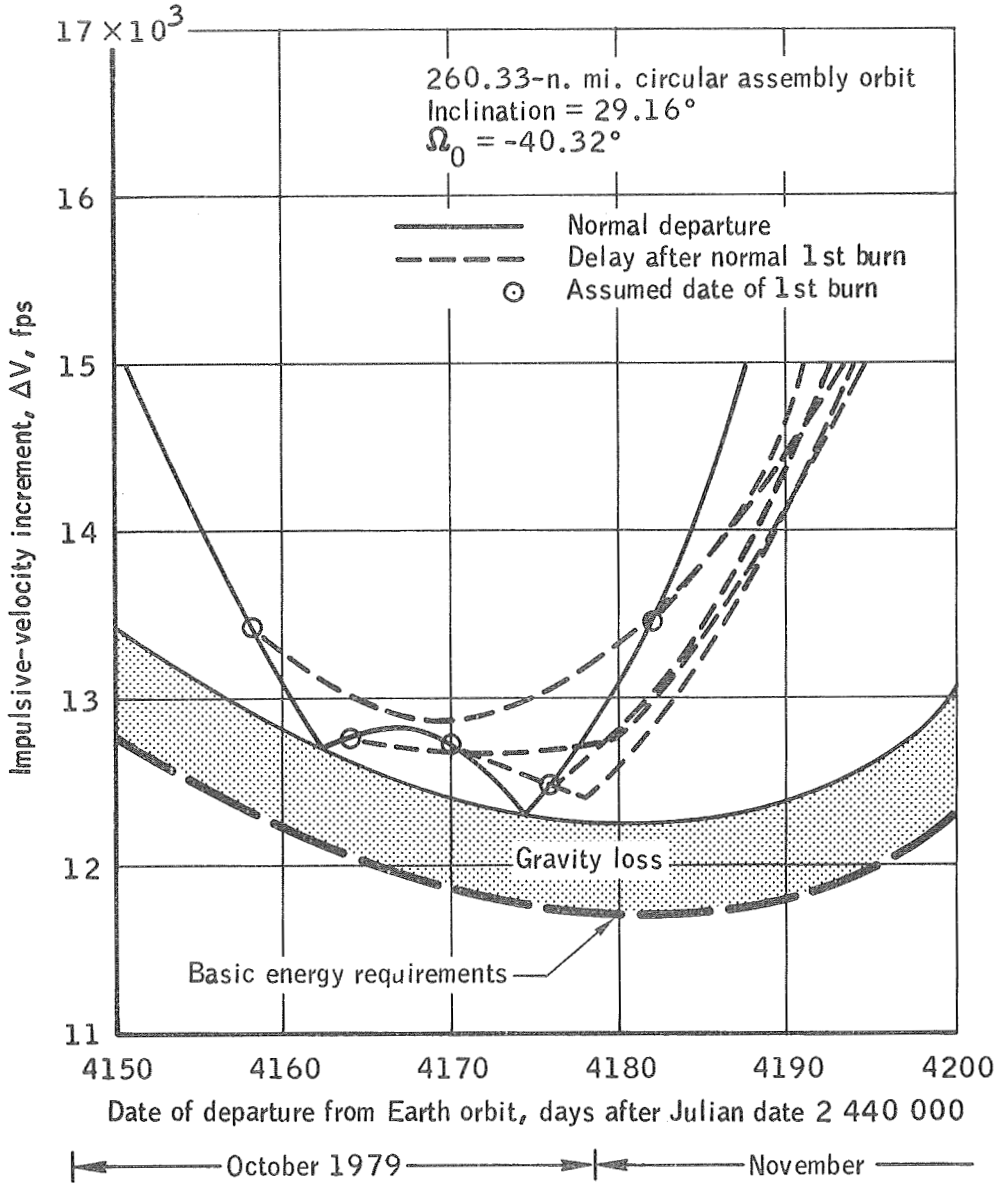

Figure 35. - Interrupted departure sequence for the 1979 mission opportunity (delay following first burn).

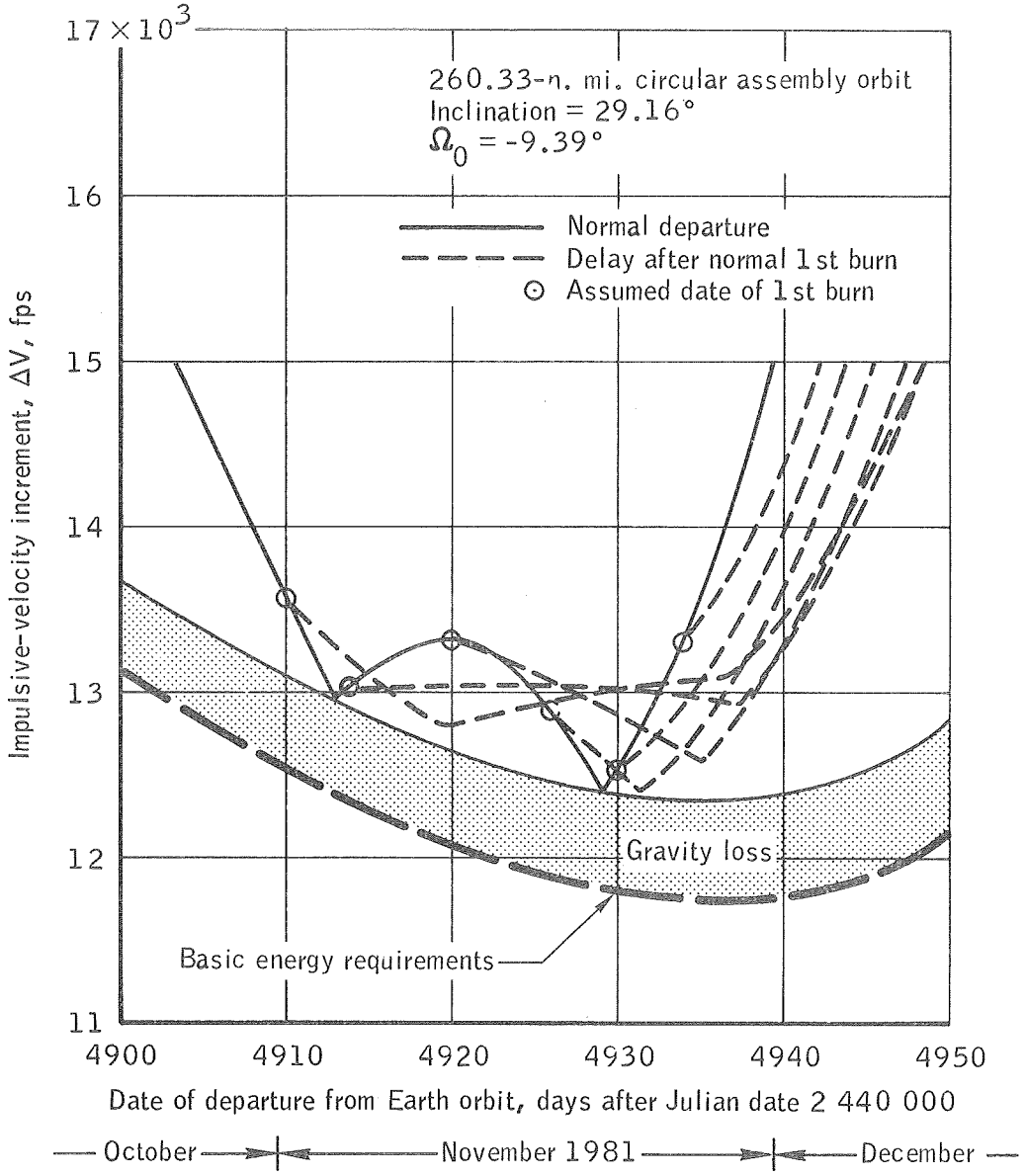

Figure 36. - Interrupted departure sequence for the 1981 mission opportunity (delay following first burn).

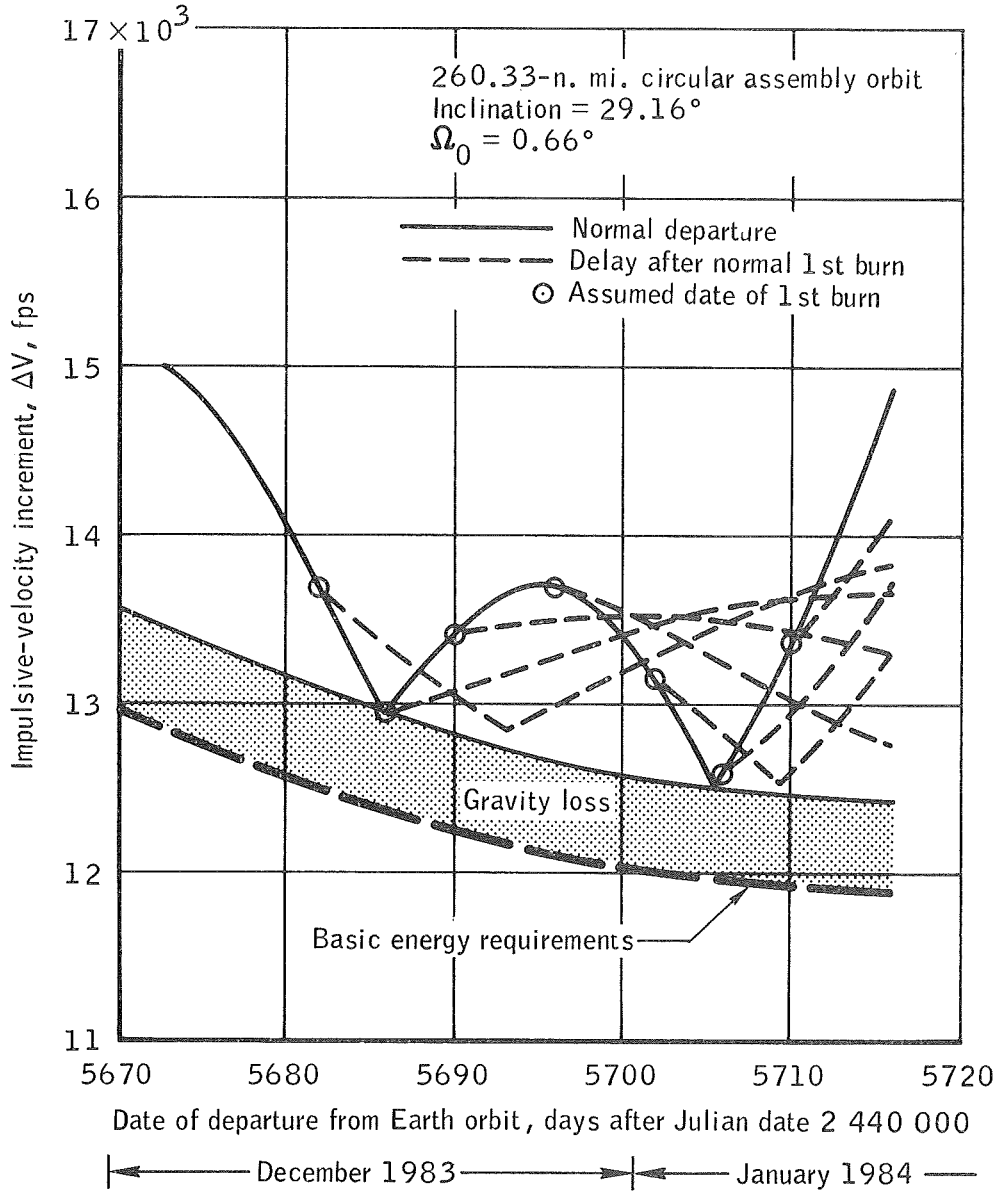

Figure 37. - Interrupted departure sequence for the 1983 mission opportunity (delay following first burn).

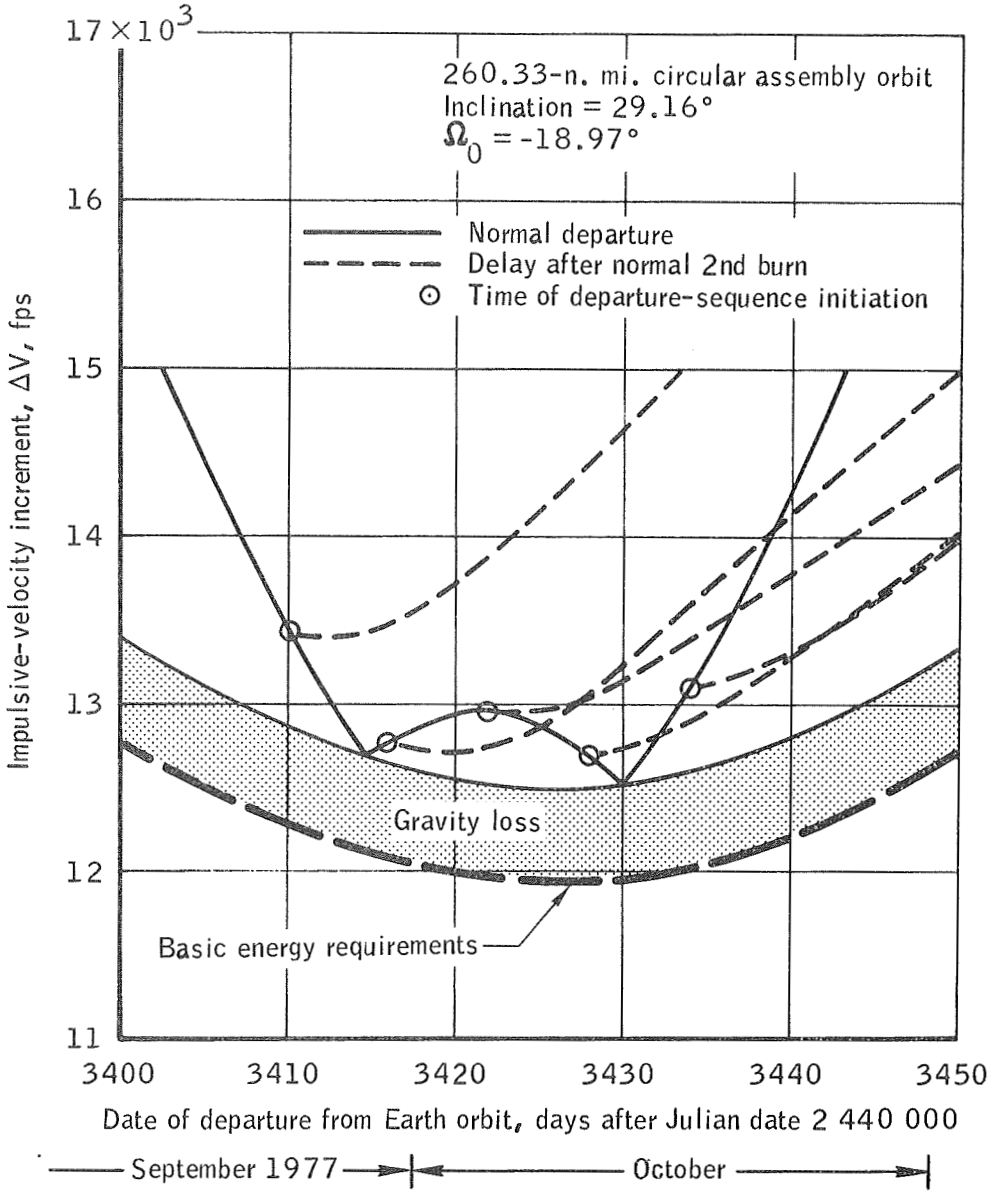

Figure 38. - Interrupted departure sequence for the 1977 mission opportunity (delay following second burn).

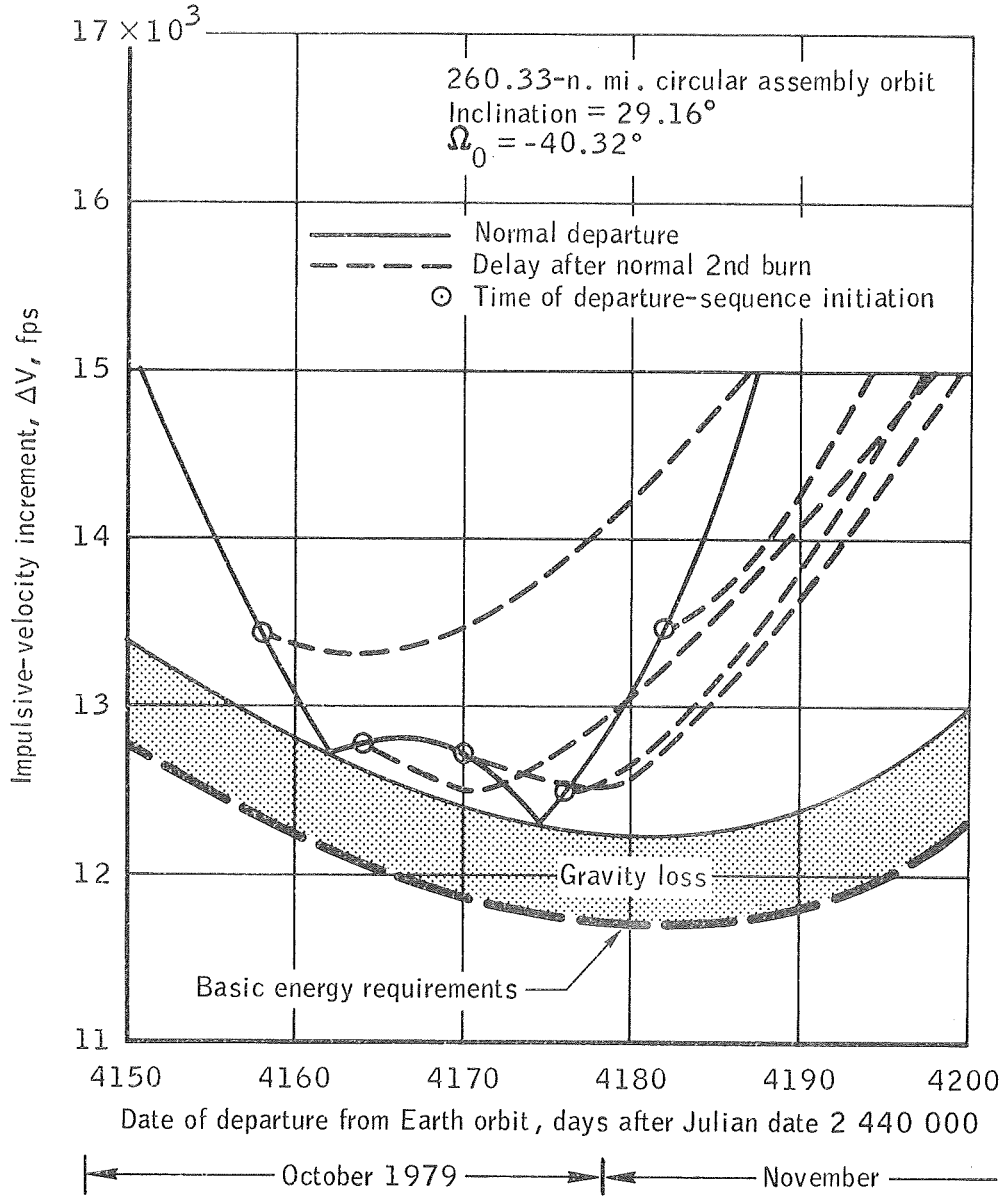

Figure 39. - Interrupted departure sequence for the 1979 mission opportunity (delay following second burn).

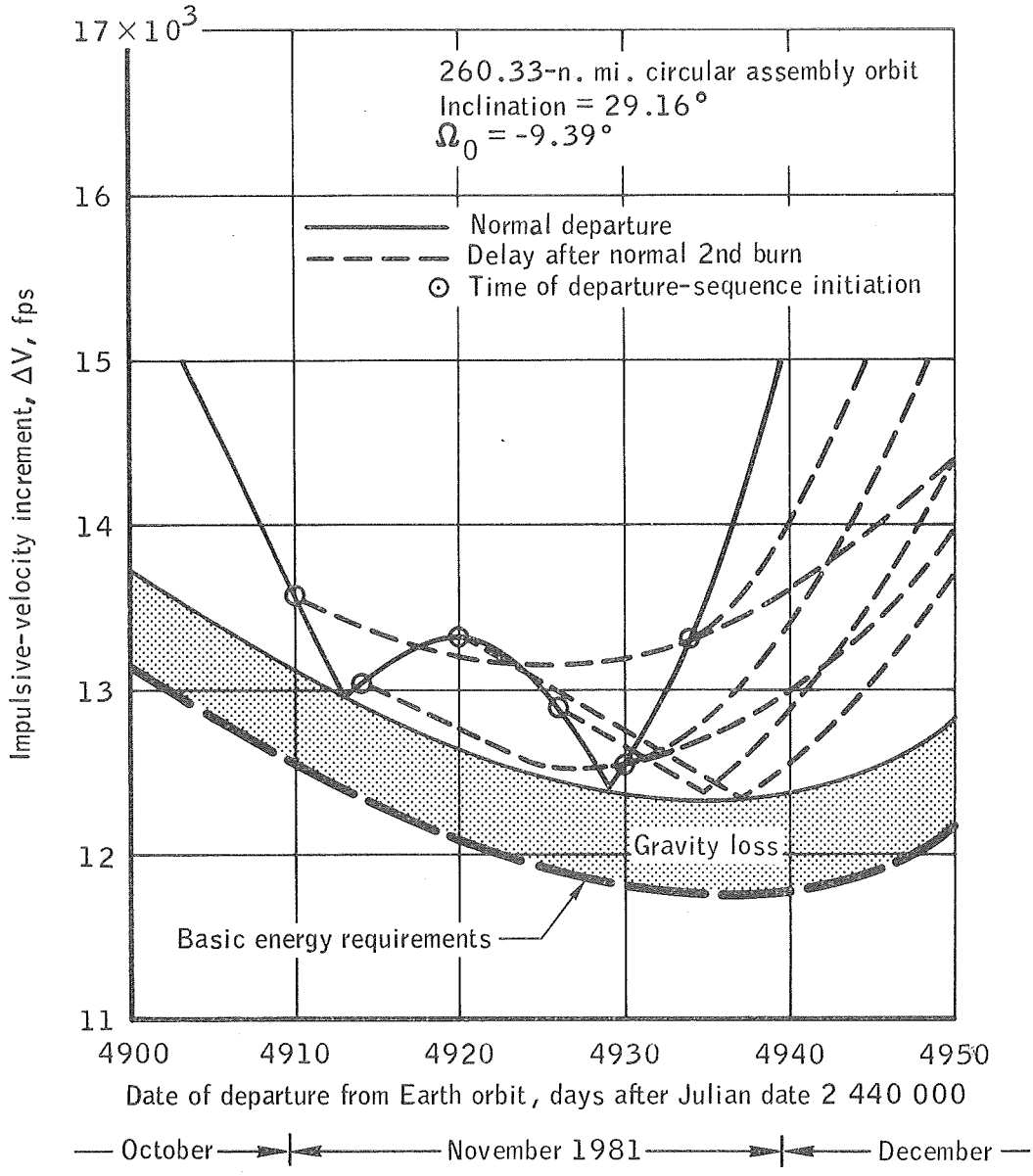

Figure 40. - Interrupted departure sequence for the 1981 mission opportunity (delay following second burn).

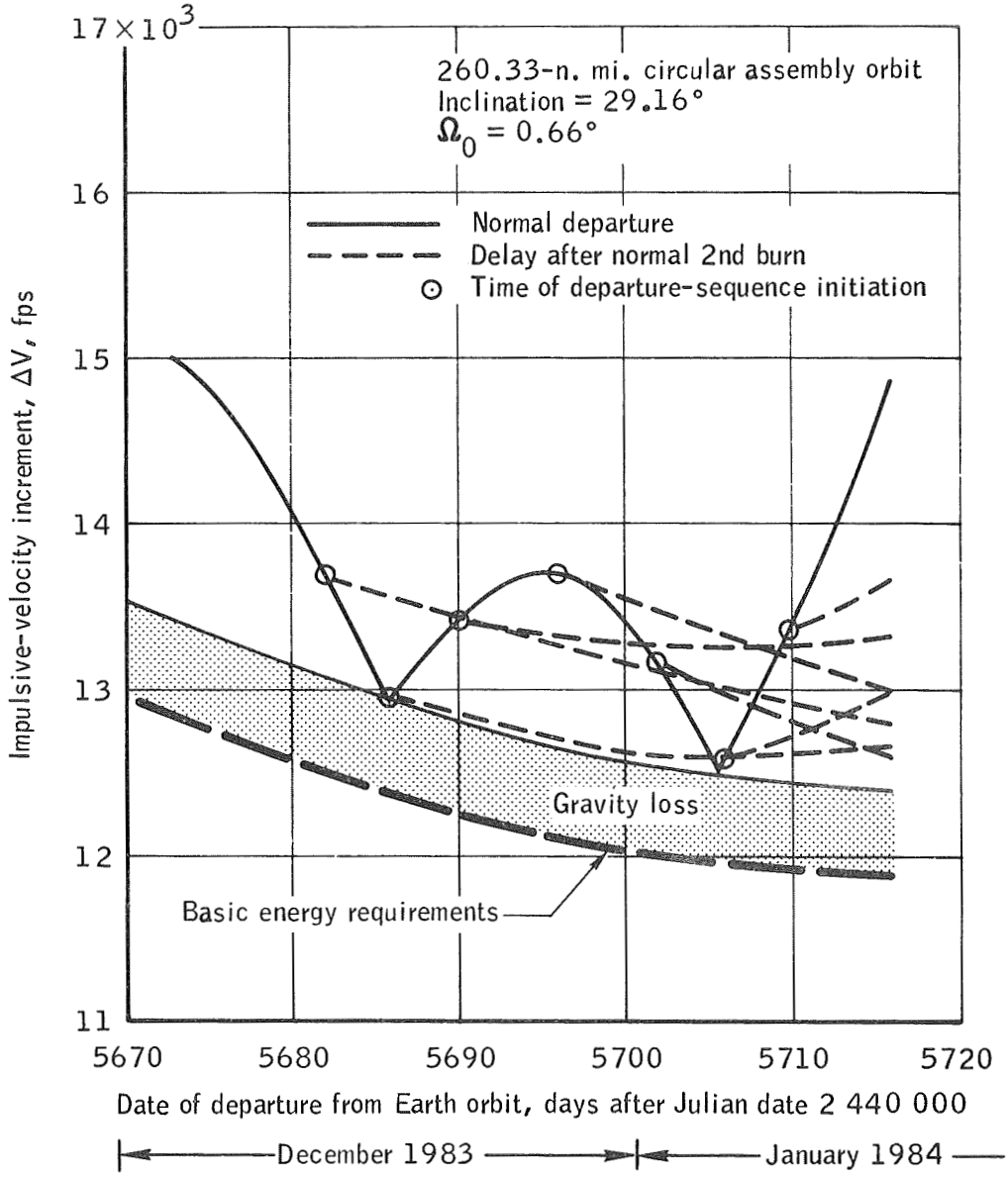

Figure 41. - Interrupted departure sequence for the 1983 mission opportunity (delay following second burn).

CONCLUSIONS

The minimum-energy mission profile for manned exploration of Mars permits the accomplishment of an increased list of scientific objectives, when compared with shorter duration mission profiles. The two most significant factors in obtaining this increase are (1) the increased payload available because of lower total energy requirements and (2) the increased Mars-orbital stay time which can be profitably used with the increased payload for scientific observation.

The performance requirements for minimum-energy profiles are nearly constant for all mission opportunities. Therefore, although, a missed mission opportunity requires a wait of approximately 2 years, as with the shorter duration profiles, major spacecraft or propulsion-system modification is not required, and a single spacecraft design can more readily accommodate all mission opportunities. The maximum Earth-entry velocity for a minimum-energy mission does not exceed 40 000 fps and is within current Apollo technology.

The orbital launch window for the minimum-energy mission and the assumed vehicle is approximately 30 days and is relatively insensitive to delayed launches or interrupted departure sequences. The first launch of a four-launch assembly can be delayed up to 30 days and still retain a 22-day orbital-departure window. The time available for launch-pad turnaround is in excess of 21 days, assuming that three pads are available and that four launches are required.

The minimum-energy mission is feasible with state-of-the-art technology. It can be accomplished with a 450 000-pound spacecraft (including 119 000 pounds of functional payload) by using cryogenic propulsion for Mars-orbital insertion and space-storable propulsion for trans-Earth injection. Four launches of an uprated Saturn V, each capable of placing 400 000 pounds of payload into a 260-nautical-mile circular orbit, provide sufficient injection velocity, assuming liquid-oxygen- and hydrogen-fueled orbital-launch vehicles.

Manned Spacecraft Center
National Aeronautics and Space Administration
Houston, Texas, July 23, 1969
909-40-30-00-72

APPENDIX

EARTH DEPARTURE HYPERBOLIC-EXCESS-VELOCITY VECTORS

Tables XII to XV are listings of the Earth-departure $\vec{V}_\infty$ vectors for Mars conjunction-class missions in 1977, 1979, 1981, and 1983. The $\vec{V}_\infty$ is defined as the planet-centered velocity vector that a spacecraft would attain after an infinite coast time on a hyperbolic trajectory if acted upon only by the departure-planet gravitational acceleration. The magnitude of this vector is given by the vis viva equation in which R, the radius from the center of the planet, approaches infinity. The direction of the vector is the direction of the hyperbolic departure asymptote translated to the center of the planet.

The $\vec{V}_\infty$ vectors listed in the tables were generated with a matched-conic program (ref. 26). The coordinate system is referenced to the true equator and the vernal equinox of date. The Julian date of departure is the time when the spacecraft is at the periapsis of the departure hyperbola. Figure 42 is a schematic representation of the tabulated data.

Theoretical analysis of the dynamic simulation suggests that the matched-conic $\vec{V}_\infty$ yields optimistic injection-velocity requirements. A single-point comparison was made between a precision-integrated trajectory and a matched-conic trajectory. The results of this point check tended to verify the theoretical analysis. Also, the matched-conic velocity vector $\vec{V}_0$ at the sphere of influence, used as a $\vec{V}_\infty$ in the geocentric two-body equations, yields an injection velocity that agrees well with the precision-integrated $\vec{V}_0$. The directions of the $\vec{V}_\infty$ and $\vec{V}_0$ vectors for a given interplanetary trajectory are essentially the same. The slightly conservative $\vec{V}_0$ values were used as the $\vec{V}_\infty$ magnitude in the launch-window analysis, and $\vec{V}_0$ is presented in tables XII to XV. The direction of the departure asymptote was that given by $\vec{V}_\infty$.

TABLE XII. - EARTH-DEPARTURE $\vec{V}_\infty$ VECTORS AND $\vec{V}_0$ MAGNITUDE FOR THE 1977 MARS CONJUNCTION-CLASS-MISSION LAUNCH WINDOW

Julian date of departure	$\vec{V}_\infty$			$\vec{V}_0$ magnitude, fps
	Magnitude, fps	Right ascension, deg	Declination, deg	
2 443 400	12 947	121.45	19.04	13 302
2 443 402	12 598	121.01	19.14	12 958
2 443 404	12 263	120.45	19.25	12 633
2 443 406	11 948	119.78	19.40	12 329
2 443 408	11 656	118.99	19.56	12 047
2 443 410	11 392	118.08	19.75	11 788
2 443 412	11 144	117.05	19.96	11 554
2 443 414	10 929	115.91	20.19	11 347
2 443 416	10 745	114.66	20.44	11 167
2 443 418	10 590	113.30	20.69	11 018
2 443 420	10 467	111.85	20.96	11 090
2 443 422	10 379	110.32	21.23	10 813
2 443 424	10 321	108.73	21.50	10 761
2 443 426	10 304	107.10	21.77	10 742
2 443 428	10 320	105.45	22.04	10 759
2 443 430	10 377	103.80	22.29	10 812
2 443 432	10 467	102.17	22.54	10 900
2 443 434	10 600	100.58	22.80	11 024
2 443 436	10 766	99.06	23.03	11 183
2 443 438	10 966	97.61	23.27	11 376
2 443 440	11 200	96.27	23.51	11 602
2 443 442	11 467	95.03	23.75	11 869
2 443 444	11 765	93.91	24.02	12 150
2 443 446	12 092	92.91	24.33	12 469
2 443 448	12 450	92.04	26.70	12 817
2 443 450	12 840	91.29	25.16	13 192

TABLE XIII. - EARTH-DEPARTURE $\vec{V}_\infty$ VECTORS AND $\vec{V}_0$ MAGNITUDE FOR THE 1979 MARS CONJUNCTION-CLASS-MISSION LAUNCH WINDOW

Julian date of departure	$\vec{V}_\infty$			$\vec{V}_0$ magnitude, fps
	Magnitude, fps	Right ascension, deg	Declination, deg	
2 444 150	12 960	151.47	17.49	13 313
2 444 152	12 588	151.62	17.79	12 951
2 444 154	12 229	151.70	18.15	12 603
2 444 156	11 885	151.68	18.57	12 269
2 444 158	11 557	151.58	19.06	11 951
2 444 160	11 245	151.38	19.61	11 650
2 444 162	10 951	151.09	20.23	11 367
2 444 164	10 676	150.69	20.93	11 102
2 444 166	10 422	150.18	21.71	10 858
2 444 169	10 191	149.57	22.56	10 636
2 444 171	9 984	148.85	23.50	10 438
2 444 173	9 804	148.02	24.51	10 266
2 444 175	9 652	147.09	25.61	10 121
2 444 177	9 532	146.06	26.78	10 006
2 444 179	9 444	144.94	28.03	9 923
2 444 181	9 392	143.74	29.35	9 874
2 444 183	9 378	142.49	30.75	9 861
2 444 185	9 405	141.19	32.19	9 886
2 444 187	9 475	139.88	33.77	9 953
2 444 189	9 591	138.57	35.41	10 064
2 444 191	9 756	137.32	37.15	10 222
2 444 193	9 979	136.14	39.03	10 434
2 444 195	10 262	135.08	41.06	10 705
2 444 196	10 614	134.16	43.28	11 043
2 444 198	11 054	133.48	45.79	11 466
2 444 200	11 610	133.10	48.71	12 003

TABLE XIV. - EARTH-DEPARTURE $\vec{V}_\infty$ VECTORS AND $\vec{V}_0$ MAGNITUDE FOR THE 1981 MARS CONJUNCTION-CLASS-MISSION LAUNCH WINDOW

Julian date of departure	$\vec{V}_\infty$			$\vec{V}_0$ magnitude, fps
	Magnitude, fps	Right ascension, deg	Declination, deg	
2 444 900	13 948	182.33	10.27	14 277
2 444 902	13 585	183.13	10.47	13 923
2 444 904	13 231	183.89	10.74	13 577
2 444 906	12 887	184.62	11.07	13 242
2 444 908	12 552	185.30	11.46	12 916
2 444 910	12 228	185.95	11.93	12 601
2 444 912	11 915	186.55	12.47	12 298
2 444 914	11 614	187.10	13.10	12 006
2 444 916	11 326	187.61	13.83	11 728
2 444 918	11 052	188.07	14.65	11 464
2 444 920	10 793	188.48	15.57	11 215
2 444 922	10 552	188.83	16.61	10 983
2 444 924	10 331	189.14	17.77	10 770
2 444 927	10 130	189.39	19.06	10 578
2 444 929	9 954	189.59	20.47	10 409
2 444 931	9 804	189.74	22.03	10 267
2 444 933	9 686	189.86	23.74	10 154
2 444 935	9 602	189.93	25.60	10 074
2 444 937	9 559	189.99	27.62	10 032
2 444 939	9 561	190.04	29.79	10 034
2 444 941	9 616	190.11	32.13	10 087
2 444 943	9 734	190.23	34.64	10 200
2 444 945	9 925	190.43	37.30	10 382
2 444 947	10 205	190.78	40.14	10 650
2 444 948	10 586	191.32	43.12	11 016
2 444 950	11 101	192.17	46.27	11 511

TABLE XV. - EARTH-DEPARTURE $\vec{V}_\infty$ VECTORS AND $\vec{V}_0$ MAGNITUDE FOR THE 1983 MARS CONJUNCTION-CLASS-MISSION LAUNCH WINDOW

Julian date of departure	$\vec{V}_\infty$			$\vec{V}_0$ magnitude, fps
	Magnitude, fps	Right ascension, deg	Declination, deg	
2 445 666	14 003	221.53	1.00	14 330
2 445 668	13 735	222.75	1.34	14 068
2 445 670	13 474	223.95	1.72	13 814
2 445 672	13 220	225.12	2.14	13 567
2 445 674	12 974	226.26	2.59	13 327
2 445 676	12 736	227.38	3.09	13 095
2 445 678	12 506	228.47	3.62	12 872
2 445 680	12 285	229.53	4.19	12 657
2 445 682	12 072	230.55	4.81	12 450
2 445 684	11 868	231.54	5.46	12 253
2 445 686	11 674	232.50	6.14	12 064
2 445 688	11 488	233.42	6.87	11 885
2 445 690	11 313	234.30	7.63	11 716
2 445 692	11 148	235.14	8.42	11 557
2 445 694	10 993	235.94	9.24	11 407
2 445 696	10 849	236.70	10.10	11 269
2 445 698	10 717	237.41	10.98	11 141
2 445 700	10 595	238.08	11.90	11 024
2 445 702	10 486	238.71	12.83	10 919
2 445 704	10 388	239.29	13.78	10 825
2 445 707	10 303	239.83	14.76	10 744
2 445 709	10 230	240.32	15.74	10 674
2 445 711	10 170	240.77	16.74	10 617
2 445 713	10 124	241.17	17.74	10 572
2 445 715	10 091	241.53	18.74	10 540
2 445 717	10 071	241.85	19.75	10 522

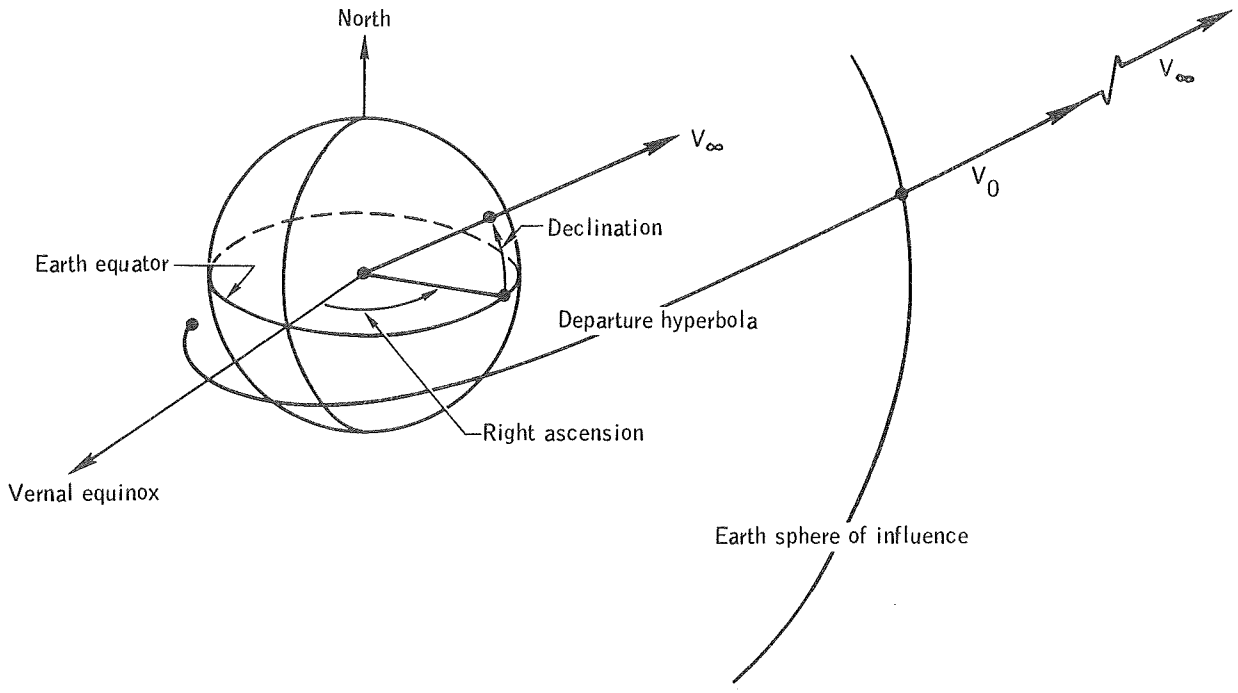

Figure 42. - Schematic representation of Earth-departure parameters.

REFERENCES

1. Anon.: Manned Planetary Flyby Mission Based on Saturn/Apollo Systems. NAA Rept. SID 67-549, Aug. 1967.

2. Anon.: Study of Conjunction Class Manned Mars Trips. Douglas Rept. SM-48662, Apr. 1965.

3. Cowls, R. S.: Tradeoff Study of a New Cryogenic Stage for Manned Planetary Exploration. Douglas Aircraft Rept. DAC-58053, Vol. II, Sept. 1967.

4. Taylor, James J.: Mode Analysis of a Low-Energy Mars Landing Mission. Proceedings of the Fourth AIAA/MSC Astrodynamics Conference, vol. 4, NASA TM X-61414, 1968, pp. 117-131.

5. Taylor, James J.; and McNeely, John T: Mars Landing Mission Mode Comparison. NASA TM X-1629, Aug. 1968.

6. TRW Systems Group: Alternative Mission Modes Study. TRW-07394-6008-R000, vol. 1; TRW-07394-6009-R000, vol. 2, Sept. 1967.

7. Deerwester, J. M.; and D'Haem, S. M.: Systematic Comparison of Venus Swing-by Mode with Standard Mode of Mars Round Trips. J. Spacecraft Rockets, vol. 4, no. 7, July 1967, pp. 904-911. (Also available as AIAA paper 67-27 at AIAA 5th Aerospace Science Meeting, Jan. 1967.)

8. Anon.: Integrated Manned Interplanetary Spacecraft Concept Definition. System Assessment and Sensitivities, Vol. II. Boeing Company D2-113544, Jan. 1968.

9. Wilson, Sam W., Jr.: A Multiple-Impulse Orbital Departure Technique for Manned Interplanetary Missions. AIAA Paper 69-126 presented at AIAA 7th Aerospace Sciences Meeting, Jan. 20-22, 1969.

10. Doll, J. R.: Three-Impulse Trajectories for Mars Stopover Missions in the 1980 Time Period. United Aircraft Corp. Research Laboratories Rept. F-110398-1, Aug. 1967.

11. Gobetz, F. W.; and Doll, J. R.: How to Open a Launch Window. United Aircraft Corp. Research Laboratories Rept. F-110058-27, Nov. 1967.

12. Johnson, Paul G.; and Row, Frank E.: Perigee Propulsion for Orbital Launch of Nuclear Rockets. NASA TR R-140, 1962.

13. Funk, Jack; and McAdoo, Stewart F.: Switching Logic and Steering Equations for Multiple-Burn Earth Escape Maneuvers. Paper presented at the Institute of Navigation National Space Navigation Meeting (Houston, Texas, Apr. 22-24) on Space Navigation — Present and Future, 1969.

14. Thibodeau, Joseph R. III: Use of Planetary Oblateness for Parking-Orbit Alinement. NASA TN D-4657, 1968.

15. Luidens, Roger W.; and Miller, Brent A.: Efficient Planetary Parking Orbits with Examples for Mars. NASA TN D-3220, 1966.

16. Ross, S. E.: Planetary Flight Handbook. Speed Contours and Auxiliary Graphs for Manned Missions to Mars and Venus. NASA SP-35, vol. 3, part 1, 1963.

17. Lowes, Flora B.; and Murtagh, Thomas B.: Navigation and Guidance Systems Performance for Three Typical Manned Interplanetary Missions. NASA TN D-4629, 1968.

18. Murtagh, Thomas B.: Planetary Probe Guidance Accuracy Influence Factors for a Conjunction-Class Mission. NASA TN D-4852, 1969.

19. Anon.: Control, Guidance, and Navigation for Advanced Manned Missions. MIT-IL R-600 (4 vols.), Jan. 1968.

20. Ross, S. E.: Final Report: Study of Interplanetary Transportation Systems Phase III. Lockheed Missiles and Space Co. Rept. No. 3-17-64-1, Apr. 1964.

21. Chovit, A. R.; and Callies, G. M.: Mission Oriented Advanced Nuclear Systems Parameters Study: Phase VI, Final Report. TRW Systems Group Rept. No. 01977-6026-R0-00, June 1968.

22. Gerbracht, R. J.; and Penzo, P. A.: Optimum Three-Impulse Transfer between an Elliptic Orbit and a Non-Coplanar Escape Asymptote. AAS Paper 68-084 presented at AAS/AIAA Astrodynamics Specialist Conference, Jackson Lake, Wyoming, Sept. 1968.

23. Deerwester, J. M.; McLaughlin, J. F.; and Wolfe, J. F.: Earth-Departure Plane Change and Launch Window Considerations for Interplanetary Missions. J. Spacecraft Rockets, vol. 3, Feb. 1966, pp. 169-174.

24. Robbins, Howard M.: An Analytical Study of the Impulsive Approximation. AIAA Paper 66-12, vol. 4, Jan. 1966, pp. 1417-1423.

25. Walters, L. G.; Koskela, P. E.; and Arsenault, J. L.: General Perturbations. Handbook of Astronautical Engineering, H. H. Koelle, Ed., McGraw-Hill Book Co., Inc., (New York), 1961, ch. 8.3, pp. 8-19 to 8-34.

26. Davis, J. Philip; and Iyer, R. Ramdas: Conic Interplanetary Mission Planning Program. Lockheed Electronics Company Computer Program Document F-181 (3 vols.), 1968.

NASA-Langley, 1969 —— 30 S-209

NATIONAL AERONAUTICS AND SPACE ADMINISTRATION
WASHINGTON, D.C. 20546
OFFICIAL BUSINESS

FIRST CLASS MAIL

POSTAGE AND FEES PAI
NATIONAL AERONAUTICS
SPACE ADMINISTRATION

POSTMASTER: If Undeliverable (Section 1
Postal Manual) Do Not Re

"The aeronautical and space activities of the United States shall be conducted so as to contribute . . . to the expansion of human knowledge of phenomena in the atmosphere and space. The Administration shall provide for the widest practicable and appropriate dissemination of information concerning its activities and the results thereof."

— NATIONAL AERONAUTICS AND SPACE ACT OF 1958

NASA SCIENTIFIC AND TECHNICAL PUBLICATIONS

TECHNICAL REPORTS: Scientific and technical information considered important, complete, and a lasting contribution to existing knowledge.

TECHNICAL NOTES: Information less broad in scope but nevertheless of importance as a contribution to existing knowledge.

TECHNICAL MEMORANDUMS: Information receiving limited distribution because of preliminary data, security classification, or other reasons.

CONTRACTOR REPORTS: Scientific and technical information generated under a NASA contract or grant and considered an important contribution to existing knowledge.

TECHNICAL TRANSLATIONS: Information published in a foreign language considered to merit NASA distribution in English.

SPECIAL PUBLICATIONS: Information derived from or of value to NASA activities. Publications include conference proceedings, monographs, data compilations, handbooks, sourcebooks, and special bibliographies.

TECHNOLOGY UTILIZATION PUBLICATIONS: Information on technology used by NASA that may be of particular interest in commercial and other non-aerospace applications. Publications include Tech Briefs, Technology Utilization Reports and Notes, and Technology Surveys.

Details on the availability of these publications may be obtained from:

SCIENTIFIC AND TECHNICAL INFORMATION DIVISION
NATIONAL AERONAUTICS AND SPACE ADMINISTRATION
Washington, D.C. 20546